Regional Geology and Fracture Network Characterisation of the Southern Chotts and Jeffara Basins, Central Tunisia

Implications for Petroleum Reservoirs

Mr. R. Y. (Ruaridh) Smith

MSc Thesis Petroleum Engineering and Geosciences
Delft University of Technology
November 2020

Regional Geology and Fracture Network Characterisation of the Southern Chotts and Jeffara Basins, Central Tunisia

Implications for Petroleum Reservoirs

by

Mr. R. Y. (Ruaridh) Smith

to obtain the degree of Master of Science (MSc.)

at the Delft University of Technology,

to be defended publicly on Thursday November 12th, 2020 at 10am CET.

Student number:	4911725	
Project duration:	October 14, 2019 – November 12, 2020	
Thesis committee:	Prof. dr. G. Bertotti,	TU Delft, Supervisor
	Dr. P. B. R. Bruna,	TU Delft, Supervisor
	Prof. A. W. Martinius,	TU Delft, Committee Member
	Dr. A. Barnhoorn,	TU Delft, Committee Member

A confidential version of this thesis and additional data used is available upon request.

TU Delft

Abstract

The Southern Chotts and Jeffara Basins are situated within the Saharan Domain of Central Tunisia, North Africa. The Southern Chotts Basin hosts reservoirs within the Triassic, Permian and Ordovician units that contain significant hydrocarbon accumulations whilst the Jeffara Basin contains outcrop analogues of the same hydrocarbon-bearing formations.

The basins experienced a late Hercynian shortening phase which involved the uplift of a major topographic high (Tebaga de Medenine). This high, in conjunction with a older regional high, the Telemzane Arch influenced the deposition and geometry of the Permian and Triassic units across both basins. This shortening event is characterised at the scale of hundreds of meters by E-W striking folds into which the mid-late Triassic and early Jurassic units are deposited. The folding is also observed at field scale (10's meters) through small fault-related folds in the Permian deposits of the Tebaga de Medenine. This late Hercynian phase occurs between the late Permian and early Jurassic in the basins.

Fracture data collected from the upper Permian and lower Triassic units (Jeffara Basin) provides an analogue to the fracture networks at depth (Southern Chotts Basin) in the Paleozoic reservoirs. A conjugate fracture system observed in the field (from fracture pavements) corroborates with the interpretation of regional shortening in the basins. Seismic attribute analysis on depth slices in the Paleozoic reservoirs also shows the conjugate system at depth. This analysis is integrated with outcrop fracture data and FMI data from wells to create an open fold distributed fracture model of the system in the basins.

This model indicates the main driver for fracture generation in the region is folding and is used to predict the fracture networks at depth. This is undertaken using discrete fracture network (DFN) modelling of the subsurface. This model is integrated with a deterministic model from the seismic time slices to create a hybrid predictive fracture model of the early Paleozoic reservoirs.

Analytical aperture modelling of the fracture model demonstrates the fractures varied in openness depending on orientation and fracture length. The conjugate set orientated at 240°and longer joints detected from seismic attributes presented the widest aperture size. These fractures in the subsurface at implications on the transmissibility of the reservoirs, especially Permian units which have low bulk rock permeability and the lower Triassic (TAGI) sequences which are susceptible to compartmentalisation.

Preface

This work was undertaken as part of the North Africa Research Group (NARG) and with Mazarine Energy (The Netherlands and Tunisia). Seismic and well data was provided by Mazarine Energy. Access to additional North African data by NARG. Thanks to Mazarine Energy for organising the fieldwork in Tunisia and special thanks to Salma Ben Amor and Ahmed Nasri for all their help. Also thanks to ETAP (Entreprise Tunisienne d'Activités Pétrolières) and ONM (National Office of Mines, Tunisia) for good discussions in the field and for sharing their knowledge of the area. Additional thanks to the TU Delft Fund (FAST Fund) for funding part of my fieldwork mission to Tunisia.

Special thanks to my supervisors Dr. Pierre-Olivier Bruna and Prof. Giovanni Bertotti for all their help and support throughout this thesis. Giovanni, thank you for all your expertise and critical analysis on my work, it has both helped develop my work and pushed it to greater heights. Pierre thanks for all the support and assistance throughout the project. Our excellent discussions both in the field and back at the university has made this project worthwhile. Your enthusiasm and support have really helped my development as a geologist and researcher. To that I thank you both. Additional thanks to Quinten Boersma and Rahul Prabhakaran in the Applied Geology section for assistance with the software used in this thesis. And to my fellow Tunisia geology researcher Jos Kwakman, thanks for the coffee breaks, the discussions about the Southern Chotts Basin and rugby and anything else that cropped up, it's been great to share this project with you.

As a culmination of my study and work in the Netherlands, I also reflect on the enjoyable two years I have spent in Delft. Thanks go to my classmates of Petroleum Engineering and Geosciences, and whilst it may have been a small class, there was a wealth of entertainment and laughs throughout the whole course. Thanks to all the lectures in the Applied Earth Science department. Coming from a purely geological background into the world of applied science and engineering it has been a great step up, and has been made easier by the excellent teaching and enthusiastic staff in all the courses. Thanks also the members of DSR-C and the general rugby community in the Netherlands who have not only given me an authentic dutch living experience but welcomed me into the small but fantastic rugby family during my time here. I can honestly say I have had some of my best refereeing experiences during the past two seasons.

My last thanks to my family (and Ginny) at home in Scotland. Without your love and support over the past years, I don't think I would have achieved anything near what I have. Further appreciation to you for taking me back for the final months of my project work during this period of lockdown and providing me with engaging and poignant discussions on work, life and everything in between. For all you have done, thank you.

Mr. R. Y. (Ruaridh) Smith
Delft, November 2020

Contents

List of Figures

List of Tables

Glossary

AFT Apatite Fission Track. 56

BBZ Baten Beni Zid. xii, 19, 20, 29, 30

DFN Discrete Fracture Network. xiii, xv, 11, 38, 39, 41, 43–45, 47, 48, 52, 57

DSDF Dip-Steered Diffusion Filter. xiv, 36, 74

DSMF Dip-Steered Median Filter. xiv, 36, 74

ETAP Entreprise Tunisienne d'Activités Pétrolières. 1, 12

FE Finite Element. 48, 52, 55, 56

FEF Fault Enhancement Filter. xiv, 36, 74, 75

FL Fault Likelihood. xiii, xiv, 47, 55, 75

FMI Formation MicroImager. 14, 27, 33–35, 41, 48, 54

JCS Joint Compressive Strength. 49

JRC Joint Roughness Coefficient. 49, 50

LPS Layer Parallel Shortening. 29, 55

MPS Multiple Point statistical Simulation. xiv, 54–56

REV Representative Elementary Volume. 53, 54, 56

SCB Southern Chotts Basin. xiii, 1–3, 6–9, 14, 22, 26, 27, 32–34, 38, 41, 43, 52–57

TAGI Trias Argilo-Gréseux Inférieur (Lower Clay-Sandstone Triassic). 1, 7, 8, 52, 56, 57

TdM Tebaga de Medenine. xi, xii, xiv, 1–3, 8, 9, 12, 14–22, 24, 26, 28, 29, 31, 53, 54, 56, 57, 67

TFL Thinned Fault Likelihood. xiii, xiv, 47, 55, 75

1

Introduction

The Jeffara Basin and the Southern Chotts Basin (SCB) (fig.1.1) are located in Central and Southern Tunisia bounded to the south by the Telemzane Arch (fig.1.2), a large regional high in Northern Africa (Soua 2014, Mejri et al. 2006, and references therein).

The late Paleozoic and Mesozoic reservoir rocks outcrop in the Jeffara Basin and are found at depth in the SCB where hydrocarbon plays are present in the Ordovician, Permian and the Trias Argilo-Gréseux Inférieur (Lower Clay-Sandstone Triassic) (TAGI) reservoirs (Bruna et al. 2019a, Soua 2014). Whilst the Ordovician reservoirs are not found at the surface, the Permian and TAGI sequences outcrop in the Tebaga de Medenine (TdM) and along the Jeffara Escarpment (Bruna et al. 2019a, Mejri et al. 2006).

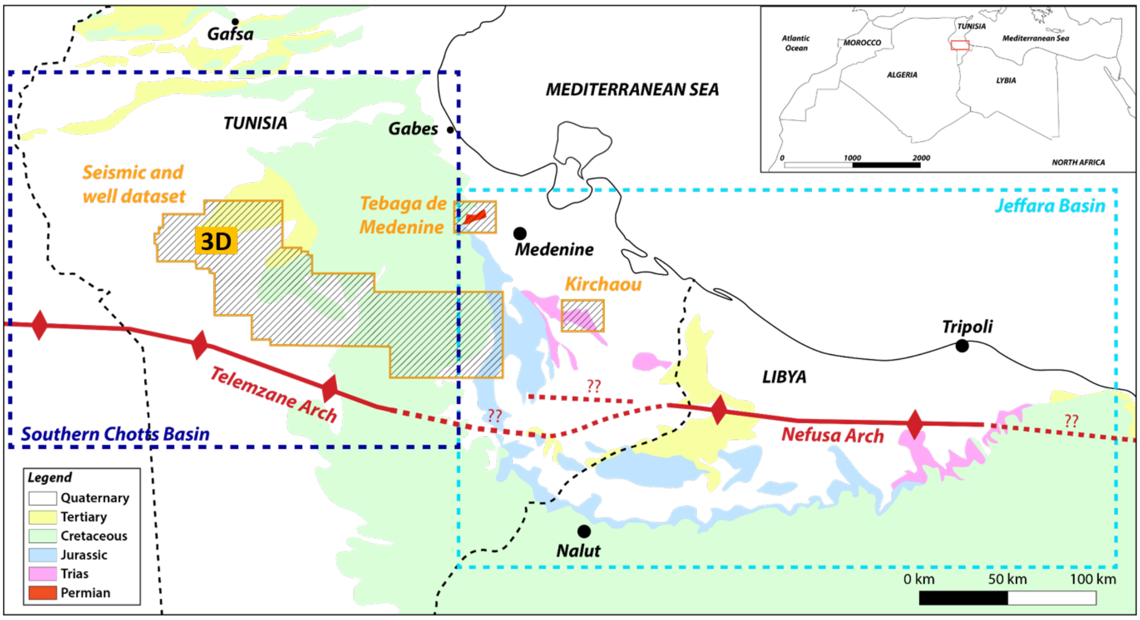

Figure 1.1: Geological Map of Central Tunisia showing location of main basins and locations of interest (yellow)

The SCB is split into several permits managed by the Entreprise Tunisienne d'Activités Pétrolières (ETAP), Mazarine Energy and Hunt Oil where average daily oil production totals 3159 bbls/day (ETAP 2020). The Zaafrane permit is in development with recent well tests indicating the potential of 2000 bbls/day and Douriet permit is currently under exploration (ETAP 2020, Mazarine Energy B.V. 2019).

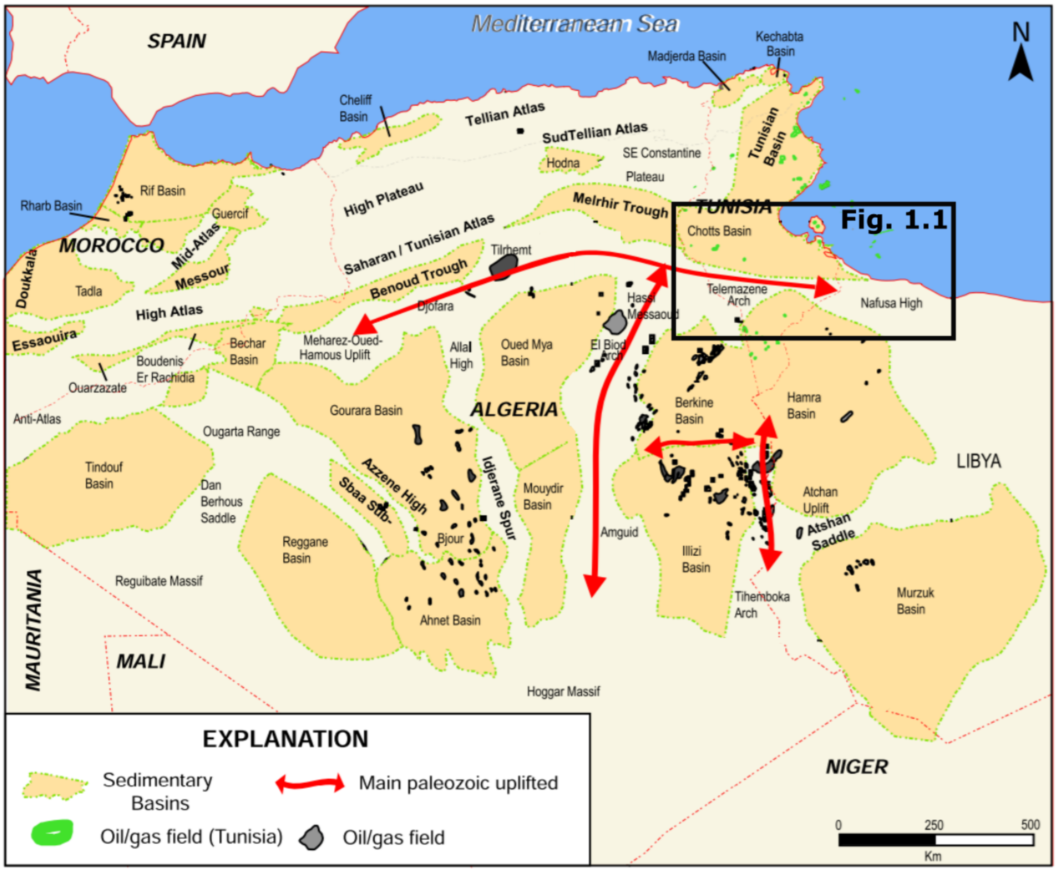

Figure 1.2: Main sedimentary basins along the North Atlantic Margin and major uplifted Paleozoic highs (Soua 2014, Lüning et al. 2000, Craig et al. 2008)

Within the Jeffara Basin, the TdM forms a series of large ridges (3-6km in length) containing the only marine Permian outcrop in Northern Africa (Mejri et al. 2006). This structure provides an insight into how the late Palaeozoic and early Mesozoic units interact with each other. The exposed units along the TdM show the geometry of the Triassic and Jurassic units on the underlying Permian and the main unconformities present between the Permian and Mesozoic layers (Raulin et al. 2011). Furthermore, the nature of the bedding within the TdM can highlight events that occurred during and after deposition of the Permian and Early Triassic. The structural nature and geological history regarding the formation of the TdM has been subject to a number of studies with varying interpretations (Raulin et al. 2011, and references therein).

Understanding the relationship between the TdM and regional history of the Jeffara Basin allows for understanding the mechanism for the formation of the main structures in the region. Fractures observed both on the surface (TdM) and at depth (SCB) can then be related to this mechanism, further understanding the drivers for fractures within the rocks. Using fracture drivers, predictions can be made about the fracture networks within the reservoirs in the SCB.

Fractures play an important role in reservoir connectivity, especially the Permian carbonate plays where bulk permeability is low (Balti et al. 2018). Determining the fracture networks at depth in the SCB plays a role in both exploration and production processes.

In addition to the main objective of further understanding the regional structure of the Jeffara Basin and SCB, the following research questions were aimed to be answered during this thesis:

1. What is the structural nature of the Tebaga de Medenine?
2. What is the regional structural history during the Permian to Cretaceous in the Jeffara Basin?
3. How does this history affect the fractures observed units at the surface?
4. How does the geological history of the region drive fracture generation in the Southern Chotts Basin
5. What are the implications of these fractures to the reservoir flow in the Southern Chotts Basin plays?

To undertake this research a number of different methods and techniques are applied. Fieldwork conducted in 2019 in the Jeffara Basin investigated the Permian and Triassic units in the TdM and along the Jeffara Escarpment. To complement this data, additional information was collected from satellite imagary along the Jeffara Escarpment. Subsurface analysis (well and seismic) primarily focused in the NW region of the SCB and on the fracture patterns present at depth. The data collected and analysed from these sources culminate into a fracture model of the Ordovician reservoirs in the SCB and a better understanding of the structures both at the surface and at depth.

2

Geological Setting and Stratigraphy

2.1. Present Day Situation

The structural setting of Tunisia is formed of three major of domains (fig.2.1) arranged mainly north to south (Bouaziz et al. 2002, Doglioni et al. 1999). The Tell (Alpine) Domain is a major fold and thrust belt related to the Cenozoic Alpine Orogeny with the Atlassic Domain situated to the south (Bouaziz et al. 2002, Perthuisot 1981, Rouvier 1977). This domain extends from the High Atlas in Morocco to the Tunisian Atlas and forms an older folded thrust belt (Bouaziz et al. 2002, Zouari et al. 1999, Zargouni 1985). The Saharan Domain forms the foreland to the Atlassic Domain in the north and is considered relatively tectonically stable, stretching across northern Africa as an area of continuous subsidence since the Cambrian Period (Fekirine and Abdallah 1998).

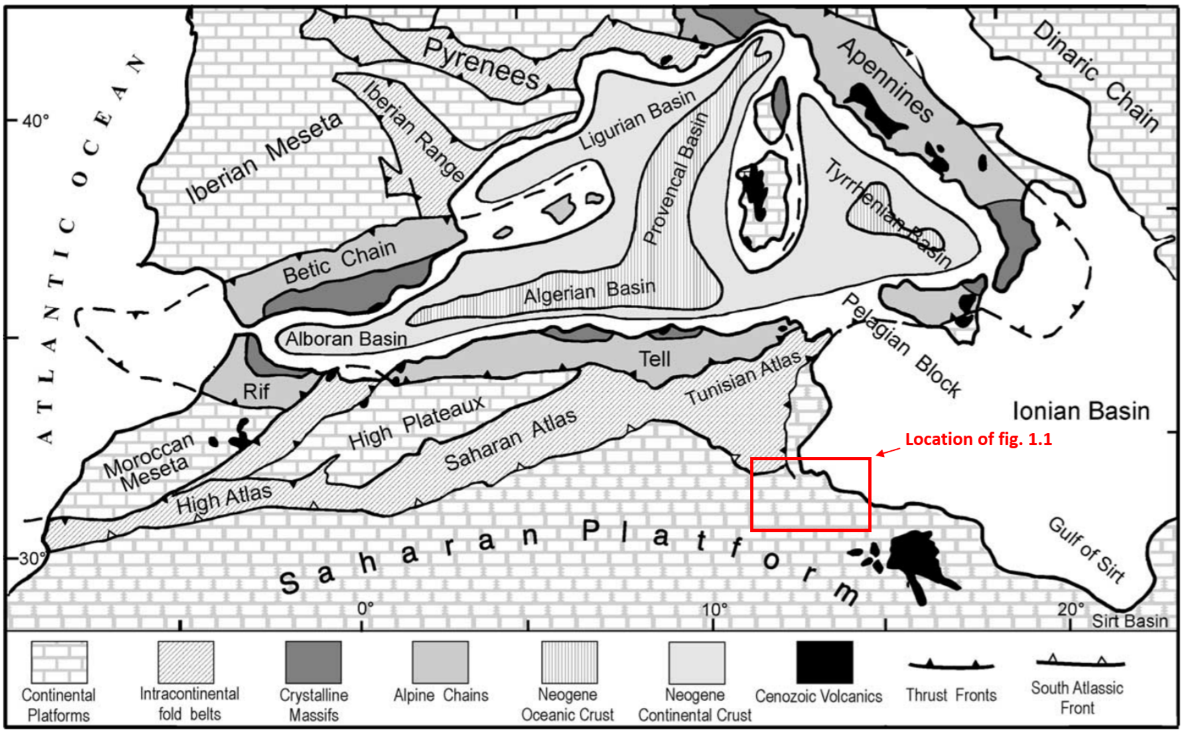

Figure 2.1: Regional Setting of Northern Africa (Modified from Bouaziz et al. (2002), Doglioni et al. (1999))

The SCB occurs just south of the Atlassic Domain along the Saharan Platform in Tunisia sharing some characteristics to the units found in the north. The Jeffara Basin, located to the east of the SCB in the Saharan Domain containing several fault systems including the Jeffara Fault System which is involved in the development of the Sirt Basin to the NE (Jabir et al. 2020, El Rabia et al. 2018, Soua 2014). These boundary between these basins is defined by the Jeffara Escarpment and both basins are bounded to the south by the Telemzane Arch.

2.2. Structural History and Regional Setting

The Saharan Domain has a considerably long continuous history compared to the northern domains (Tell and Atlassic) which have been affected by recent events from the Alpine orogeny (Lüning 2005). The basement of the Saharan Domain relates to Archean to Paleaeoproterzoic metamorphic units overlain by the deposits from the Pan-African Orogeny during the late Proterozoic (680-550Mya) which formed Gondwana (Dhaoui et al. 2014, Condie 2003, Ferjani et al. 1990, Bishop 1975).

During the late Proterozoic to Cambrian (”Infracambrian”) several half-grabens and pull-apart basins formed from dominant extensional and strike-slip regimes (Bruna et al. 2019a, Soua 2014, Lüning et al. 2009). This continues into the Cambrian where the E-W trending Telemzane Arch forms as a half graben controlled by normal fault movements creating an arch (Lavier and Buck 2002). By the early Ordovician the arch is a prominent feature influencing the distribution of major reservoirs and source rocks in the region (El Gassi, El Atchane and Hamra Formations) (Bruna et al. 2019a, Soua 2013, Fabre 1988).

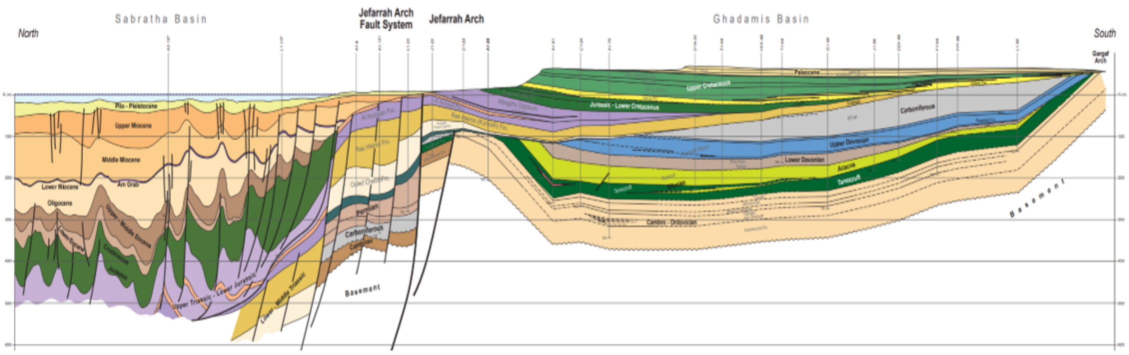

Figure 2.2: Regional cross-section over Telemzane Arch (Jeffara Arch) (Reeh et al. 2019)

Between the early Ordovician and the Carboniferous, there are several phases of extensional and compression (Taconian and Caledonian Orogenies), marked by a series of unconformities affecting deposition and preservation of units (Lüning 2005, Guiraud et al. 2005, Boote et al. 1998). During this period the Telemzane Arch continues to be a prominant arch high, affecting the distribution and thickness of major petroleum units (Soua 2014, Aissaoui et al. 1996, Scotese and Barrett 1990, and references therein). A major source rock (Frasnian) deposited during the Devonian is partially eroded in this region during the Caledonian and Hercynian orogenies (Daniels and Emme 1995, Ross and Ross 1988, Tissot et al. 1984). Prior to the onset of the Hercynian Orogeny, the Telemzane Arch experiences major uplift during the late Devonian through thermal doming affecting the distribution of younger sediments Frizon de Lamotte et al. (2013).

The Hercynian Orogeny (collision between Laurentia and Gondwana) initiated in the Carboniferous affecting the entire region through reactivation of faults, block tilting and folding, including further uplift of the Telemzane Arch causing the onlap of the Carboniferous and Permian deposits onto Devonian and older units (Frizon de Lamotte et al. 2013, Stampfli and Borel 2002, Stampfli et al. 2001). This phase causes several unconformities in the region including the complete removal of the Carboniferous and remaining Devonian in the SCB (Jabir et al. 2020, Mejri et al. 2006). It is generally considered that this orogeny culminates by the late Permian (Galeazzi et al. 2010, Villeneuve et al. 1991).

From the Triassic and Jurassic, North Africa experiences a period of extension related to the opening of the Tethys Ocean, into which the early Triassic sands (TAGI) are deposited over the Hercynian Unconformity (fig.2.2) (Frizon de Lamotte et al. 2013, Bouaziz et al. 2002, Boote et al. 1998).

A series of unconformities mark the transition between the late Jurassic and lower Cretaceous and collectively grouped as the Austrian Unconformity relating to the structural movements along the African-South American margin and strike-slip roation with Eurasia (Bodin et al. 2010, Lazzez et al. 2008). The Alpine phase (collision and rotation between Africa and Eurasia) is marked in the Saharan Domain by the Cretaceous-Tertiary Unconformity. From this period on, non-deposition and tectonic stability in the domain continues from the Pliocene to the present day (Galeazzi et al. 2010, Lazzez et al. 2008, Mejri et al. 2006).

2.3. Stratigraphy of the Jeffara and Southern Chotts Basins

The various regional tectonic phases in North Africa (section 2.2) are present in the stratigraphy of the Jeffara Basin and the SCB. The uplift and continued presence of the Telemzane Arch as a prominent folded high in the region affected the distribution of the deposits found in the basins (Frizon de Lamotte et al. 2013, Bouaziz et al. 2002). The earliest effect, observed in the Ordovician sand deposits of the El Atchane and Hamra Formations (fig.2.3) (Bruna et al. 2019a, Mejri et al. 2006). Overlying these deposits an important Devonian regional source rock (Fegaguira Formation) which underlies the Permian carbonates (Bouaziz et al. 2014, Derguini 2005). The basins are predominately filled with Mesozoic sediments (including reservoir units, TAGI) and thick formation packages (up to 500m) of the Jurassic and Cretaceous were deposited during the Tethyian extension and Austrian Orogeny (Bouaziz et al. 2014, Bodin et al. 2010).

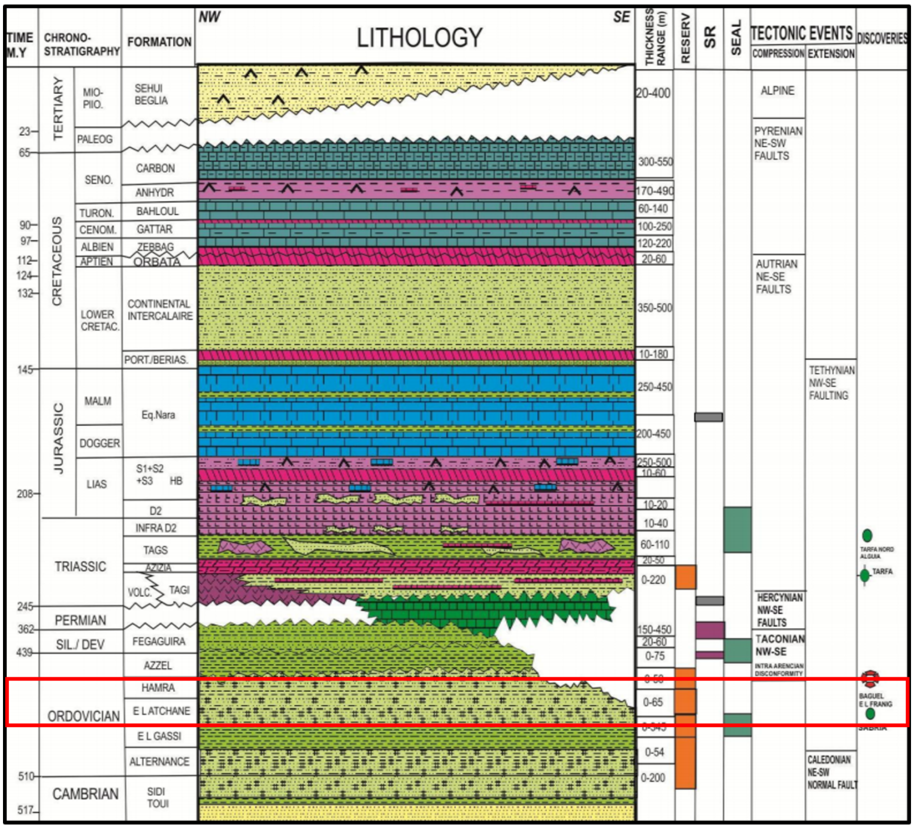

Figure 2.3: Stratigraphy of the Southern Chotts Basin with Ordovician units studied in this work (Red box) (Bouaziz et al. 2014, Derguini 2005)

There are several major hiatuses and erosional phases observed in the Jeffara Basin and SCB from the Taconian, Caledonian and in particular the Hercynian Orogenies, in which the complete Carbonifeous and majority of the Permian, Silurian and Devonian deposits are removed or undeposited (Bouaziz et al. 2014, Soua 2014). This has been constrained through seismic analysis and previous basin modelling studies on the SCB (Bruna et al. 2019a, Mejri et al. 2006).

One of the more important phases is the Hercynian Orogeny which affects the entire region Bruna et al. (2019a). The timeline of this orogeny is complex with a number of different stages involved in the overall event, thus making reconstructions difficult in places (Galeazzi et al. 2010, Villeneuve et al. 1991). The orogeny is marked by two major unconformities, at the end of the Carboniferous and the end of the Permian, the latter observed as an angular unconformity in the Jeffara Basin around the TdM (Jabir et al. 2020, Bruna et al. 2019a, Raulin et al. 2011).

The TdM forms the only Permian exposed units in Tunisia and the only outcrop of marine upper Permian deposits in Africa, therefore providing an excellent area for analysing the formations and structure (Raulin et al. 2011, Kilani-Mazraoui et al. 1990). The Permian exposures form reef bioherms (fig.2.4) of which there are at least 3 sequences in the TdM (Zaafouri et al. 2017, Toomey 1991). These complexes are formed along slope breaks in the shallow marine environment where increasing base level encourages vertical carbonate growth (Zaafouri et al. 2017, Harris 1985). Well data suggests that the Permian units around the TdM are up to 4000m thick (Zaafouri et al. 2017, Raulin et al. 2011). In the SCB, well data suggests the Permian thickens to the north due to the effects of the Telemzane Arch during deposition (Bruna et al. 2019a, Bouaziz et al. 2014, Mejri et al. 2006).

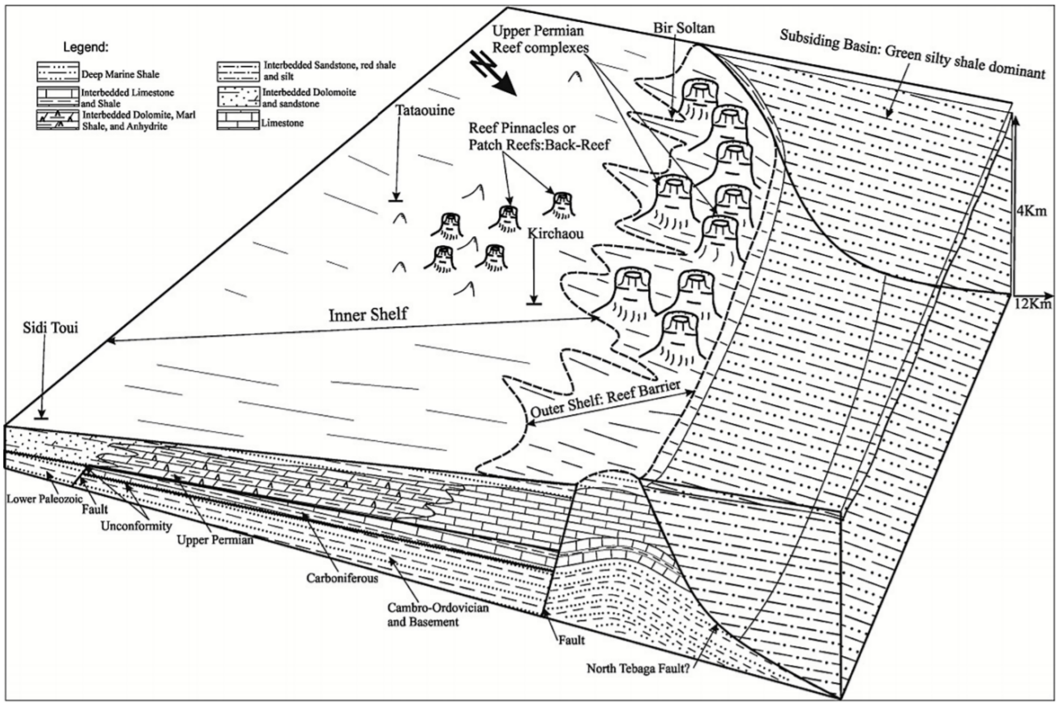

Figure 2.4: Late Permian carbonate platform and reef complexes (bioherms) reconstruction (Zaafouri et al. 2017)

In the Jeffara Basin, the basal Triassic units (TAGI) conformably overly the Permian carbonates and together form a major angular unconformity with the Cretaceous deposits. This is attributed to the final phase of the Hercynian Orogeny (Jabir et al. 2020, Raulin et al. 2011). The timing and mechanism of late Permian to early Jurassic structures around the TdM and the Jeffara Escarpment are controversial. The current accepted interpretation suggests block tilting along the main E-W faults during the early Triassic, although this interpretation will be discussed further in this thesis (Raulin et al. 2011, Bouaziz 1995, Busson 1972, Mathieu 1949).

South of the TdM, the Mesozoic stratigraphy (figs.2.5 & 2.6) of the Jeffara Basin is best observed and represents the mid Triassic to Cretaceous deposits. Mid-upper Triassic sand deposits outcrop in Jebel Rehach and Sidi Toui (east of the Jeffara Escarpment) into the basin. This area has been affected by strike slip movements along the main Jeffara Fault System, likely during sedimentation (Raulin et al. 2011, Bodin et al. 2010). The middle to late Mesozoic units dip gently towards the west (fig.2.5) along the escarpment and show minimal structural movements. They are predominately formed of carbonate and evaporitic deposits (fig.2.6) related to base level cyclic variation during these periods (Galeazzi et al. 2010, Lazzez et al. 2008). There are several unconformities in the upper Mesozoic deposits, namely Middle Albian Unconformity and Cimmerian Unconformity and are marked in seismic and well data from the SCB and outcrop analysis in the Jeffara Basin (Raulin et al. 2011, Bodin et al. 2010). These are attributed to the Austrian Orogeny (Bodin et al. 2010, Lazzez et al. 2008).

The effects of the Alpine phase (late Cretaceous) is observed in both basins by an unconformity and a period of non-deposition continued into the Pliocene, from which evaporite and mud deposits have continued to the present day (Galeazzi et al. 2010, Lazzez et al. 2008, Mejri et al. 2006).

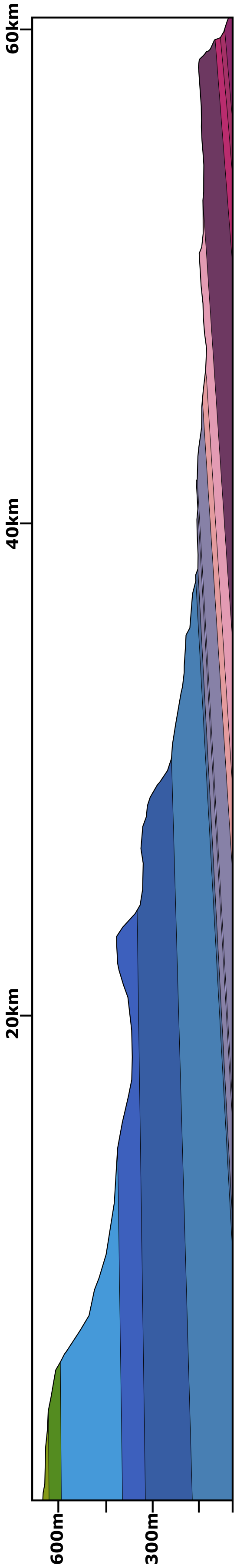

Figure 2.5: Section through the Jeffara Escarpment and Plain showing the Mesozoic deposits

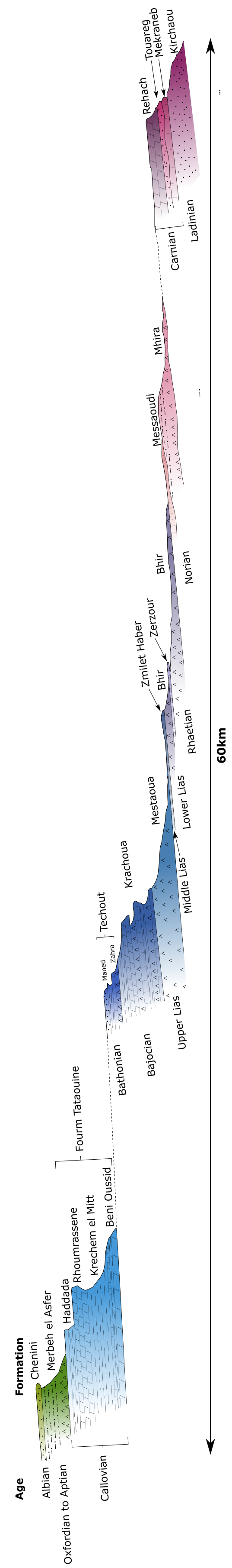

Figure 2.6: Stratigraphical section of the Mesozoic formations in the Jeffara Basin and Escarpment (adapted from Faycel Ferhi [ETAP Geologist])

3

Data Integration

This chapter presents the integration of different data types from various sources utilised in the project.

To be able to understand and make interpretations of the regional geology and the effects of fractures a number of different data sources are required. The main sources used in this research is as follows:

- Fieldwork and Outcrop Data
- Satellite Imagery
- Seismic Data
- Well Data

These data sources can be integrated into a number of processes for interpreting subsurface geology and fracture patterns both on the surface and predictions at depth. To do this several software packages are also utilised to improve the workflow and are as follows:

- ArcGIS - Data integration and visualisation, and aperture modelling
- Dynamic 3-Point Geological Plane Solver - Satellite dip calculator for cross sections
- FracPaQ - Matlab script for interpreting fractured pavements
- Midland Valley MOVE - Cross section analysis and DFN modelling
- OpendTECT - Seismic attribute analysis
- Petrel - Seismic interpretation and cross section analysis
- SKUA GOCAD - DFN modelling
- Techlog - Well Interpretation

3.1. Fieldwork

Fieldwork was undertaken for 14 days between November and December 2019 in collaboration with geologists from Mazarine Energy, ETAP and the National Office of Mines. Fieldwork aimed to collect a number of different data types to build cross-sections and to investigate fracture network characteristics. The fieldwork focused on outcrops (fig.3.1) around the Tebaga de Medenine and Djerba Rehach near Kirchaou.

The TdM area contains the only marine Permian outcrops in Africa and form topographic highs orientated E-W. The outcrops highlight the angular unconformity between the mid-late Mesozoic units and the Permian-early Triassic units. This made it a good exposure for investigating the nature and timing of the major unconformity and to make interpretations of the structure of the units. Bedding orientation and dip measurements were collected from this area and fracture data (type, orientation, pavement images) obtained from several stations along the Tebaga (see Appendix B.1).

Djerba Rehach (near Kirchaou) is a major Triassic and lower Jurassic outcrop to the south east of the Tebaga. Fracture data was obtained from several stations in this area (Triassic units) to compare with fractures observed in the TdM (see Appendix B.2).

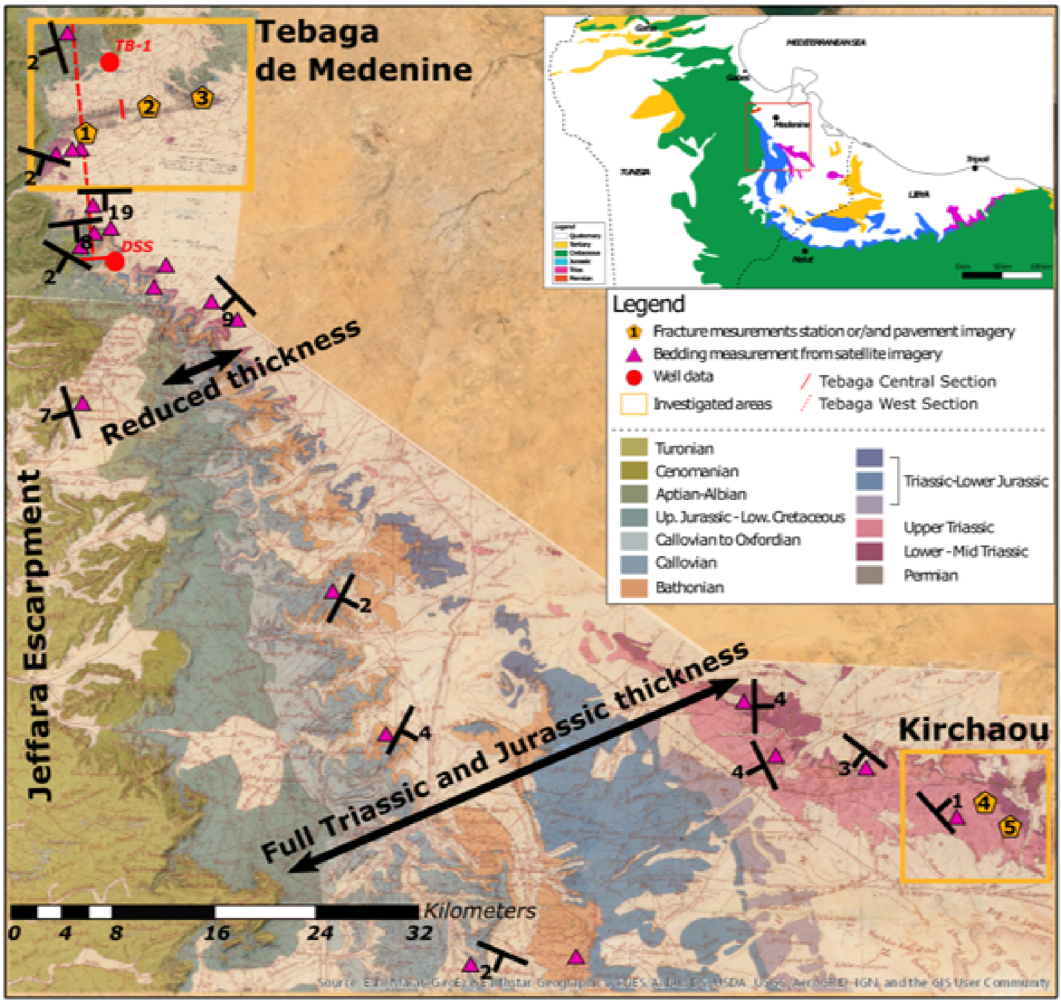

Figure 3.1: Geological map (Busson 1965) showing the locations of the fieldwork areas (orange boxes, see Appendix B) and satellite measurements. Wells from (Soua 2014, Mejri et al. 2006).

3.2. Satellite Analysis

Due to the low structural inclination of the mid-late Mesozoic units, obtaining reliable bedding measurements in the field is difficult. However, satellite data can be used to trace near horizontal lying beds to then measure the orientation and dip angle using the 3 point rule (see appendix D). This process is undertaken using the Dynamic 3-Point Geological Plane Solver developed using NASA World Wind 3 open source virtual globe application (see appendix D) which uses topographic satellite data to calculate bedding attitude Jamieson and Herman (2014).

Bedding data was obtained along the Jeffara Escarpment and Djerba Rehach (fig.3.1) in the Triassic, Jurassic and Cretaceous deposits. Two transects were also taken at stages from the Tebaga de Medenine.

3.3. Seismic Data

Seismic data provides valuable information for linking the surface to the subsurface. Several 2D seismic lines and a 3D cube (fig.3.2) are used to make regional interpretations and create cross-sections. Mazarine Energy provided a number of 2D seismic lines within their concession that were integrated into two large scale cross-sections (N-S [250km] and E-W [450km]). Further seismic images were obtained from previous studies in the region.

Both regional lines and horizon interpretations are corrected for Time-Depth using well tops to present more accurate subsurface interpretations.

A 3D seismic block was also provided by Mazarine Energy. This seismic data was used for extracting seismic attributes in fracture detection and characterisation. For this process, Petrel and OpendTect were utilised in calculating and analysing the fractures detected from the seismic attributes.

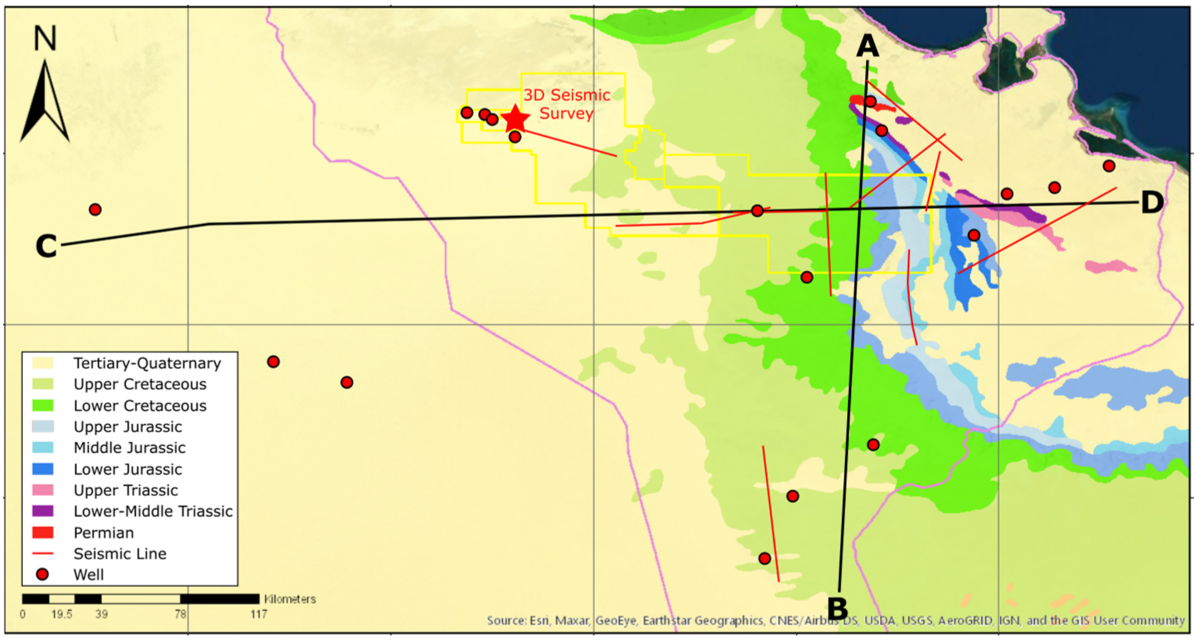

Figure 3.2: Regional geological map (Redfern et al. 2019) showing the seismic sections and wells used for the geological history analysis and fracture modelling. Regional cross-sections are shown (black lines)

3.4. Wells

Well data from the region (fig.3.2) was utilised from a number of sources in this project. A variety of data information (well location, horizon tops, petrophysical data etc.) was available dependent on the data source. Mazarine Energy provided full well data, including the well logs and Formation MicroImager (FMI) images for interpretation. The NARG database provides percentages of geological units for select wells from which horizon tops were calculated. Literature sources vary in quality, but provide good insights into the subsurface geology in both basins.

Data from literature were analysed with data from Mazarine Energy and NARG to understand the subsurface effectively. Most literature data came in the form of correlated logs and within regional cross-sections. These were then incorporated into the regional cross-sections presented in this report.

3.5. Gravity Data

Gravity data was used to locate the structural highs and lows in the region. Gravity and topography data is sourced from the open-access Nasa and CNES Topex/Poseidon Satellite with a resolution of 1.5km (global 1-minute grids) (NASA and CNES 2019, Sandwell and Smith 2009). Using the topography data, Bouguer gravity corrections were calculated using the sea level datum and a Bouguer reduction density of 2.67g/cm^2 was used (IAG 1967). Previous studies of the area have tested lower reduction densities for the sediments in the region, however it was found that these different densities only increased the magnitude of the of the anomalies and did not affect the overall appearance of the output (Gabtni et al. 2009). An area of 50,000km^2 covering the Jeffara Escarpment, SCB and the northern section of the Ghadames basin was analysed in ArcGIS to illustrate the anomalies present.

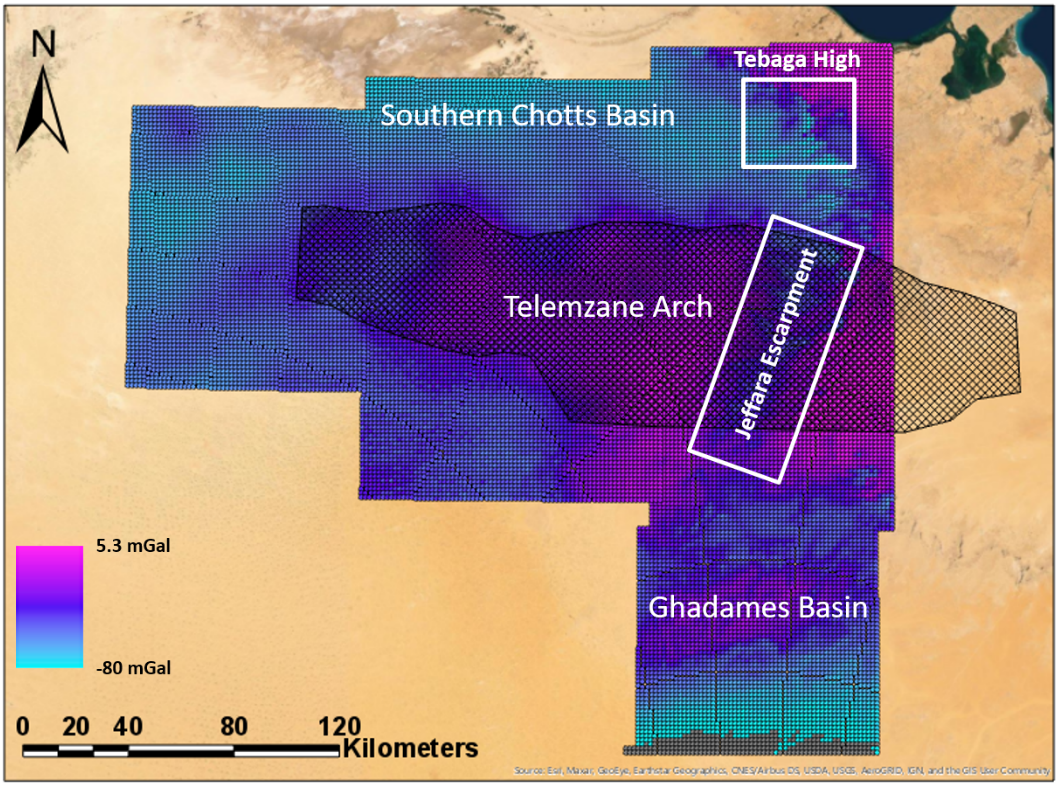

Figure 3.3: Bouguer Anomaly map of the region showing the main basins and highs. Tebaga High (TdM) and Jeffara Escarpment situated in white boxes

4

Multiscale shortening in the Tebaga de Medenine and Jeffara Basin

This chapter will discuss new interpretations of the Permian to Jurassic units in the Jeffara Basin. These are best observed in the TdM where the Permian outcrops. Through understanding this structure and the nature and timing of the Hercynian Unconformity conclusions can be made on the regional geological history of the Jeffara Basin.

4.1. Previous Interpretation of the Hercynian Unconformity and the Tebaga de Medenine

The Hercynian Orogeny (described in Chap.2) was a complex event with major vertical uplift phases at the end of the Carboniferous and end of the Permian (Soua 2014, and references therein). This makes interpreting the Hercynian Unconformity difficult in the geological record. Whilst Soua (2014) places this unconformity the end of the Permian in Tunisia (fig.4.1), many geologists attribute the end of the Hercynian phase in this region to the top Carboniferous (Raulin et al. 2011, Bouaziz 1995).

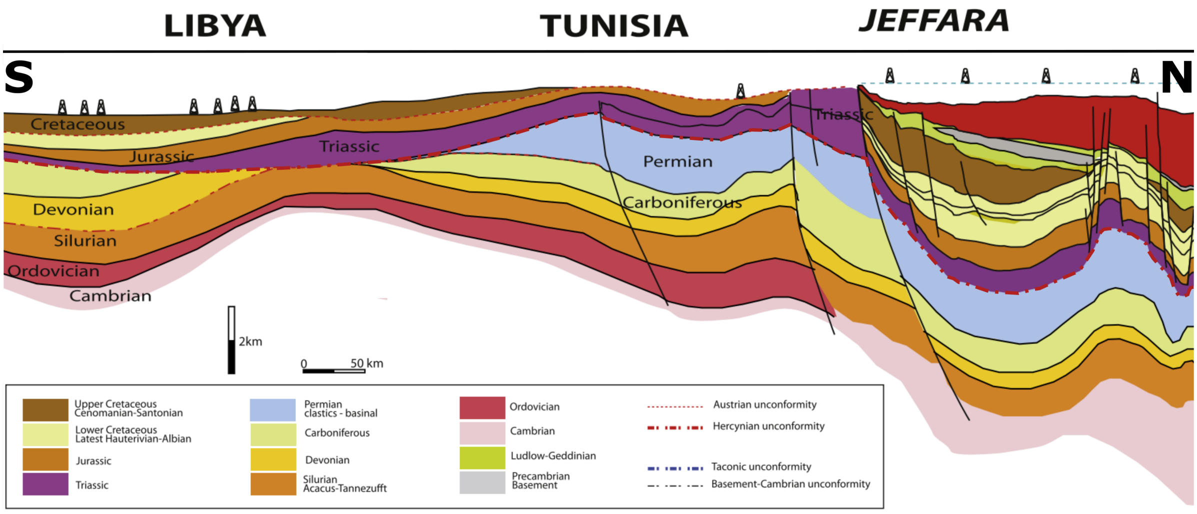

Figure 4.1: Cross section through the Jeffara Basin showing the Hercynian Unconformity at the top Permian (modified from (Soua 2014))

However outcropping at the TdM in the Jeffara Basin is a angular unconformity where the late Paleozoic units (Upper Permian) which are dipping 30°south, are overlain by near horizontal Mesozoic sediments. Several hypotheses have been presented over the last 80 years to explain the structure of the Permian deposits in the TdM and the significance it has on the geological history of Central Tunisia (Raulin et al. 2011, and references therein).

Mathieu (1949) first proposed that the tilted structure of the TdM was the result of shortening causing folding prior to the deposition of the middle Jurassic units. This interpretation was based on the presence of small reverse faults and folding along the TdM (Bouaziz 1995, Mathieu 1949). Transcurrent faults have been suggested more recently in relation to this event and is dated to late Triassic based on an unconformity within the Carnian units forming an asymmetrical anticline (Bouaziz et al. 2002, Bouaziz 1995).

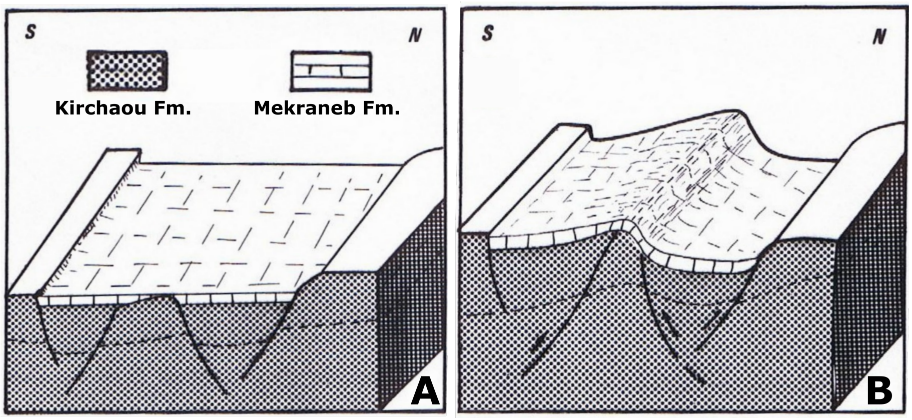

Figure 4.2: Modified interpretation by Bouaziz (1995) showing A. Ladinian. B. Ladinian to Lower Carnian the reverse faults which inherit previous extensional faults forming an asymmetrical anticline fold.

Similar ideas that point towards vertical uplifts during the middle Triassic creating a monocline (fold) structure causing onlap geometries (fig.4.3) of the Mesozoic units on the TdM have been suggested (Busson 1972).

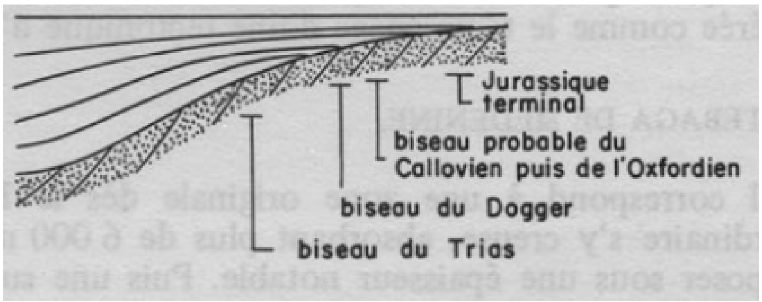

Figure 4.3: Interpretation by Busson (1972) showing the vertical uplift of the Permian with pinch out geometries of the Mesozoic units.

The current generally accepted interpretation suggests that the structure of the TdM is part of extensional block tilting (fig.4.4) from the late Triassic to early Jurassic (Raulin et al. 2011). Raulin et al. (2011) suggests that this large scale block tilting (fig.4.4) is controlled by inherited E-W trending major faults (Azizia Fault System) that were initially formed in the early Paleozoic. This fits the general continental scale mechanics occurring in the east Mediterranean and Atlas systems where rifting is taking place in the Neo and Apline Tethys (Frizon de Lamotte et al. 2011, and references therein). However, there is uncertainty in the subsurface interpretation of Raulin et al. (2011) due to the lack of seismic data (seen in fig.4.4) as this work is a synthesis field and well data only.

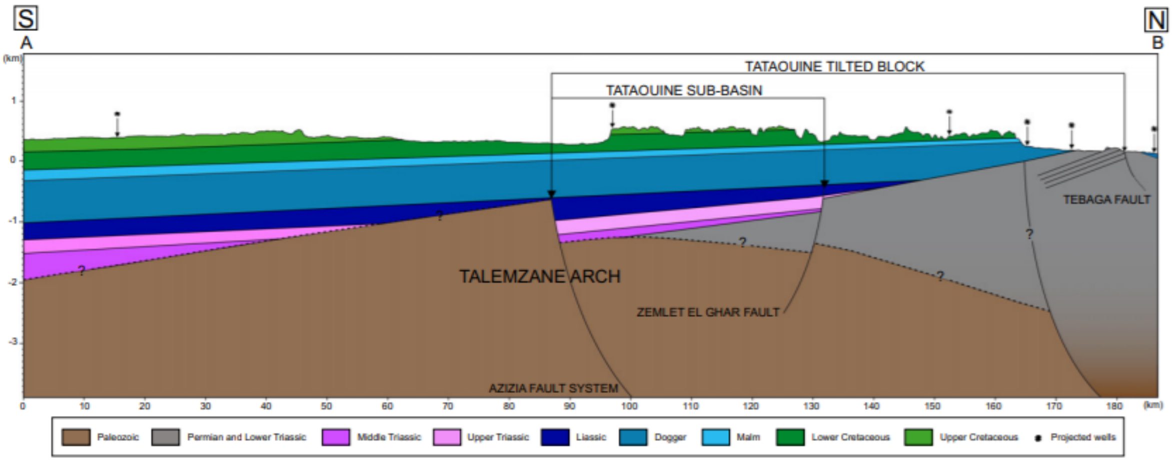

Figure 4.4: Cross-section interpretation from Raulin et al. (2011) using borehole, field and subsurface data showing the large scale block tilting in the Jeffara Basin.

At the scale of the TdM Raulin et al. (2011) also interprets the intensely brecciated Permian rocks to fracture corridors and damage zones around the normal faults (fig.4.5). This would require significant deformation and stress to cause the widespread fracture patterns as presented in figure 4.5, which is difficult to completely attribute to normal fault which accommodate much less deformation than folding for example (Fossen 2016). The interpretation also suggests that while folding is observed in the field, it is related to localised compression in the extensional blocks occurring on the hanging walls of normal faults (Roure et al. 1992).

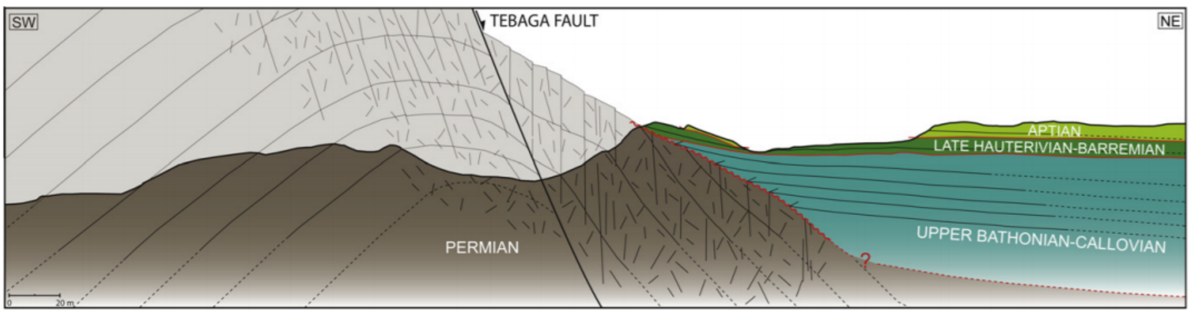

Figure 4.5: Interpretation by Raulin et al. (2011) showing the extensional faulting forming widespread fracturing and brecciating the Permian units in the TdM. The Jurassic sediments fill the drag syncline.

4.2. Shortening in the Tebaga de Medenine

The TdM is composed of Upper Permian shallow marine deposits and which form large E-W trending ridges. There are three main sectors studied in the TdM (fig.4.6): 1) Merbah Crouz (East), 2) Baten Beni Zid (Center), 3) Cheguimi (west). The general bedding along the Permian units in the TdM is a 30°dip to the south, which are observed along the main slopes of the Tebaga (fig.4.7). However, in depth analysis in the three sectors shows that the Permian bedding is dipping North and South up to near vertical in dip angle (fig.4.6). These bedding measurements line in a consistent N-S pattern indicating that the Permian units are folded with an fold axis of 091/7.

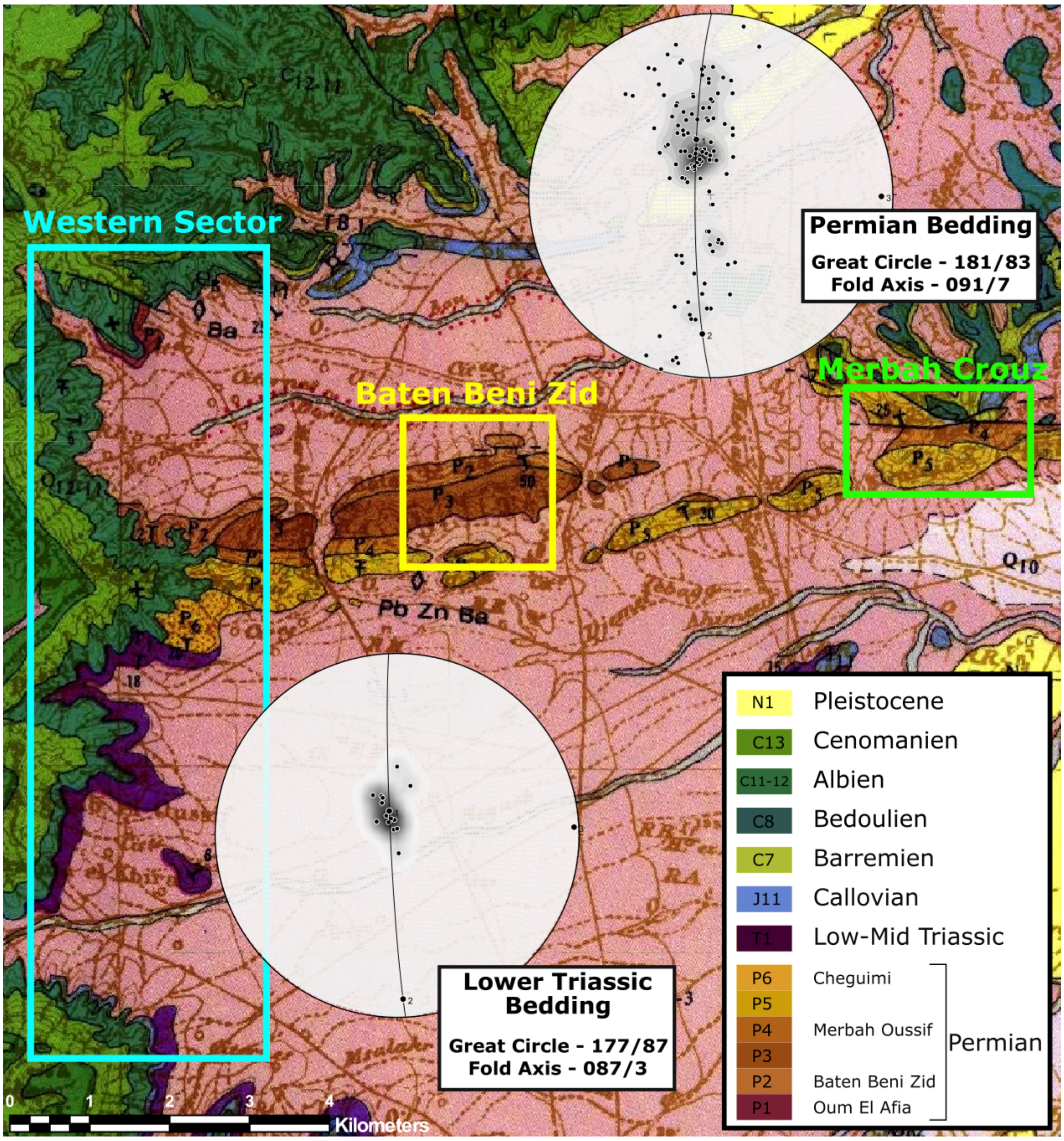

Figure 4.6: Map showing the three main sectors analysed in the TdM and the bedding stereoplots of the Permian and Lower Triassic.

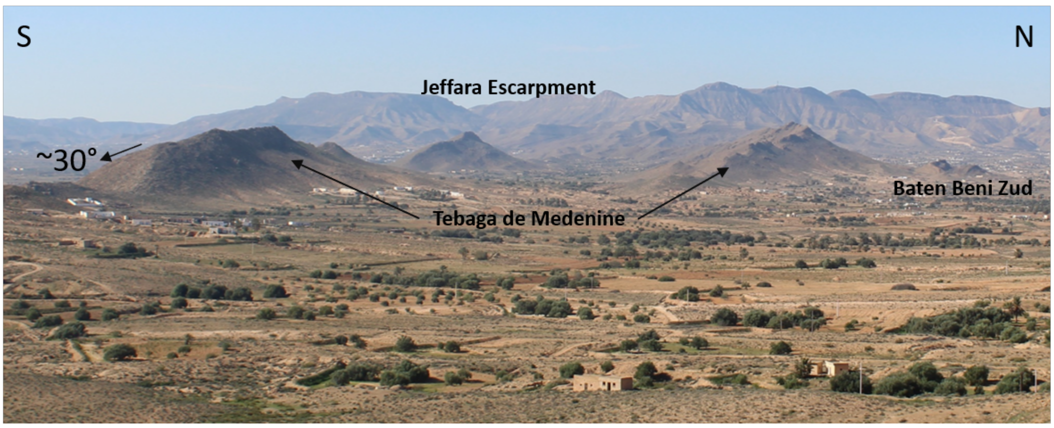

Figure 4.7: Panoramic view of the TdM (foreground) and the Jeffara Escarpment (background) taken from Merbah Crouz looking west.

In the BBZ there is evidence of fault-related folding (fig.4.8) occuring in the Permian units. The fault strike is E-W and show reverse movement (observed through the slickenlines on the fault planes). This configuration of folded bedding and reverse faults is found across the TdM in both Merbah Crouz and the western sector. In Merbah Crouz, a fault zone is also observed related to the reverse faulting which causes significant brecciation in the Permian units. In the western sector the folding and deformation is also found in the lower Triassic units which conformably overly the upper Permian. The configuration observed in the three sectors requires intense deformation and the reverse nature of the faults and folded beds suggests a N-S orientated shortening phase affecting the upper Permian and lower Triassic units.

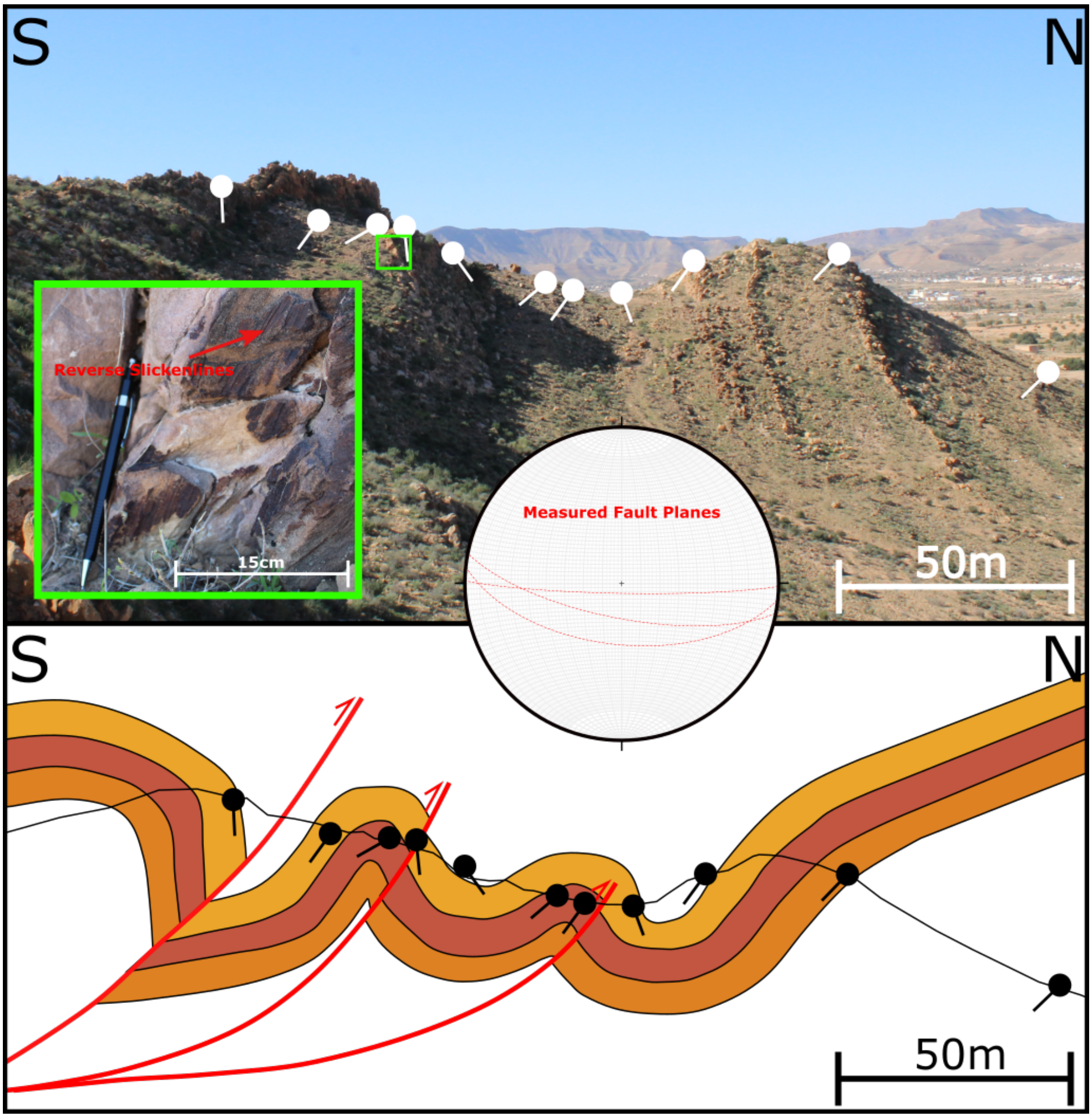

Figure 4.8: Section through the BBZ showing the fault related folding in the Permian units. Slickenlines were also observed showing reverse movement on the fault planes.

Overlying the Permian and lower Triassic units in the TdM is the Cretaceous forming an angular unconformity best observed in Cheguimi (west). The Cretaceous beds dip 4°to the west. The Jurassic is absent from the sequences in the western TdM and only outcrops to the north and south of the structure. This implies that the Jurassic has likely not deposited over the TdM.

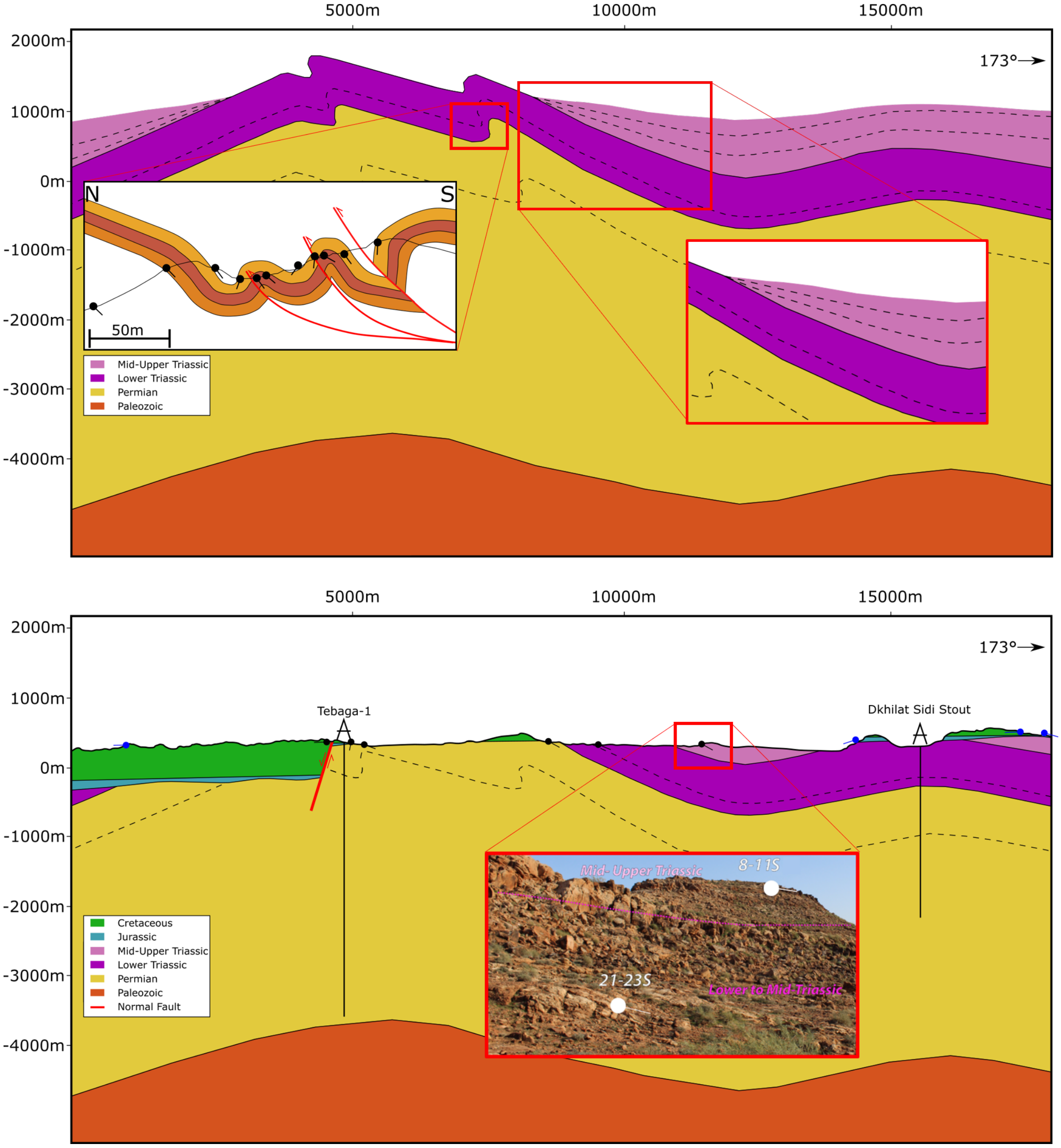

Figure 4.9: Western TdM section showing: Above) Situation during the middle Triassic around the TdM. Field image from BBZ showing fault-related folding. Middle Triassic units forming a wedge-like geometry onto the TdM. Below) Present day situation (black ticks - field measurements; blue ticks - satellite measurements). Field image from Hamaïma el Kbira

.

5km south of the TdM at Hamaïma el Kbira, the middle Triassic outcrops unconformably overlying the lower Triassic units. The orientation of the middle Triassic beds is southwards similar to the underying early Triassic, however the dip angle is shallower (8°). The nature of the shallower bedding away from the TdM suggests that the middle Triassic is forming a wedge unconformity onto the Tebaga. In addition to this, 10km south of the TdM, the middle Triassic units dip towards the north, implying these beds are gently folded. This indicates that the TdM composed of the upper Permian and lower Triassic formed a topographic high onto which the middle Triassic deposits. Furthermore, this high is still uplifting during the middle Triassic causing the wedge unconformity and gentle folding in these units (fig.4.9).

4.3. Regional Shortening in the Jeffara Basin

Further south away from the TdM along the Jeffara Escarpment, the main units observed are the middle-upper Triassic, lower Jurassic and Cretaceous. Satellite analysis shows there is an unconformity between the middle-upper Triassic and lower Jurassic. There is also an unconformity between the lower Jurassic and Cretaceous (fig.4.10).

The Triassic and Jurassic sequences increase in thickness to the south along the escarpment and thin towards the north where the TdM lies. As mentioned previously, the Jurassic does not outcrop at the western section of the TdM where there is the angular unconformity between the upper Permian and Cretaceous and only outcropping to the north and south of the structure. This indicates that the Jurassic did not deposit over the upper Permian and lower Triassic units in the TdM. Therefore the topographic high (Tebaga High) must have been present during the early Jurassic and possibly active to control deposition of the units and causing the wedge geometry onto the high and the thickness changes to the south.

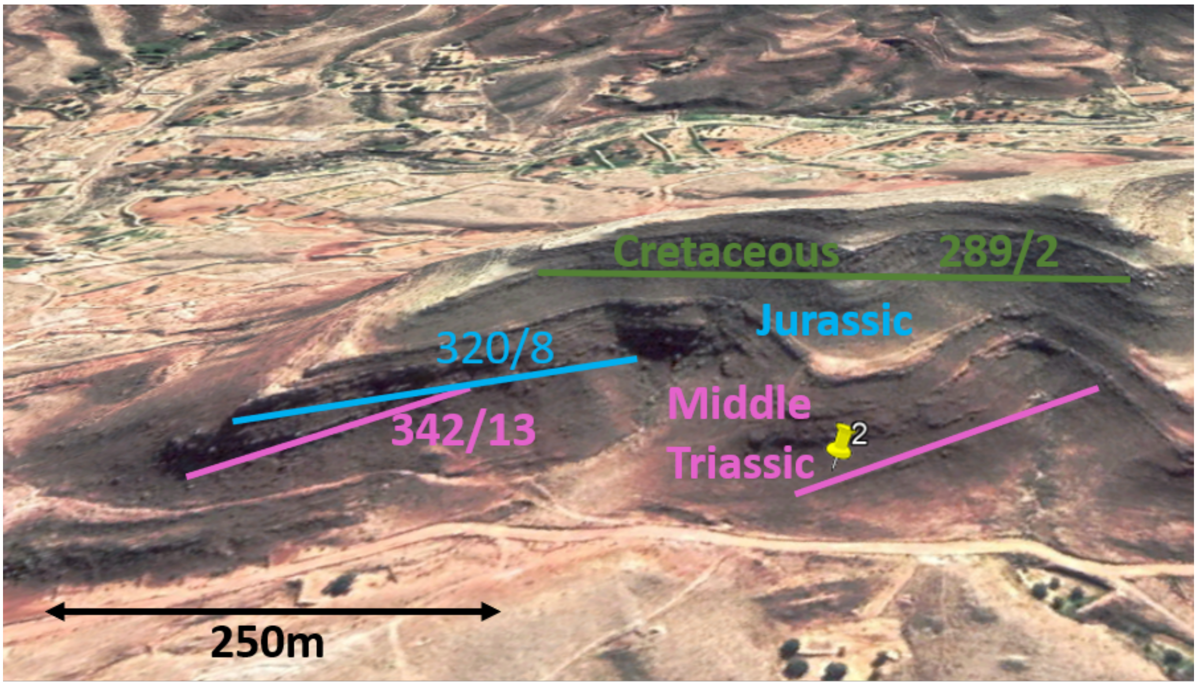

Figure 4.10: Satellite imagery showing a transect (facing south) through the Mesozoic units in the Jeffara Escarpment

Analysis of the Mesozoic beds along the escarpment show gentle folding in the middle-upper Triassic and lower Jurassic. This folding is in a similar orientation as the folding in the TdM, with the fold axis striking approximately E-W.

There is a variation in wavelengths in the folding between the Permian/lower Triassic, mid-upper Triassic and Jurassic (fig.4.11). Varying wavelengths are primarily associated with different thicknesses between the units (periodic folding) which is observed in the different folding of the Permian/lower Triassic and mid-upper Triassic (Fossen 2016). Away from the TdM along the escarpment, the Jurassic is thicker than the Triassic. The wavelengths of the folds show the lower Jurassic units have a longer wavelength compared with the middle-upper Triassic corresponding with the thickness variations. Furthermore, the longer wavelength of the lower Jurassic units could also correspond with a decrease in shortening intensity where this phase is culminating in the early Jurassic.

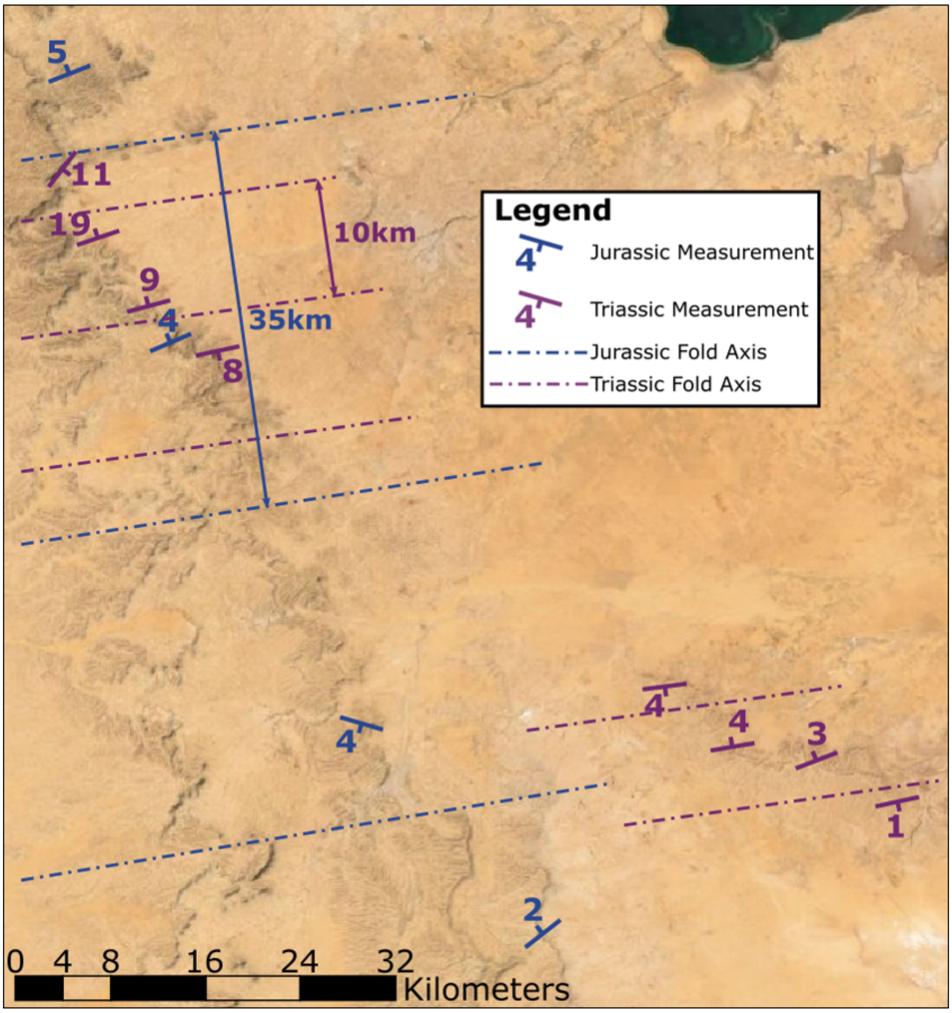

Figure 4.11: Interpreted fold axis for Triassic and Jurassic units showing the different wavelengths identified.

Regional interpretation from multiple data sources (outcrop, satellite, well and seismic) are incorporated into two large scale cross-sections. The N-S section (fig.4.12) covers the Jeffara and Ghadames Basin. It shows two major highs (Tebaga High and Telemzane Arch) which control the deposition of several units. The late Paleozoic and early Mesozoic units are folded in the TdM and thin towards the Telemzane Arch. This indicates that the Telemzane Arch is forming a prominent high and is active during the deposition of the late Paleozoic and early Mesozoic. This is also observed through the lack of the Permian deposits to the south of the arch in the Ghadames Basin. The Permian units form bioherm carbonates from which deposition will be controlled by basin dynamics, specifically topographic highs such as the Telemzane Arch. These deposition of these deposits is likely to be focused in certain parts of a basin and this can explain the absence to the south.

After the deposition of the Permian and lower Triassic units, an intense shortening phase initiated causing the folding and formation of the Tebaga High. In seismic from Zaafouri et al. (2017), the folding is also observed in the underlying Paleozoic units. This shortening continues through the Triassic into the early Jurassic causing gentle folding and wedge structures onto the high.

The E-W section (fig.4.13) provides an insight from the Jeffara Basin to the SCB. Gravity analysis shows towards the west, the Telemzane Arch is orientated WNW-ESE and whilst the Triassic and Jurassic thin towards the structure, it is a less prominent feature than in the east. In the east, the Triassic units increase substantially in thickness and a series of extensional faults are observed related to late Mesozoic extension in the region.

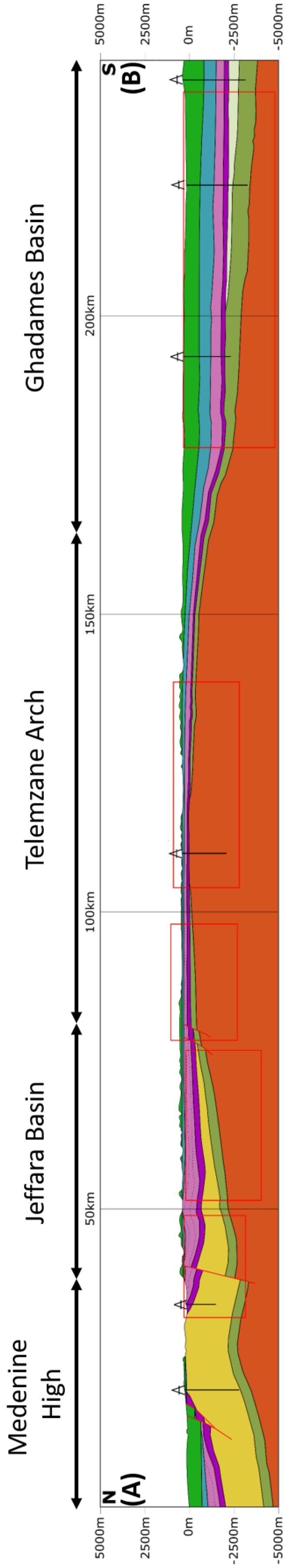

Figure 4.12: Seismic lines and wells interpreted in the N-S regional cross-section (see fig.3.2 for line of section). See figure 4.14 for legend.

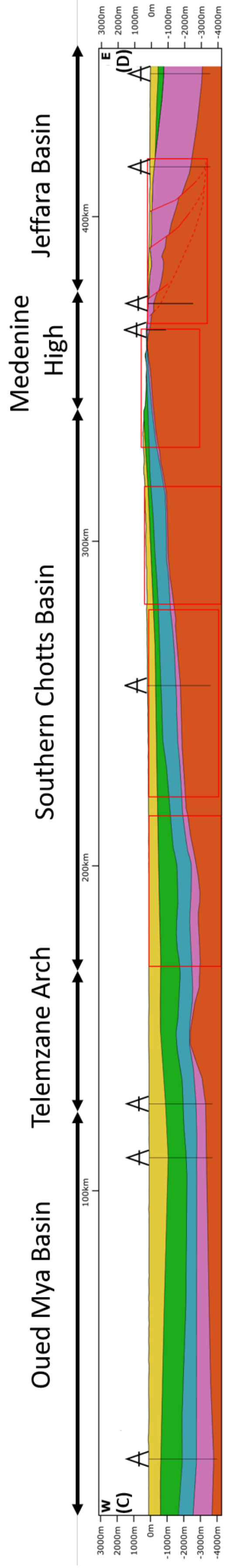

Figure 4.13: E-W section across the Southern Chotts Basin and the onshore Jeffara Basin (see fig.3.2 for line of section). See figure 4.14 for legend.

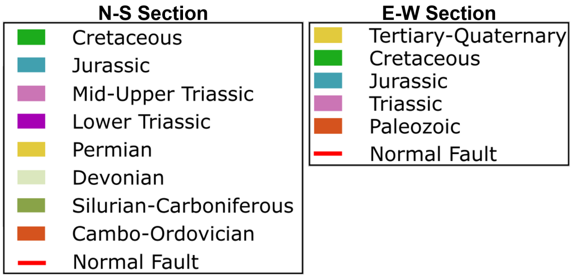

Figure 4.14: Geological legend for: Left) N-S Section (fig.4.12). Right) E-W Section (fig.4.13)

4.4. Implications of Shortening in the Regional Setting

4.4.1. Proposed Late Hercynian Shortening Phase

The evidence from the TdM and the Jeffara Basin indicate that a shortening phase occurred in the region affecting the Paleozoic and Mesozoic units. This shortening phase is represented in a series of N-S sections presented in figure 4.16.

The Telemzane Arch forms a prominent high during the Carboniferous. The arch continues to be active into the Permian causing the thinning of the Permian units towards the structure and the absence of deposition of the Permian in the Ghadames basin to the south (fig.4.16A). A phase of shortening is initiated by the end of the Permian and intensifying during the middle Triassic. This causes large scale folding in the region and also fault-related folds in the TdM. The folding creates a topographic high (Tebaga High) which, whilst active causes the wedge geometry of the middle-upper Triassic deposits onto the flanks (fig.4.16B). This shortening phase culminates by the early Jurassic where gentle folds are observed in the lower Jurassic units. The TdM is still a prominent topographic high in this period causing thickness variations and preventing the Jurassic from depositing over the Tebaga (fig.4.16C). Post shortening, the Cretaceous deposits over the underlying late Paleozoic and early Mesozoic units and a period of extension causes normal faulting in the region which is observed in the present day situation (fig.4.16D).

There are 4 unconformities represented in these scenarios (fig.4.15). 1) Main Hercynian Unconformity, 2) Late Hercynian Unconformity, 3) Base mid Jurassic, 4) Late Jurassic. The unconformity at the base middle Triassic marks the major shortening phase which forms the Tebaga High onto which the mid-upper Triassic units deposit onto. This is one of the two major Hercynian Unconformities, the other situated at the base Permian which marks the uplift of the Telemzane Arch.

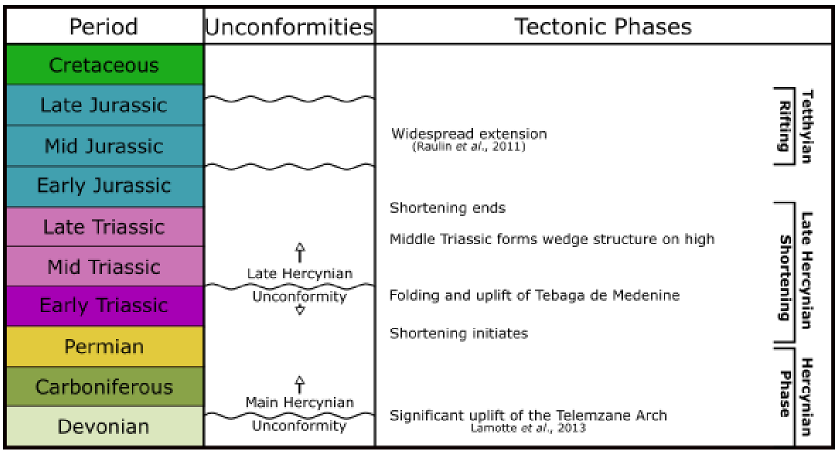

Figure 4.15: Tectonic history of the Jeffara basin, showing the four main unconformities identified

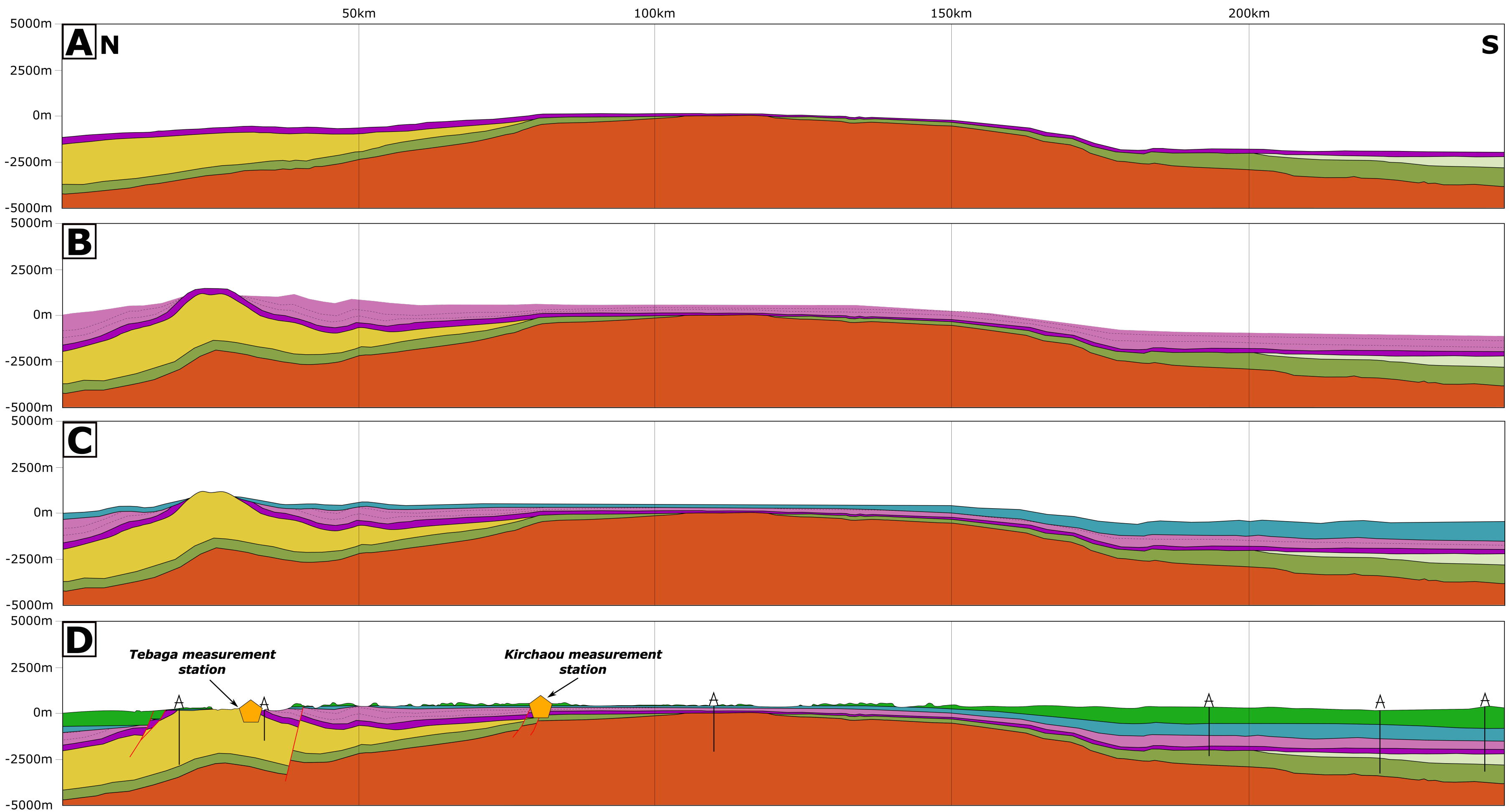

Figure 4.16: Regional NS cross-section (263 km) through the Tebaga de Medenine and the Telemzane Arch down to the Ghadames Basin. A) to D) is a reconstruction of the structural events occurring in the area of interest. A) Situation at the time of deposition of the Lower Triassic. The Permian deposits are controlled by the presence of the Telemzane Arch. B) Situation at the end of the Upper Triassic. At that time the Tebaga was a prominent structure (active) and the Mid- to Upper Triassic is pinching out on its flanks. C) Situation during the Jurassic. The Tebaga de Medenine is achieving its activity and variations of thickness are still visible. D) Present-day situation and marked with the measurement stations we investigated during fieldwork.

4.4.2. Tebaga High in the Southern Chotts Basin

The regional nature of the shortening phase which affected the TdM means this structure should observed in large scale. Work undertaken on 2D seismic in the SCB to the west of the Jeffara Basin shows the upper Permian displaying and E-W trending positive topographic anomaly at depth indicating a topographic high is present (Bruna et al. 2019a). This is important as this can link with the TdM extending the Tebaga High westwards. Furthermore, previous research indicates that this structure can also be related to the ”Matmata Arch” (Ferjani et al. 1990) which is direct extension of the Tebaga High westwards. This structure is observed to cause thinning of middle Triassic onto the topographic high and a significant high in both basins (fig.4.17). This establishes a link between the surface geology in the Jeffara Basin and the subsurface of the SCB.

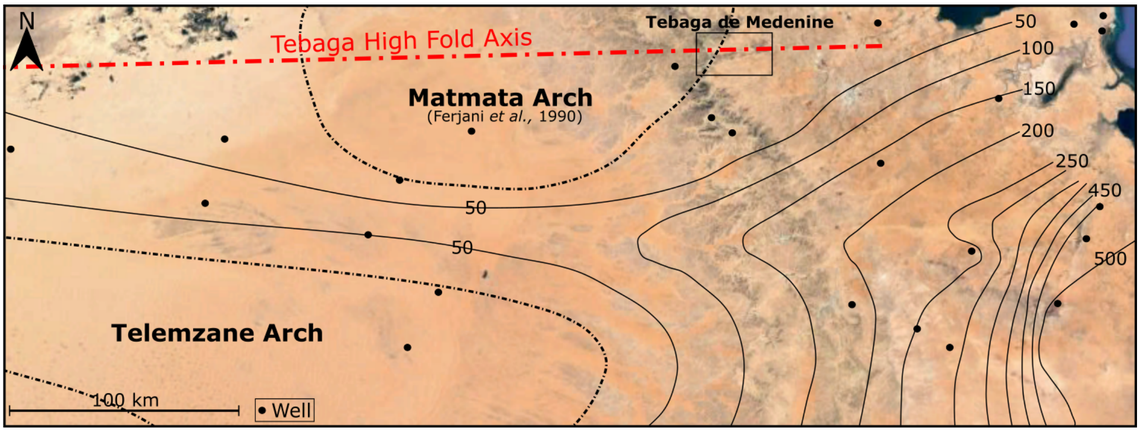

Figure 4.17: Isopach map of the Middle Triassic showing thinning towards the Matmata Arch (part of the Tebaga High fold axis). Modified after Ferjani et al. (1990).

4.4.3. Integration into Regional Dynamics

It is important to link the shortening phase observed across the Jeffara Basin into the wider geological context at regional and tectonic scale. The Hercynian Orogeny is known to culminate in the late Carboniferous across Northern Africa which formed the large E-W anticlines such as the Telemzane Arch (Bodin et al. 2010, Galeazzi et al. 2010, Boote et al. 1998). These anticlines are exposed and eroded during the Permian allowing for the Permian to onlap the Carboniferous (fig.4.16A), constrained through seismic analysis. The period of shortening that occurs during the Permian and Triassic is related to a late Hercynian Phase which interacts with the E-W anticlines. This phase is active during the late Permian and early Triassic forming the TdM and culminating by the latest early Jurassic. This provides a link between the major Hercynian events of the Carboniferous and Permian and the extensional Tethys events that occur from the Jurassic (Mejri et al. 2006). Raulin et al. (2011) and others suggest the Triassic and Jurassic deposits in the Jeffara Basin are linked to extension in the Neo-Tethys Ocean (Ionian Basin) to the north. However it is conceded that major basin extension and development does not occur until the mid-late Jurassic (Callovian) (Raulin et al. 2011, Keeley 1994, Garfunkel and Derin 1984). The proposed shortening phase in Central and Southern Tunisia is unlikely to have a significant relationship to the Neo-Tethys opening to the north and occurs prior to the major extension in the Jurassic. Therefore, a late Hercynian shortening event is plausible in the time frame between the Permian and middle-late Triassic which is followed by a major rifting (Tethys opening and the breakup of Pangea) event as described in literature during the mid-late Jurassic and Cretaceous (Jabir et al. 2020, Gharbi et al. 2020, Raulin et al. 2011, and references therein).

5

Characterisation of fractures in the Jeffara and Southern Chotts Basins

Linking the deformation described in Chapter 4 to the fracture networks plays an important role in reservoir characterisation and development of the fields. Fractures can both aid and hinder fluid flow in the reservoir and play key roles in how the industry extracts hydrocarbons. It is therefore useful to understand what the aspect of the fractures are at depth and the contribution of these to overall reservoir flow. This chapter will focus on characterising the fractures present in the Jeffara Basin (surface fractures) and the SCB (subsurface fractures) through several data sources (fieldwork, well and seismic). The results of which will be integrated in the fracture modelling in chapter 6.

5.1. Fractures and Fracture Drivers

Fractures are mechanical discontinuities within rock units affecting the permeability and subsurface flow patterns in either a positive or negative way (Bisdom et al. 2016b, Narr et al. 2006, Nelson 2001). Open fractures can act as natural pathways for hydrocarbons improving flow patterns in low permeable rocks (e.g. Paleozoic reservoirs in the SCB) whereas closed fractures can hinder these pathways impacting on production (Bisdom et al. 2016b, Zeeb et al. 2013, Nelson 2001).

A combination of several techniques is required to effectively model fracture networks and flow pathways in the subsurface. The seismic (attributes) and well (FMI logs) data are useful tools to gauge the subsurface fracture patterns however there are significant limitations when solely relying on these data sources. The resolution of seismic data limits the amount of data that can be derived while data derived from wells are too spatially sparse causing greater uncertainty to modelling and prediction. Surface data from field analogues can provide additional detail on the fracture networks (e.g. fracture orientations, length and density). However, it is not always straightforward to make direct comparisons between the surface analogues and the subsurface as process such as diagenesis, PT variation and exhumation can cause misinterpretations of the fractures (Bruna et al. 2019c, Li et al. 2018). Therefore whilst it is useful to integrate outcrop analogues with the subsurface to data when characterising and modelling fractures, care must also be taken when evaluating the fracture data.

It is important to understand the uncertainties involved with surface to subsurface fracture characterisation as in-situ regional stresses can also play a role in the fracture networks at depth (Bisdom et al. 2016b, Gale et al. 2014, Amadei et al. 1987). The most useful method of integrating this data is determining the fracture drivers (faults and folds) through field analogues which are then used to predict the fracture sets in the subsurface.

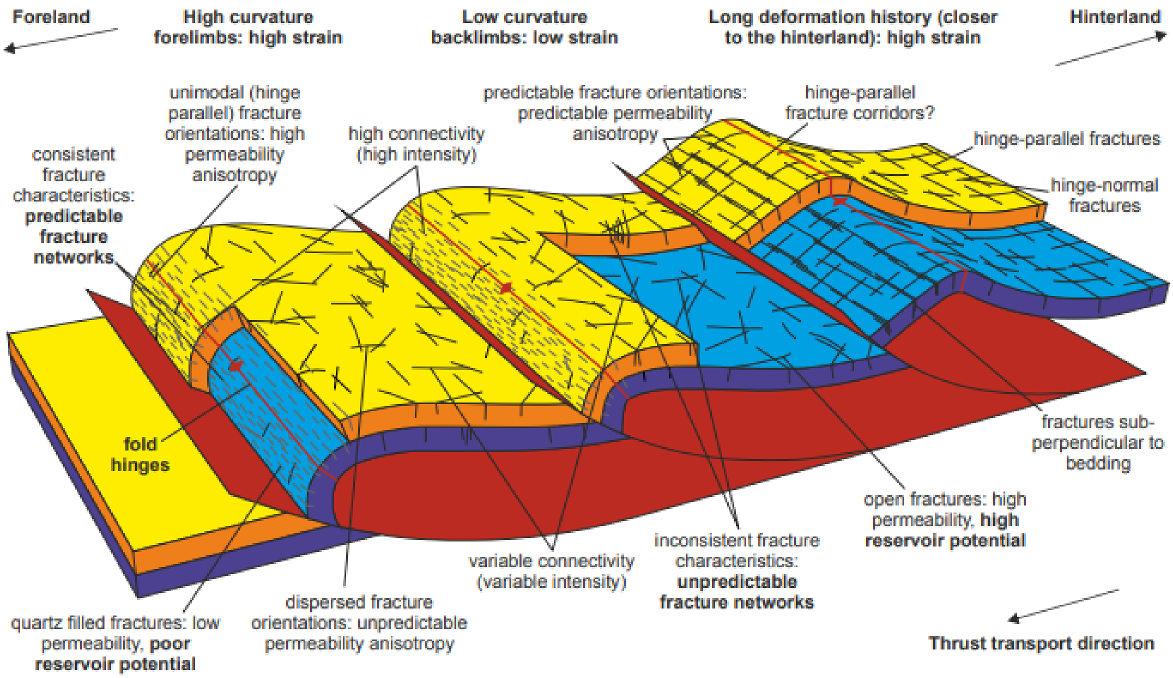

Figure 5.1: 3D diagram showing fractures formed due to fold and fault drivers (Watkins et al. 2018)

Faults can influence the regional stress regimes, causing the development of fractures along the fault and around propagating faults where there is a variation in high and low stress (Bisdom 2016, Blenkinsop 2008, Hilley et al. 2001). This driver causes localised fracturing.

Folding is another main driver in the development of fractures and can be an important factor in forming large scale fracture networks (Watkins et al. 2018, Cosgrove 2015). Figure 5.1 shows the variety of fractures that can occur in shortening system and the likely density of the networks (Watkins et al. 2018).

While faults and folds are the main drivers for fractures in the subsurface other drivers may also affect fracture development. Burial-related fractures form though the increase of stress through deepening burial and thickening of overburden (Bisdom 2016). Far-field stresses can also cause fractures through movements on tectonic plate scale and these fractures are useful when linking local geology to the regional scale events (Bisdom et al. 2016b, Bisdom 2016, Ishii 2016, Rohde 1986).

Through understanding which drivers or what combination of drivers are involved in the formation of fractures, which relates to the geological history (see Chp.4), predictions can be made on the nature of the fractures and networks in the subsurface and this can be used in the modelling of the fracture networks within the reservoirs.

5.2. Surface Fracture Characterisation in the Jeffara Basin

Surface characterisation in the Jeffara Basin was carried out through the fieldwork mission in Nov 2019. Several fracture stations and pavements were observed in the TdM (Permian) and Kirchaou (Triassic). Fracture stations were areas where fracture measurements were taken whilst pavements were areas where image scans were acquired using a selfie stick. Pavement images were interpreted and analysed through the open-source software FracPaQ (Healy et al. 2017).

5.2.1. Fracture Stations and Pavements

Fracture Station Data

There were 5 main fracture stations (fig.3.1) where fracture data was collected from the Permian and Triassic units. These fracture stations provided a good insight into the orientations of the main fracture sets within these units that could be implemented into the fracture modelling. In the TdM, several fracture sets were observed and unfolded to correct for bedding attitude.

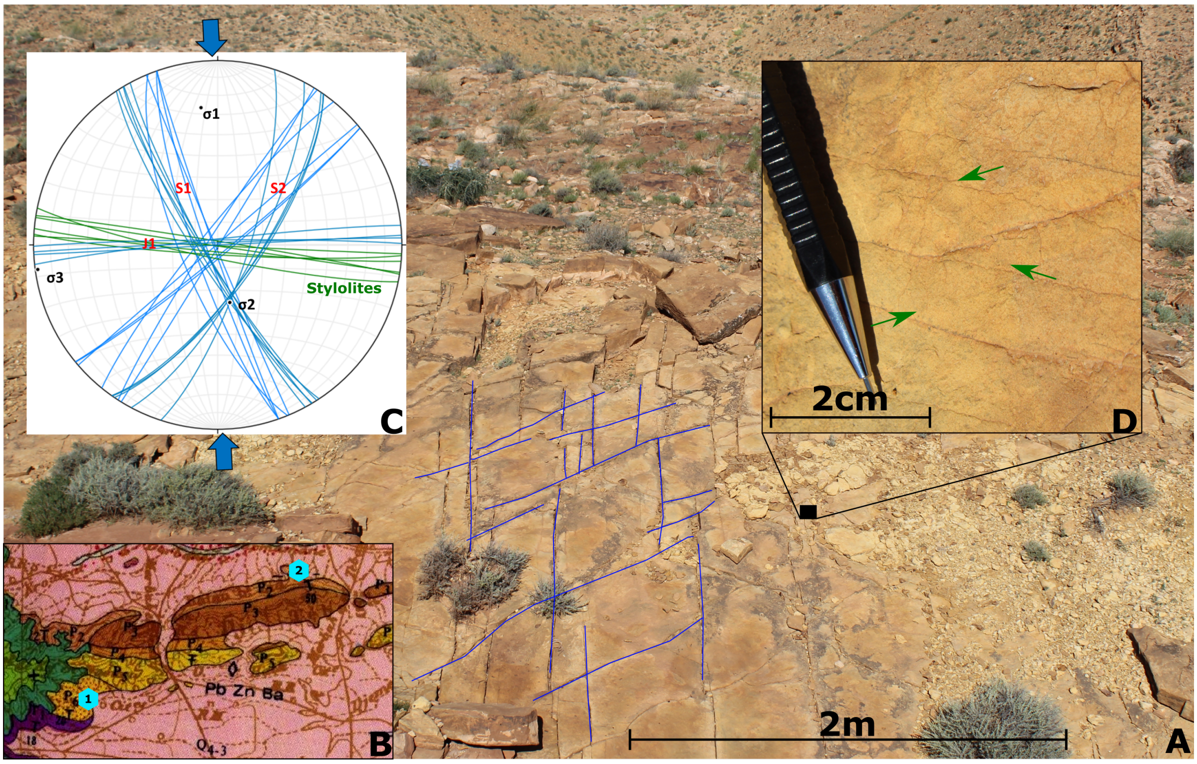

Figure 5.2: A. Fracture Station 1 showing the interpreted fractures. B. Location of fracture station in the TdM. C. Stereonet showing the interpreted fractures at the station (blue - joints, green - stylolites). D. Stylolites identified in the rock that indicate a principle horizontal stress in the N-S direction.

Conjugate fractures (S1 and S2) observed in TdM can be used to show the principle stresses acting on the rocks (fig.5.2 A). These fractures form during shortening with the acute angle (60°) indicating the principle (horizontal) stress direction. In the TdM this direction is N-S (fig.5.2 C). This set of fractures are observed throughout the TdM. This is important in relating these sets in a distributed fracture network system. It is likely that during Layer Parallel Shortening (LPS) these fractures begin to form throughout the region, thus becoming a major fracture set in the system.

Tectonic stylolites were also located across the TdM (fig.5.2) within the carbonate layers. A compressional $\sigma 1$ can also be measured from these features providing the main principle stress. The stylolites strike E-W with the peaks orientated N-S corroborating with the ($\sigma 1$) orientation of the conjugate fractures. The stylolites also imply there is dissolution occurring in the units. This could be a source of the calcite that is then deposited in the fractures found elsewhere, which could have implications on the flow capacity in the network. However, it is also suggested that stylolites can be drains in the reservoir due to the high connectivity and this could be a consideration (Bruna et al. 2019b).

An additional two fracture sets (fig.5.3) were observed in the Baten Beni Zid area (BBZ) of the TdM. These sets were perpendicular to one another. At the BBZ these fractures are mainly orientated in a N-S and E-W striking pattern. However, compared with the conjugate sets of fractures, these sets were localised to the BBZ and were not distributed throughout the TdM. These could be related to the intense deformation occuring in this location which is amplifed by several small faults in the area (fig.4.8). Due to the isolated nature of these fractures in the BBZ they are unlikely to form a major fracture set at depth and be part of the distributed fracture system.

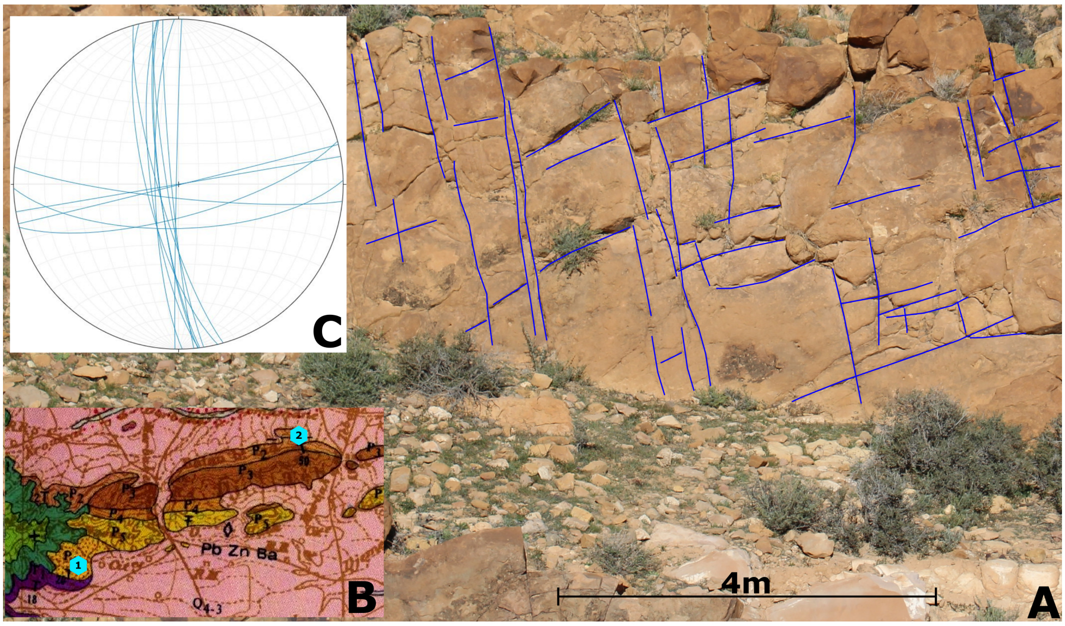

Figure 5.3: A. Fracture station 2 located in the BBZ showing interpreted fractures. B. Location of station. C. Steronet showing the interpreted fractures at the station.

In Kirchaou, conjugate fracture systems are present in the Triassic units indicating horizontal maximum stress in the N-S direction. These fractures were infilled with calcite which could indicate that sealed fractures also occur at depth. Also observed in these units are echelon and horsetail fractures (fig.5.4) which are commonly associated with shear movement in this case showing dextral movement. The shear fractures in Kirchaou show more localised deformation likely related to nearby strike-slip faulting. This faulting occurred during the extensional tectonics experienced in the basin in the late Mesozoic after the major shortening event.

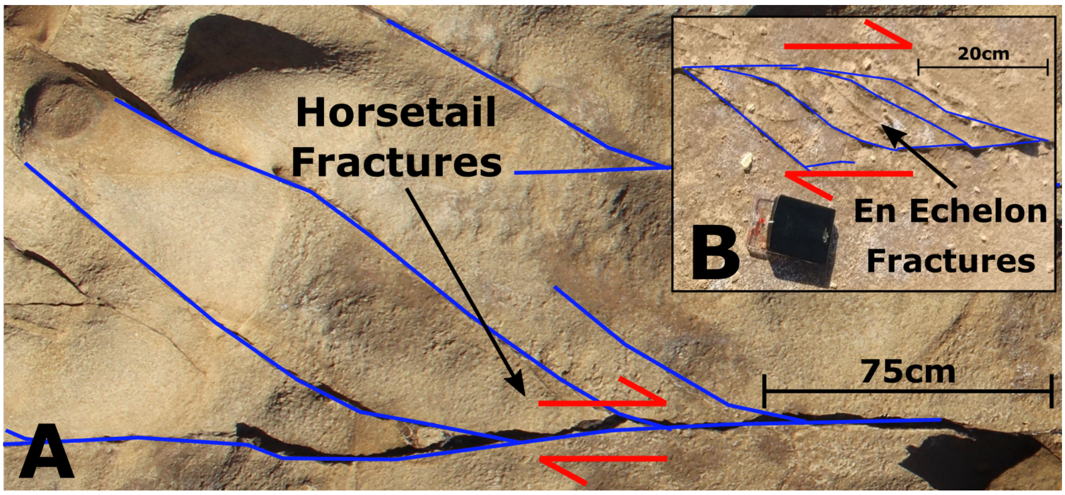

Figure 5.4: Dextral shear fractures observed in Kirchaou. A. Horsetail fractures. B. En Echelon fractures.

Fracture Pavement Analysis

Five pavements (fig.3.1) were imaged in the field. Pavements 1, 4 and 5 were interpreted (fig.5.5) and analysed through FracPaQ and show the array of fractures in the Permian and Triassic units in the Jeffara Basin. The pavements vary in size from $172m^2$ to $2000m^2$ however all provide detail into the fractures present in the units. Pavement analysis allows for additional features (intensity (P21), spacing etc) of the surface fracture networks to be assessed and interpreted which are incorporated into the modelling stage.

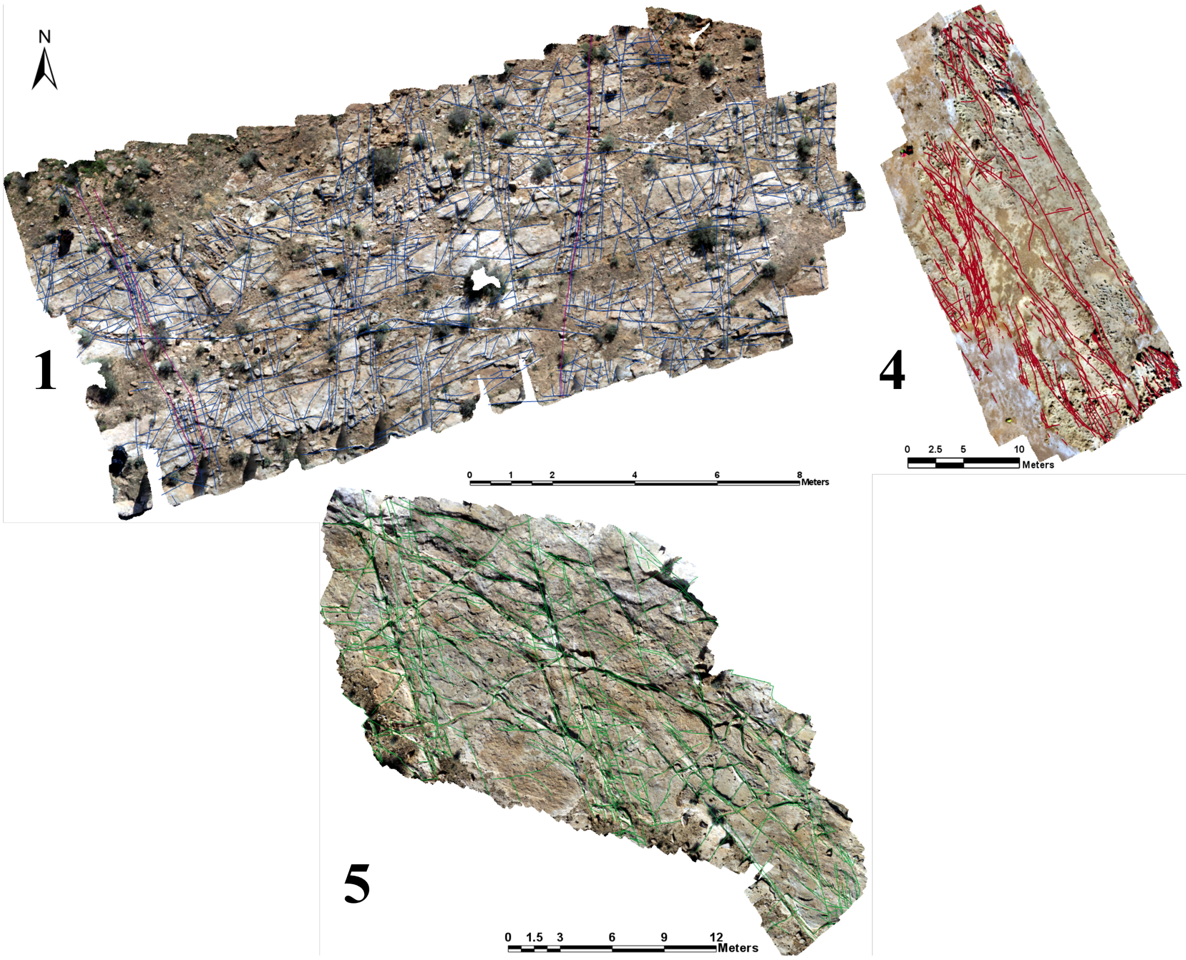

Figure 5.5: Fracture pavement interpretations. Location of pavements in figure 3.1

Pavement 1, located on the western sector of the TdM. This pavement contained conjugate fractures and karst related fractures. Pavements 4 and 5 are located in Kirchaou within the Triassic sandstone units. These pavements present conjugate sets of fractures along with interesting shear fractures such as echelon and horsetail fractures (fig.5.4). These fractures show orientations (fig.5.6 A-C) predominately in N-S, NW-SE and NE-SW directions. These pavements (rose diagrams) show slight variation from the main conjugate system, this is likely due to some rotation related to the faulting nearby associated with the Jeffara Fault System.

Areal fracture intensity (P21) is calculated from the pavements. This is an important characteristic of fractured pavements and provides a measurement for the amount of fractures in a certain area. The pavement P21 output (fig.5.6 D-F) indicates that whilst there is a variability in the fracture intensity at the scale of pavements (10's meters), P21 values are approximately around 0.25-0.45m/m^2. The variability in the output creates some uncertainty in the result but provides a good initial estimate of fracture intensity which is an input in modelling.

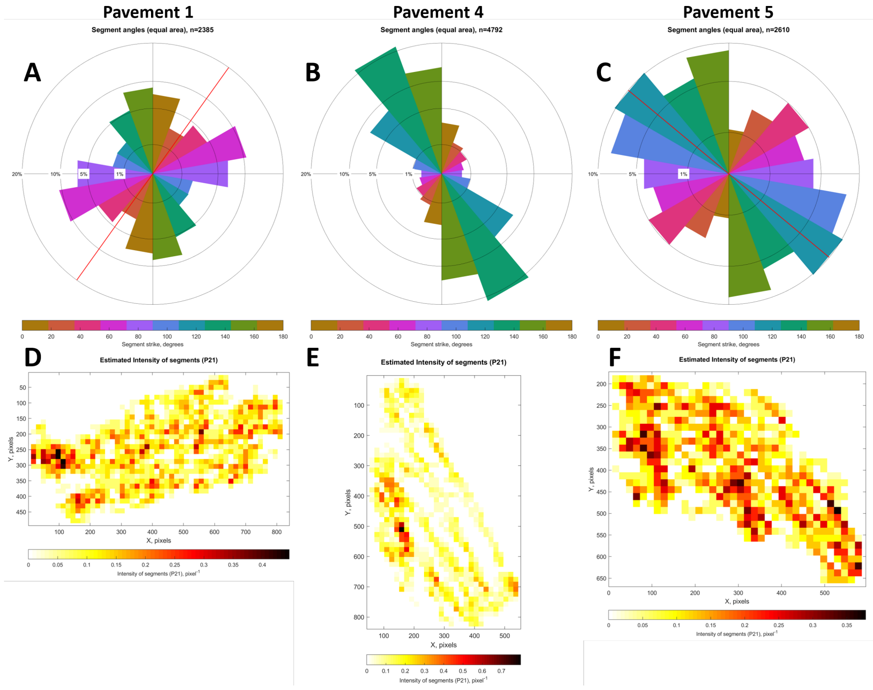

Figure 5.6: A-C. Rose diagrams showing the orientations of the interpreted fractures on each pavement. D-F. Calculated P21 fracture intensity of each pavement.

5.3. Structural Link between the Jeffara and Southern Chotts Basins

In order to understand the fractures in the subsurface reservoirs of the Southern Chotts Basin, it is important to define the structural link between the SCB and the Jeffara Basin. The data fro the surface provides the main fracture driver characteristics of the fractures in the Permian and early Triassic units of the Jeffara Basin. This main driver is regional shortening culminating in the formation of large scale open folds. This folding forms the conjugate fractures with the N-S orientated σ_1 and the stylolites. These are distributed throughout the folding system as the fracture sets were observed in multiple locations along the folds (fig.5.7).

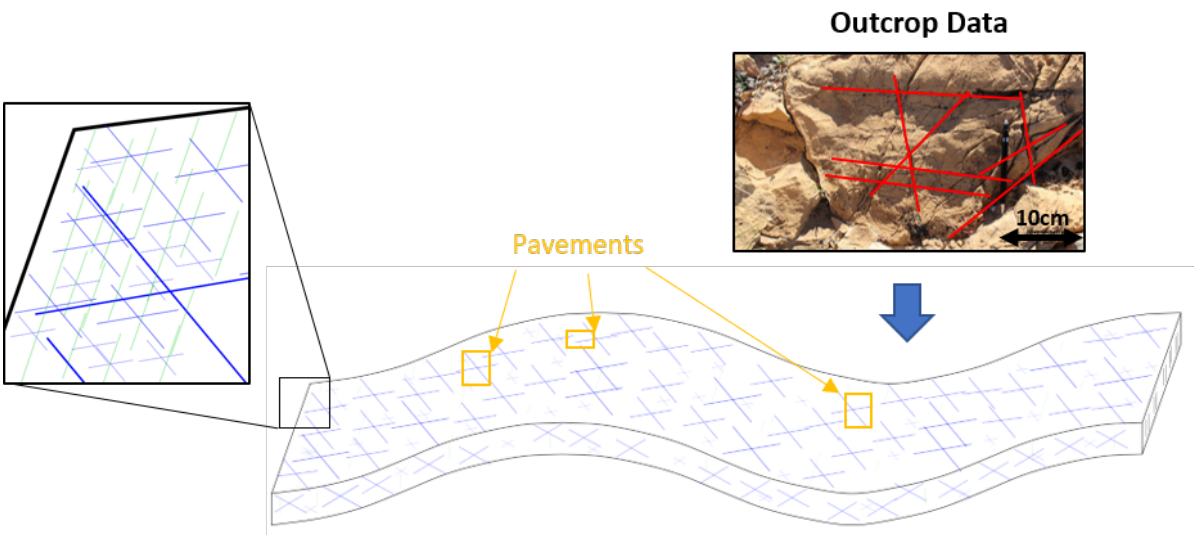

Figure 5.7: Schematic model indicating the main distributed fracture sets in the open fold system from outcrop analysis

This regional shortening can be interpreted to the SCB through the Tebaga fold axis. This fold axis trends E-W and extends into the SCB at least 150km (fig.5.8) and corresponds with the subsurface topographic high, the Matmata Arch (Ferjani et al. 1990). Further to the west in the SCB a high is also observed through palinspastic restorations (Bruna et al. 2019a).

The late Hercynian regional shortening event that has affected the Permian and Triassic units in the Jeffara Basin affects the same units in the SCB through the Tebaga fold. Therefore it is predicted that the open fold fracture sets presented in the schematic model (fig.5.7) will be also be observed in the earlier Paleozoic units, underlying the Permian, at depth in the SCB such as the El Hamra and El Atchane Ordovician reservoir units.

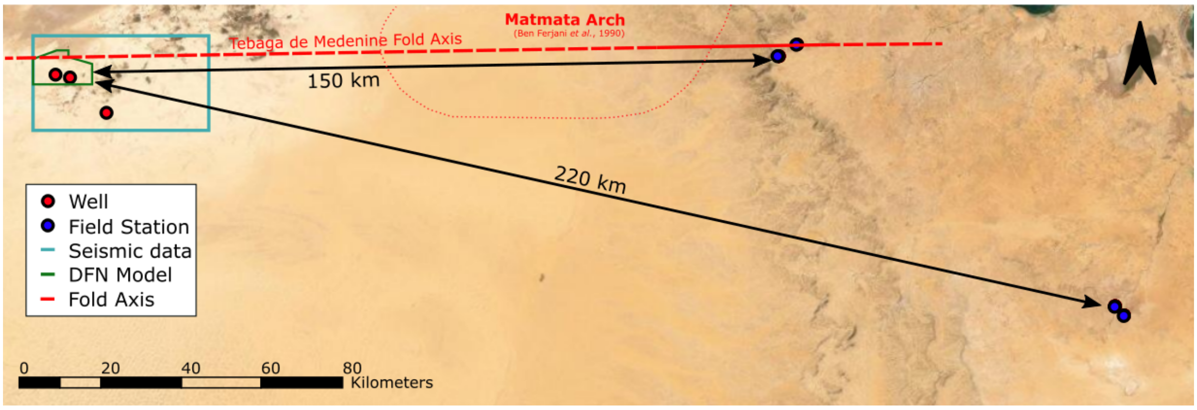

Figure 5.8: Map showing the link via the Tebaga fold between the outcrop fracture analysis in the Jeffara Basin and the subsurface data (well and seismic) in the SCB.

5.4. Subsurface Fracture Characterisation of the Southern Chotts Basin

Subsurface data for fracture characterisation was acquired from both well and seismic data. FMI logs from four wells in the Sabria block were interpreted for fractures. Data from the 3D seismic cube was analysed through seismic attributes to illustrate fractures at depth (see Chapter 3 for more detail on the wells and seismics). The well and seismic information provide data at different scales when interpreting the fractures at depth. Wells provide point data at small scale (m's) whereas seismic data can provide 3D information of the fractures but at a larger scale (10's m to km's). By utilising both data sources, the fractures in place can be better understood. Fracture analysis in the subsurface focuses on the Ordovician reservoirs in the SCB which are affected by the late Hercynian shortening event.

5.4.1. Well Data

Well data was used to detect fractures within the reservoir units and determine the main orientations and fracture intensity. The FMI data was interpreted in Techlog to identify fractures present in the 3 wells around the permit blocks. These wells were Well-1, Well-2 and Well-3.

The two main reservoirs of interest in this region are situated in the Ordovician layers (table. 5.1). Therefore the focus of the well analysis will be on the fractures in and around these units. Both units sit below the Hercynian Unconformity and therefore expect similar compressional features as observed in the Permian deposits analysed on the surface.

Table 5.1: Table showing the depths of the Ordovician reservoirs in each well. Depth in meters - MD (TVDSS)

Unit	Boundary	Well-1	Well-2	Well-3
Reservoir 1	Top	3635 (-3600)	3681 (-3607)	3580 (-3522)
	Bottom	3700 (-3664)	3743 (-3669)	3642 (-3584)
Reservoir 2	Top	3700 (-3664)	3743 (-3669)	3642 (-3584)
	Bottom	3747 (-3711)	3802 (-3728)	3715 (-3657)

From these interpretations the orientations of the fractures in the wells can be analysed (fig.5.9). The conjugate system observed in outcrop is also found in the wells (Dip Azi - 300°& 65°[Well-2 Well-3]), shown as green. There is a N-S striking orientation (Dip Azi - 271°& 268°[Well-1 Well-2]), shown in blue. An E-W striking orientation is observed in Well-2 and Well-3 shown in red.

The conjugate fractures (green) show similarties with the conjugates observed in outcrop. This indicates that the structural link from the late Hercynian event is present at depth in the SCB. It should also be noted that there is variation of fracture orientation in the wells, possibly due to the picking and local in-situ stresses at depth. This is an important restriction to consider when modelling the distributed fracture networks since for these the focus is on the prominent fractures that are observed throughout the network.

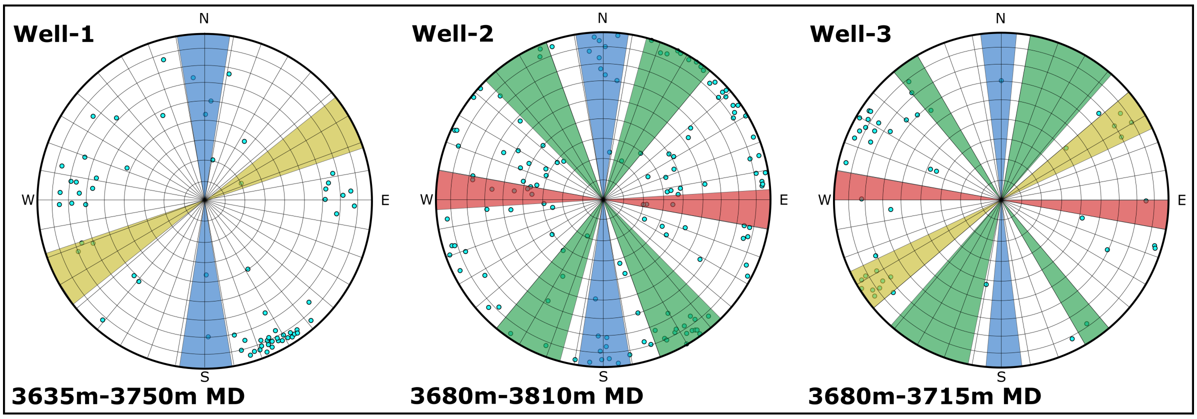

Figure 5.9: Rose diagrams of each well showing the strike of the interpreted fractures in the reservoir units. Blue dots are the azimuth points.

The wells also provide important data on the intensity (P10 and calculated P21) of the fractures. Using the Terghazi correction, P21 values are calculated for the zones (table 5.2). Well-1 and Well-2 showed varying values for the P21 corrected fracture intensity. In the Well-1 around the reservoir units the P21 is calculated to 2.5m^{-1}/m^{-2} whereas in the Well-2 the intensity is 4.1m^{-1}/m^{-2}. The Well-3 P21 corrected values are much lower. This could be due to less fractures being identified from the FMI logs. The high values for the Well-2 could be due to being around a fault zone which enables more fracture generation, however it will not be representative of the overall fracture network in the subsurface. Therefore, it is likely the P21 intensity value would be lower.

Table 5.2: Table showing the Intensity (P21 corrected) values for each well in the reservoir zones

Well	Well-1	Well-2	Well-3
Intensity (P21 Corrected)	2.49	4.10	1.55

Fracture H/L ratios are difficult to accurately calculate from wells due to how fractures intersect the borehole. Therefore, rough estimations on fracture height are gauged from the traces in the FMI and can be compared with estimations from fracture length in seismic. Fractures do vary in height, however are approximately around 4m. Integrating this with the fracture lengths from seismic will be useful for estimating the fracture H/L ratio. This is important in fracture modelling as it influences the connectivity of the fracture network. The larger the H/L ratio, the larger the vertical permeability which is one of the outputs that is of importance in fracture networks.

Aperture from the wells is also difficult to estimate given the quality of the images. Furthermore, there are some fractures within the well data that are healed. An initial estimate from the wells indicates a fracture aperture of around 0.45mm. From previous studies in the north regarding open fractures using core data, fracture aperture could be up to 2.5mm, however the average aperture is approximately 0.94mm (Roskam 2016). However there is uncertainty in estimating aperture from both FMI and core data. Aperture measurements from FMI is commonly overestimated and core analysis is undertaken at surface conditions and this uncertainty may require additional modelling.

5.4.2. Seismic Data and Attributes

3D seismic data is used for detecting fracture signatures in the subsurface. This is undertaken using seismic attributes to highlight lineations and fracture zones. There are various conventional seismic attributes (similarity, curvature etc) that can highlight these features, however a recently developed workflow (fig.5.10) utilising open source software (OpendTect) to apply unconventional attributes (fracture density, fracture proximity etc) to 3D seismic cubes which is more effective in detecting and highlighting fractures (Jaglan et al. 2015, Brouwer and Huck 2011).

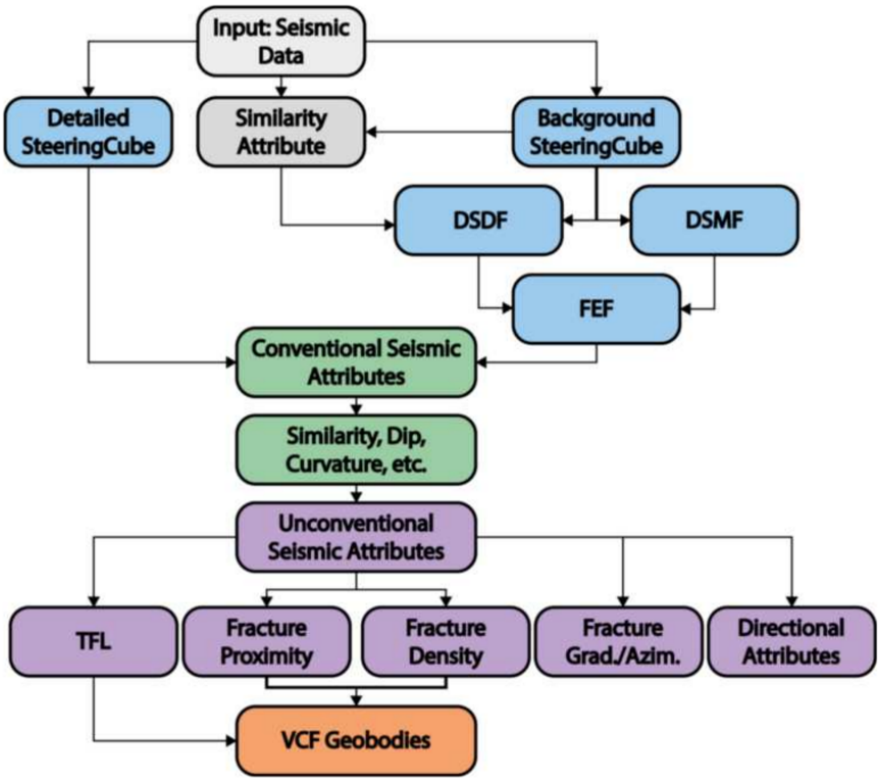

Figure 5.10: Workflow for extracting structural data from seismic attributes using OpendTect (Jaglan et al. 2015)

Seismic Attribute Workflow

Before information regarding the fractures can be extracted, a steering-cube needs to be created from the seismic volume. The steering-cube is a dip-azimuth volume with localised dips of seismic events calculated at every sample point (Nederveen 2018, Jaglan et al. 2015). Two types of steering-cube can be created (Detailed or Background) which differ by the amount of filtering applied. Background steering-cube is heavily filtered and emphasises dip trends of seismic events and therefore is the preferred option in defining and enhancing attributes (Jaglan et al. 2015, Brouwer and Huck 2011).

Filtering is then applied to the steering-cube to condition the data for fault and fracture detection. This process is separated into three main steps:

1. Conditioning and smoothing the data through DSMF

2. Enhancement of fault and fracture lineations through DSDF

3. Combining both steps 1 and 2 to create a structually enhanced seismic cube through FEF

DSMF is filter which smoothes the seismic volume and removes background noise and therefore improving the continuity of seismic reflectors (Jaglan et al. 2015). This filter is used in conjunction with other filters (e.g. DSDF) as small fault zones may be filtered out by the median filter size.

DSDF improves the sharpness of the fault zones through replacing the central amplitude of reflectors are replaced by better quality nearby amplitudes and in the proximity of faults and fault zones, the good seismic reflectors are shifted to the fault edges, thereby sharpening the fault plane (Jaglan et al. 2015, Brouwer and Huck 2011).

The outputs of these two filters are combined into the FEF which enhances the fault and fracture zones within the seismic for use in later attribute processes (Jaglan et al. 2015).

Fault Likelihood and Thinned Fault Likelihood attributes are calculated using the FEF. These attributes are defined by the power of semblance to output likely faults and fractures in a ratio of 0 to 1. The Thinned Fault Likelihood attribute outputs thin lineations from which structural interpretation can be undertaken.

For this work, fracture detection and measurement are the priorities when applying seismic attributes. Both conventional and unconventional attributes are applied. Similarity and curvature attributes are calculated to highlighting large fractures and faults aiding in understanding the length of fractures. Unconventional attributes such as fracture proximity and density highlights the regions within the seismics that contain fracture zones. This combined with the fracture azimuth attribute provides the nature of the fractures in the subsurface. See Appendix E for additional workflow and results from the seismic attribute analysis.

Seismic Attribute Results

The conventional attributes generally provide qualitative results regarding proximity and nature of the faults and fractures, however they are not useful for obtaining quantifiable results. Orientations of these lineations can be better constrained using the fault likelihood and the thinned fault likelihood attributes (fig.5.11 A). 1300 lineations were detected from the thinned fault likelihood attribute (fig.5.11 B). These are similar to the orientations observed in the wells with the main conjugate system identified (green). The E-W orientation (red) is also prominent in the fractures as is a N-S orientation (blue). These do correspond with fracture sets observed in the wells and are likely to be distributed background sets which can be included in the modelling.

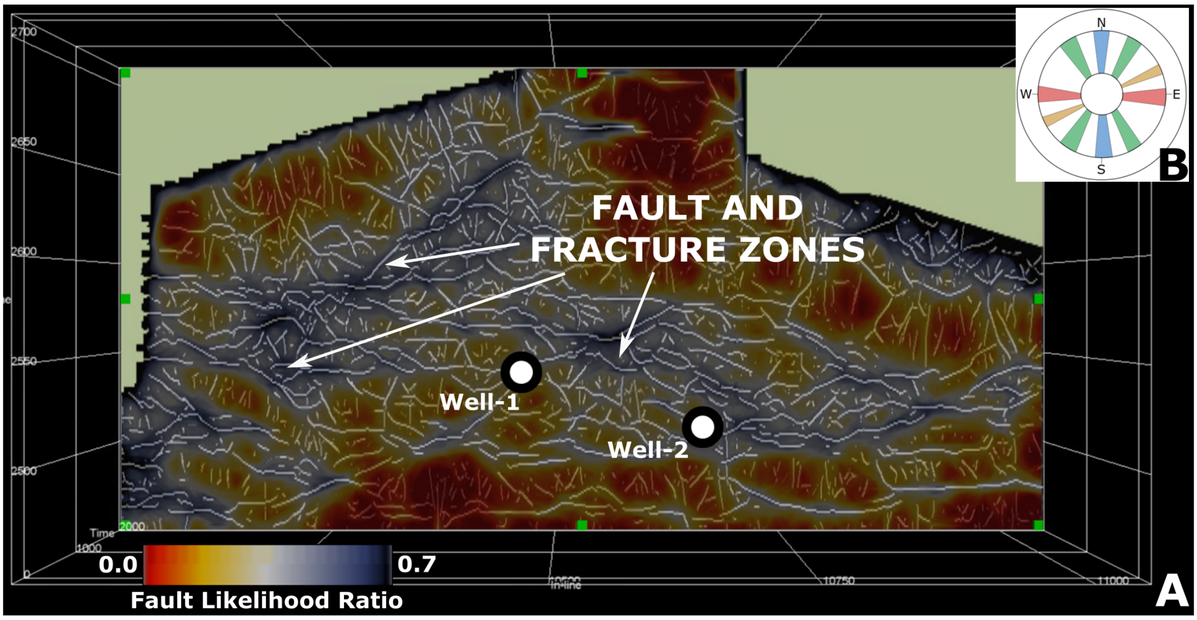

Figure 5.11: A. Fault Likelihood and Thinned Fault Likelihood attributes showing locations of faults and fractures zones in the target reservoirs. B. Rose diagram showing the strikes of identified faults and fractures.

Fracture density (fig.5.12) is also calculated to gauge the density zones in the area. These are computed through inputting the fault likelihood attribute and calculating the ratio of ”number of traces classified as being fractures” to the total number of traces present” in a given scan radius on the Z (time) plane. The output of this processing attribute shows that the fractures are densely populated around the center of the seismic region. Well-1 is observed to be in a region of low fracture density whilst Well-2 is located in a higher fracture density zone. Whilst this seismic attribute is a ratio, the qualitative results correspond well with the fracture intensity values estimated from wells.

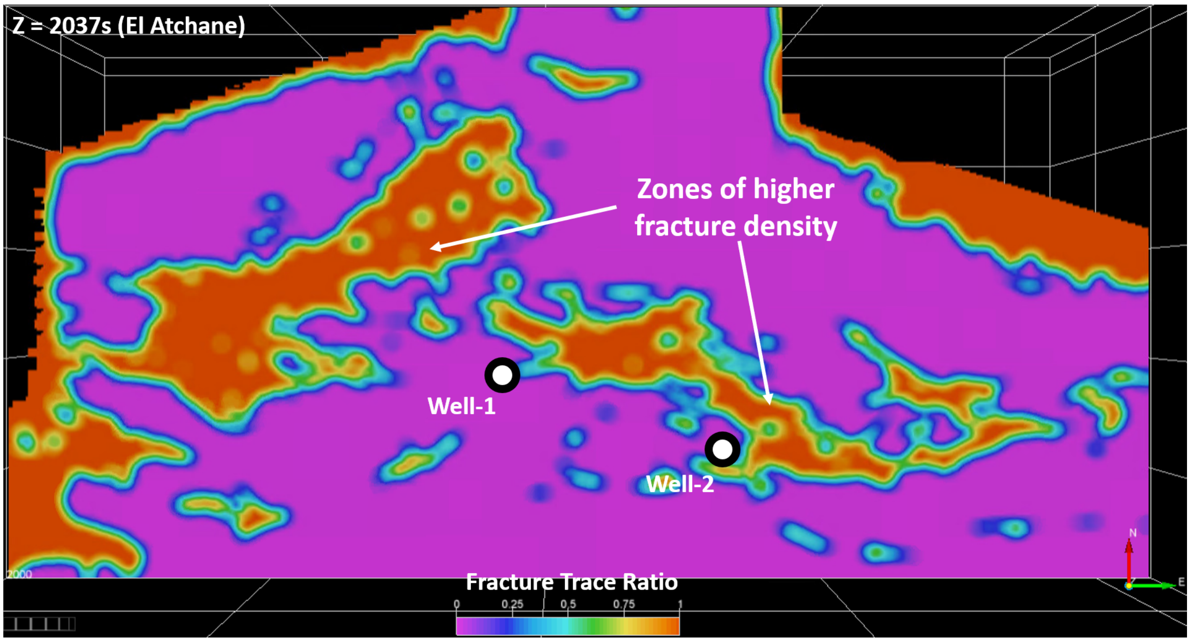

Figure 5.12: Fracture density output for Z=2037ms (Reservoir 2). Radius of scanning = 125m, fault likelihood threshold = 0.4.

Seismic processing can also provide information on the fracture length at depth. This is an important input in association with the H/L ratio estimation for the DFN modelling. Using the thinned fault likelihood, planes are extracted (fig.5.13) from which fracture data (length, strike, dip) are calculated. This output shows on average length of the fractures in the reservoir region is approximately 22m. This value does vary from around 10m to a 4000m, with the majority of fractures are below 50m. There is some uncertainty to the seismic resolution which can be tested during the modelling phase to assess the sensitivity of the fracture length.

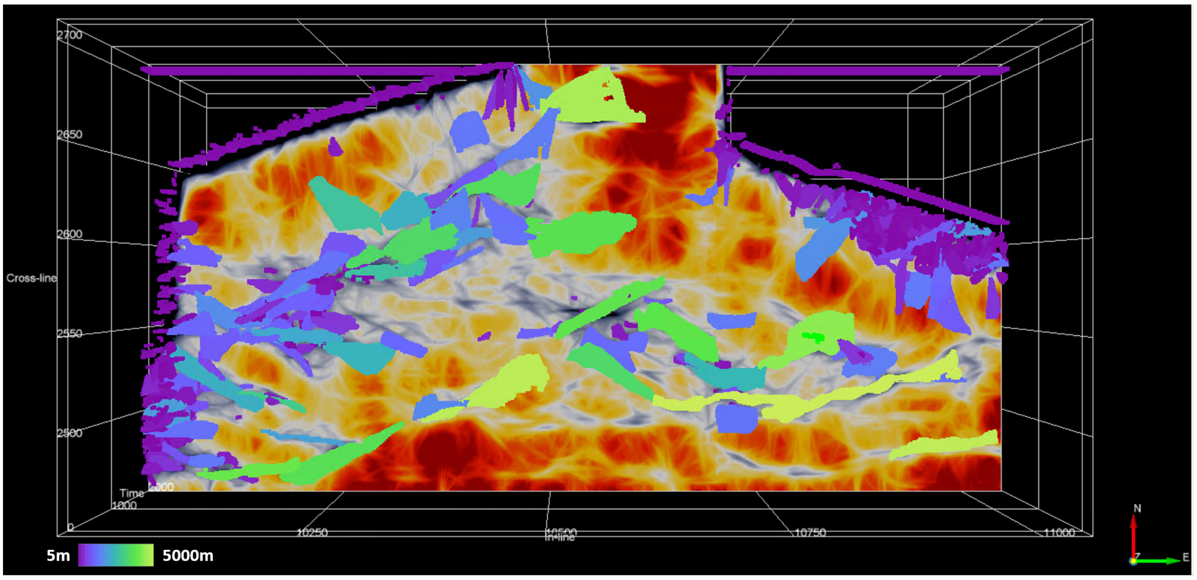

Figure 5.13: Extracted fracture data from the fault liklihood attribute.

5.5. Integration into the Geological Framework

The data from the surface and the subsurface can be integrated into a fracture framework that forms is the basis for the input to the DFN model. The data from the surface provides the characteristics of the main driver to the fractures in the Paleozoic and early Triassic units in the Jeffara Basin and SCB. The conjugate system of fractures is viewed as distributed throughout the folding (as observed through the pavement analysis), these fractures are also observed at depth in the Palaeozoic reservoirs of the SCB.

The observed fractures are characterised by NNE-SSW and NNW-SSW striking conjugate fracture sets linking well with the interpretations of the geological history. These fractures are also observed in the subsurface (65°& 300°in Well-2 and the seismic data). In the subsurface, N-S and E-W striking fracture sets are also observed distributed throughout the units. These fracture sets are likely to be background joints that formed prior to the late Hercynian event that formed the conjugate sets. Therefore, whilst they are not observed in the late Permian and early Triassic units, they are found in the earlier Paleozoic. Given the distribution of the these four fracture sets, they can be integrated into a fracture model units in the Jeffara Basin and SCB (fig.5.14). This model incorporates the open fold model which influences the conjugate fracture sets and the earlier formed background joints in the Paleozoic.

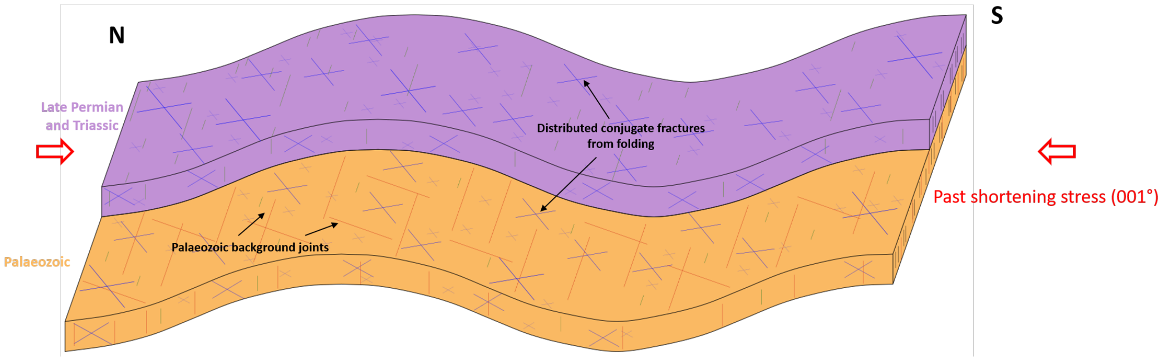

Figure 5.14: Fracture model showing the joint sets observed in outcrop (conjugate sets) and in the subsurface (background joints and conjugates)

Integrating the data from the surface and subsurface fracture characterisation is important for the understanding of the network that is used in the fracture modelling. Fracture lengths, estimated from the seismic data indicate fractures are approximately 22m long to a maximum of 50m with H/L rations estimated between 1.5 - 3 depending on the set. Fracture intensity, calculated surface pavements indicate the areal fracture intensity (P21) is approximately 0.065m^{-1}/m^{-2} falling within the preferred range for fracture intensity. However, well data (P10) updated to P21 using the Terghazi correction indicate a variable areal intensity between 1.55m^{-1}/m^{-2} and 4.1m^{-1}/m^{-2}. The Well-2 is affected by the nearby fault zone and therefore less representative of the whole region. The Well-3 found a low fracture density which better represents the overall intensity of the fractures at depth and corresponds better with the pavement results. It is also a possibility that the well fracture interpretation could over pick fractures or include drilling-induced fractures into the intensity calculations. Therefore, the pavements provide a better estimation for fracture intensity and is estimated as approximately 0.065m^{-1}/m^{-2}.

These results provide the necessary inputs for stochastic DFN modelling and deterministic modelling of the subsurface units which is important for predicting fracture networks and quantifying the fractures contribution to reservoir flow.

6

Fracture Modelling of the Southern Chotts Basin

Fracture modelling is an important step in characterising reservoirs at depth. Data from the surface and subsurface is used in combination with the fracture driver understanding to create discrete fracture network (DFN) and deterministic models that can predict networks in the SCB. Fracture aperture modelling is undertaken on the final fracture model to analyse which fracture sets are more likely to be open under the current regional stress regime. The modelling provides an insight into the possible flow paths in the reservoirs.

6.1. Fracture Modelling

DFN modelling is a process of distributing fractures throughout a 3D model stochastically using set input parameters. This is a vital process in understanding the networks in naturally fractured reservoirs and quantifying the fracture contribution to reservoir flow. The main factors that are established using DFN modelling are the geometry of the fracture system and the transmissivity (flow effectiveness) of the individual fractures (Jing and Stephansson 2007).

The main inputs for stochastic DFN modelling are **Fracture Intensity**, **Fracture Orientation**, **Fracture Size (length)** and **Fracture Aperture** which are derived in the modelling through probabilistic functions. Fracture orientation and size are common attributes of fractures that can be easily measured both in the field and at depth in well/core analysis. Fracture intensity and aperture are more complicated to derive but both vitally important parameters for fracture network modelling.

Fracture intensity (fig.6.1) is a measurement of the number of fractures per unit length of a scanline (P10), fracture trace length per unit area (P21) or area of fracture per volume of rock (P32) (Dershowitz et al. 1992). P32 is the output value used in the DFN modelling. Unlike fracture density which only considers the number of fractures in a given dimension (line, area or volume) fracture intensity considers the size in the dimension and therefore is directly related to the conductivity (flow) and storativity of the fractures (Niven and Deutsch 2010, Dershowitz et al. 1992). Fracture intensity is calculated in the different dimensions through FMI data (P10) or pavement imaging (P21) from which an initial estimate on the ”area of fractures per unit volume” (P32) can be estimated.

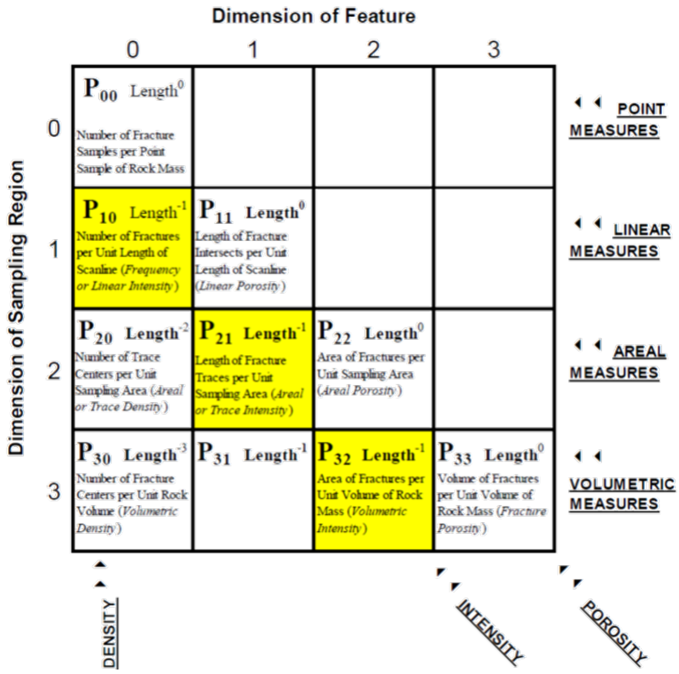

Figure 6.1: Features of fractures (density, intensity and porosity) in different dimensions.

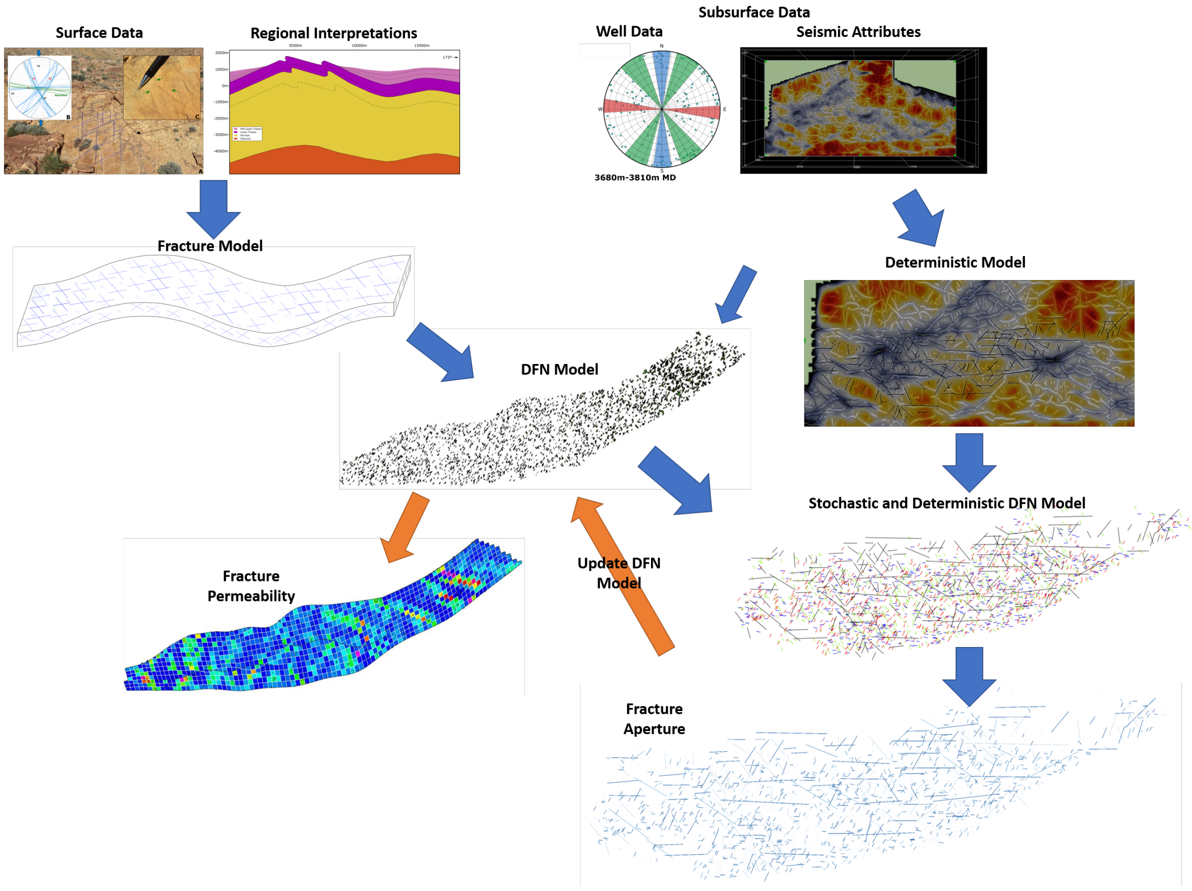

Figure 6.2: Fracture Modelling workflow

The fracture data acquired from pavements, seismic and wells (Chapter 5) is used as input for the modelling stage. Surface and subsurface data is integrated into the DFN model to output a stochastic fracture network model of the Ordovician reservoirs (fig.6.2). From this an estimate on fracture permeability can be calculated within the model. Using seismic attributes, additional fractures are traced (deterministic) to better represent larger fractures present at depth. This final model is used for analytical aperture modelling to test the current openness of fractures and which fractures are likely to contribute to reservoir flow.

6.2. Data Input and Volume Model

6.2.1. Volume Model

A volume model (fig.6.3) created in Petrel is used as a framework to receive a distribution of fractures. The model focuses on the Ordovician reservoir units in the SCB. The model is split into 3 regions (north, centre, south) based on the major faults that run through the volume. The Well-1 covers the North and Centre regions, whilst the Well-2 covers the South region. The seismic attribute work extended through all the regions. The Well-3 lies outwith the volume model to the south east but is still applicable to modelling the subsurface reservoirs.

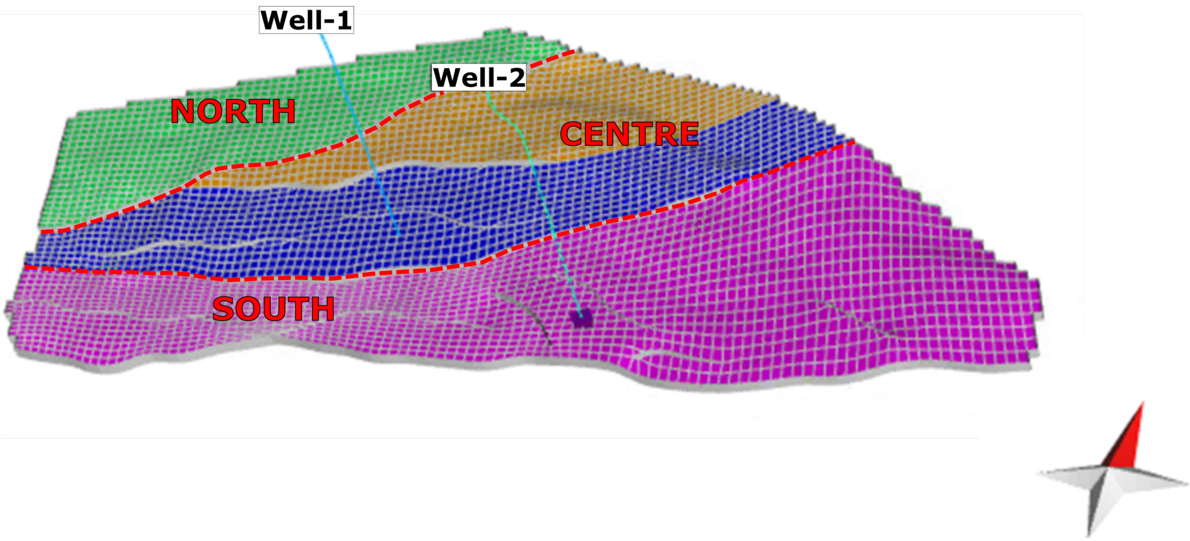

Figure 6.3: Initial volume model and main defined regions.

6.2.2. DFN Model Input

The software MOVE requires several inputs to create the DFN model of the fractures, these include fracture orientation, intensity (P32) and length.

Table 6.1: Input fracture sets to DFN model

Set	Azimuth	Dip Angle	H/L	Estimated Aperature (mm)	Note
1	240	80	0.8	0.94	**Conjugate 1**
2	302	85	1	0.94	**Conjugate 2**
3	3	90	1	0.94	**Background Joint**

Table 6.2: Input fracture intensity for each region

Sector	Region	Intensity (Model 1)	Intensity (Model 2)
0	North	0.06	0.035
1	North	0.06	0.035
2	Center	0.06	0.042 (conjugate) 0.033 (Joint)
3	South	0.06	0.075 (conjugate) 0.05 (Joint)

6.3. DFN Fracture Models

The stochastic DFN modelling process is driven by the interpreted fracture driver of open folding, i.e. the distribution throughout the system of conjugate fractures which are observed in outcrop and subsurface data. Furthermore, also integrated into the DFN model from well data, is the consistent E-W striking fractures which forms background joints.

Due to software and computational limitations, only one region is modelled. The seismic attribute analysis showed that the central region contained the most fracture zones and therfore would be the most promising for fracture modelling. Model 1 uses the parameters based solely on the input values and provides a basic initial fracture network model. Model 2 uses output values from Model 1 in order to update the model. This includes updating the input values for fracture intensity (P32) and varying fracture orientation distribution to better represent the fracture networks at depth.

6.3.1. Model 1 - Central Region

Model 1 contains three fracture sets (table 6.1) in which the orientations of these fractures are set to constant. Fracture lengths are set to a normal distribution estimated with average of 22m and standard deviation of 3m to fit around the fractures detected in the seismic attribute analysis. Fracture aperture is set to constant for all sets of fractures at 0.94mm based on estimates from Roskam (2016). The model set the fracture intensity at 0.06 (table 6.2) which is the estimate from the pavements on the surface.

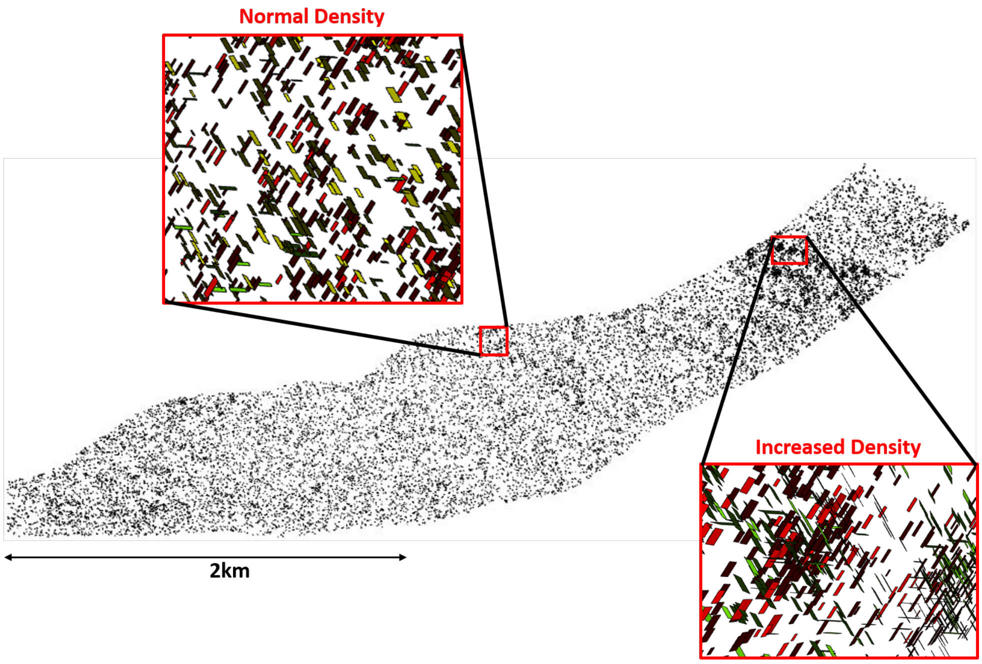

Figure 6.4: DFN model 1 fracture output

The output of the model shows distributed fracture network (fig.6.4). There are zones in the northwest of the region that are densely populated in fractures. These could then represent good zones for flow in the reservoir.

The output P32 intensity values (table 6.3) from model 1 show that whilst the estimated input value (0.063 m^2/m^3) for the sets 1 and 2 fractures matches the output, fracture set 3 output value is lower (0.0331 m^2/m^3). Therefore, set 1 and 2 fit fit well in the model, however the intensity value for set 3 will need to be updated in model 2.

Table 6.3: Table showing outputs from Model 1

Fracture	Conjugate	Background Joints
Number of Fracs	724670	724583
Fracture Area (m^2)	4.59E+09	2.43E+08
Fracture Volume (m^3)	4.30E+05	1.30E+04
Average P32 (m^2/m^3)	0.0625	0.0331
Average Fracture Porosity (-)	5.89E-05	1.83E-06

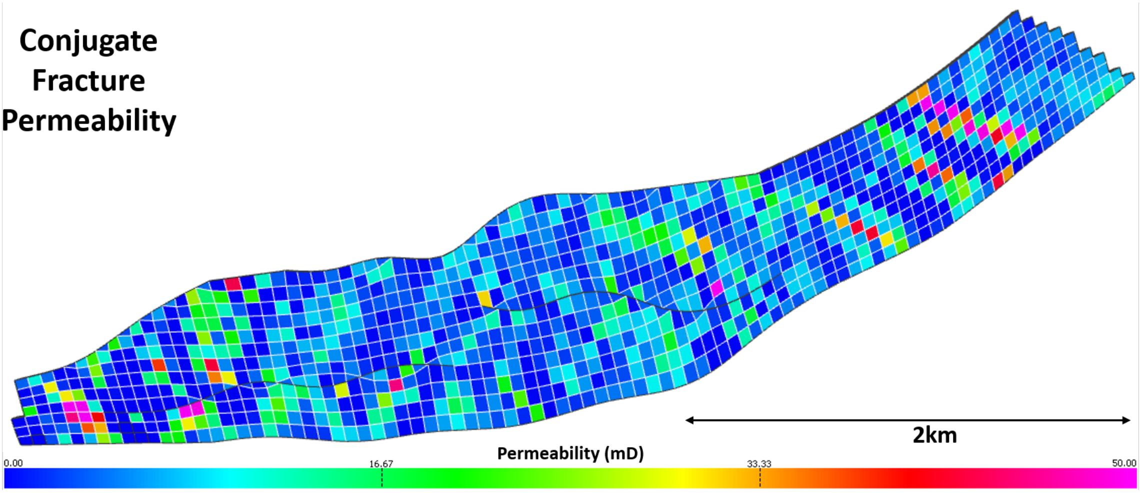

Figure 6.5: DFN model 1 fracture permeability output

The permeability outputs (fig.6.5) show the zones where fracture permeability is good in the central region. The fracture sets show permeability values ranging between 16mD to 33mD. Higher permeability zones are also observed to be orientated similar to the conjugate fractures indicating zones where flow could be increased through the sets (assuming they are open). The major assumption for these fractures is that the aperture is constant at 0.94mm based on the wells. Therefore, aperture modelling will be used to better estimate the fracture openings.

6.3.2. Model 2 - Central Zone Updated

Model 2 uses the results of model 1 and updates the Central Zone to create a more accurate stochastic fracture model of the region. The results from Model 1 showed that the conjugate set fracture intensity (P32) fitted well into the volume, however the background joints fitted poorly (P32 = 0.033 m^2/m^3). Therefore this model will integrate both the conjugates and the joints into the Central Zone with varying P32 values.

Fracture orientation distribution is also updated as these will be calculated based on fisher distributions which better represent the variation in fracture orientation (Gutierrez and Youn 2015, Fisher 1953). The fracture pavement measurements calculated from outcrop estimate the fisher distribution k value to be approximately 50 indicating a low variation in orientation of each fracture set.

Model 2 will also use a different fracture length distribution technique to better represent the fractures at depth. The power law distribution is used regularly in stochastic fracture modelling (Gutierrez and Youn 2015). The exponents used in the power law process are calculated using lab testing on different rocks types. For the sandstone reservoirs used in this modelling, an exponent of 1.8 is used based on previous studies on sandstone (Gutierrez and Youn 2015, and references therein).

Modelling Results

Similar to Model 1, the major fracture zones are located in the northeast and southwest regions (fig.6.6) of the central zone. These fractures show strong orientations of fracture sets 1 and 2. They are also well connected throughout the Central zone. This is an important attribute for the fractures as it enables better flow through the system.

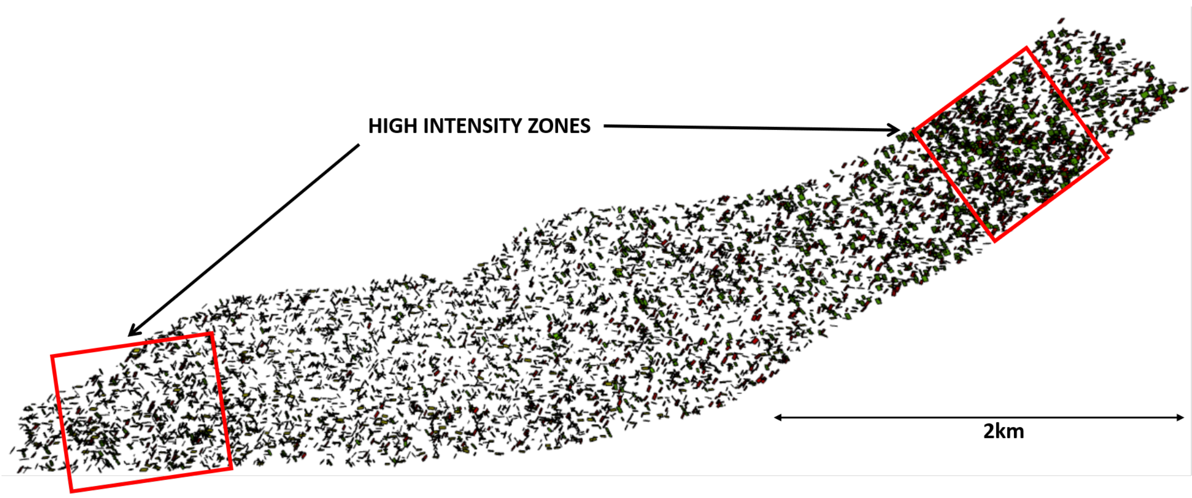

Figure 6.6: Model 2 generated fractures showing higher intensity zones

The are flow zones (fig.6.7) present in the model which could positively influence reservoir flow. These are orientated as the conjuate sets, possibly indicating longer, well connected fractures in these zones. Fractures can be up 50m in length and when these larger fractures are connected, they form higher permeability zones. In this model, aperture is calculated based on fracture length, with an average aperture of 0.94mm.

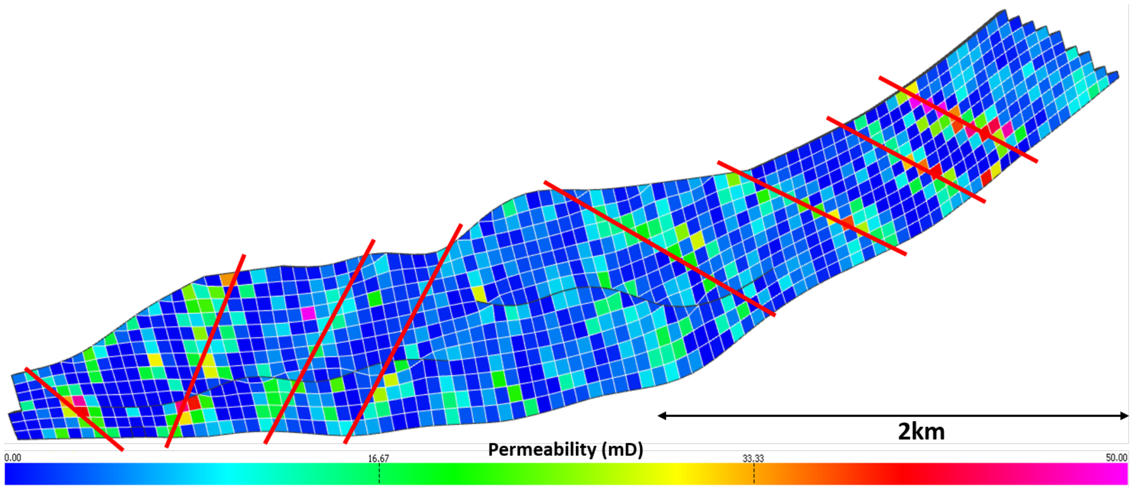

Figure 6.7: High permeability zones where flow could be enhanced

These flow zones are completely stochastic and the result of the model generating more or larger fractures in these areas. To fully relate this model to the subsurface a deterministic model is be created. This directly incorporates the fractures observed at depth in the fracture model and also picks out longer fractures which are not modelled in the DFN modelling process.

6.3.3. Hybrid Fracture Model

Seismic analysis shows certain areas where there are larger fractures and also zones where fracture density is increased. Therefore to create a fracture model that is representative of both the DFN and the subsurface analysis a final model is created. This involves tracing additional longer fractures observed in the TFL seismic attribute (fig.6.8) from a 2D depth slice. This adds a deterministic model to the stochastic DFN model and builds on the generation of fractures in MOVE (which mainly represent the system interpreted throughout the field and well) linking in the subsurface data (seismic).

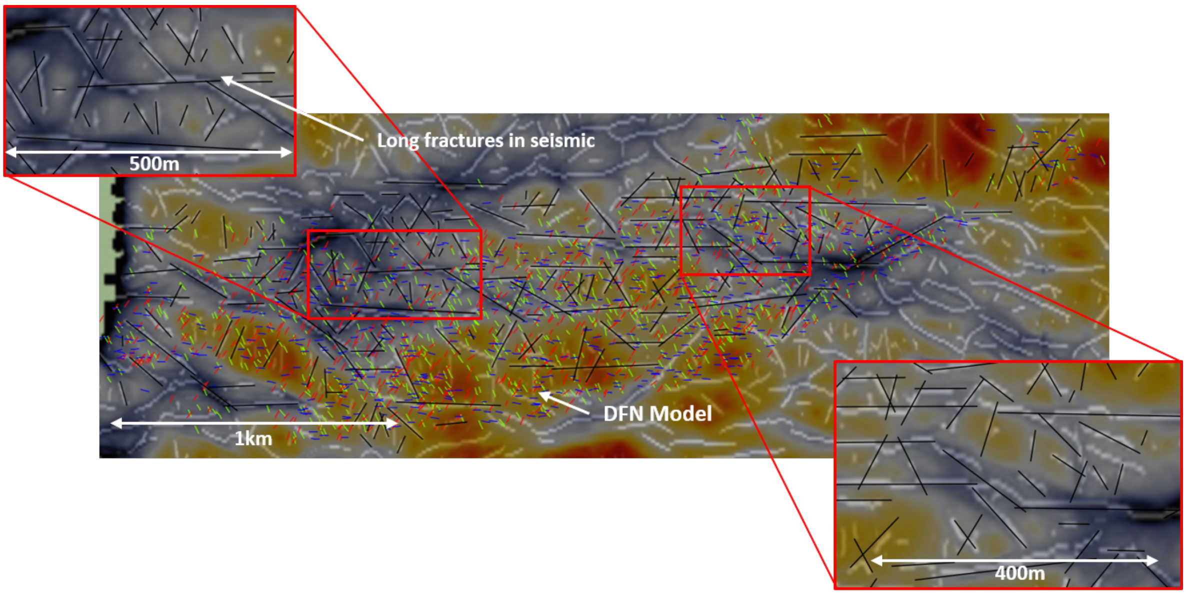

Figure 6.8: FL and TFL seismic attributes used to identify longer fractures in the subsurface for deterministic modelling. Overlain by DFN model to form hybrid fracture model.

The deterministically derived fractures in this model vary from 25m to 200m in length with orientations that are similar to fracture sets 1-3. In addition there are also fractures striking approximately N-S. This, similar to the E-W striking fractures (set 3) form a background joint that is observed only in the subsurface data.

By combining the same depth slice of the DFN model with the traced fractures, a hybrid fracture model is created (fig.6.9). This model shows the smaller fractures modelled from the DFN modelling stage and the larger fractures that are visible through seismic.

This final hybrid 2D fracture model can be used in the aperture modelling to test the ability for the smaller and larger fractures in allowing flow in the current stress conditions at depth.

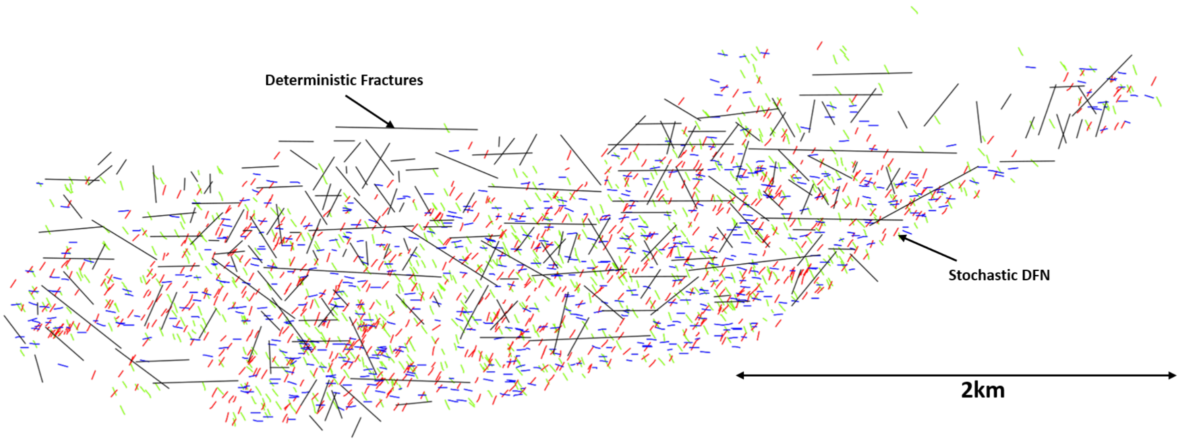

Figure 6.9: Final fracture model showing the stochastic DFN model fractures and the deterministic fractures from seismic

6.4. Fracture Aperture Modelling

Fracture aperture is an important characteristic of fracture networks in the subsurface. The aperture of the fracture determines the transmissibility of the network and how easily fluids can flow through. It is therefore vital to understand which fractures are open (large aperture) and are closed (small to zero aperture) and to what extent they are open. The DFN and hybrid fracture models use data from the FMI and cores to estimate the fracture aperture. However, both of these data sources commonly overestimate the aperture size. Therefore to understand which fracture sets are open at depth in the current stress regime, aperture modelling is undertaken.

6.4.1. Geometrical Aperture Modelling Methodology and Parameters

There are several methods of modelling fracture aperture which include using Finite Element (FE) solvers which can be used in fluid flow calculations, however for this work an analytical approach is more appropriate to gauge the openness of the fractures in the current stress regime (Bisdom et al. 2016a, Barton 2014, Barton and Bandis 1980). The analytical approach presented by (Bisdom et al. 2016a) provides a method through which mechanical aperture (fig.6.10) can be predicted for a fracture network on a 2D horizontal plane.

There are two forms of aperture within the fracture network (fig.6.10) that control fluid flow, mechanical (kinematic) and hydraulic aperture (Bisdom et al. 2016a, Olsson and Barton 2001, Marrett et al. 1999). Mechanical aperture is defined as the direct opening between two fracture walls and hydraulic aperture is the fracture space which controls fluid flow within the network.

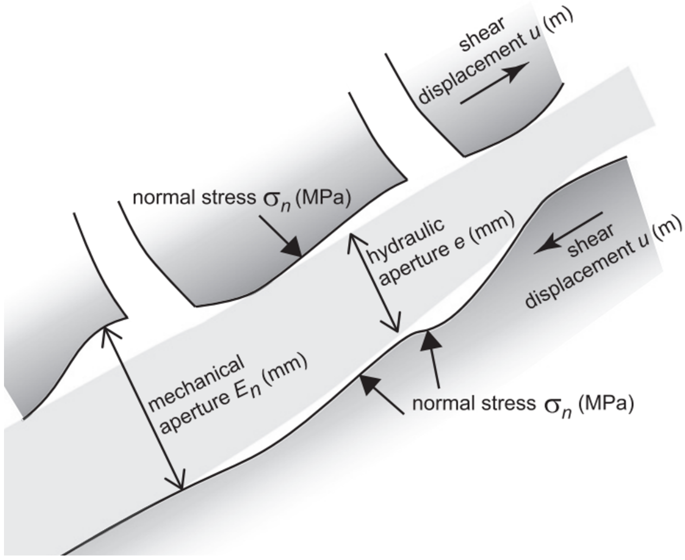

Figure 6.10: Fracture variables controlling mechanical and hydraulic aperture (Bisdom et al. 2016a)

The methodology of the analytical modelling involves analysing the relationship between in-situ stress and fracture geometry and the resulting aperture (Bisdom et al. 2016a). First analysis looks at the effects of the maximum horizontal stress on a single fracture in the network, which then corrected for the affect that length or block size has on the normal stress applied to the fracture:

$$\sigma_{n,single} = \sigma_1(-0.33\cos[\alpha\pi] + 0.65)$$

where α is the angle between the maximum horizontal stress and the fracture strike.

$$\sigma_{n,length} = \sigma_{n,s}(-0.083\ln(L) + 1.055)$$

where L is the fracture length or block length.

The normal stress applied to each fracture $\sigma_{n,L}$ is then used in calculating the mechanical aperture (E_n) of each fracture in combination which additional parameters concerning the fracture wall roughness and compressive stress of the rock (Bisdom et al. 2016a, Barton et al. 1985):

$$\mathbf{E_n} = \mathbf{E_0} - (\frac{\mathbf{1}}{\mathbf{v_m}} + \frac{\mathbf{K_{ni}}}{\sigma_{\mathbf{n,L}}})^{-\mathbf{1}}$$

where E_0 is the constant initial aperture (a function of Joint Roughness Coefficient (JRC) and Joint Compressive Strength (JCS)), v_m is the maximum closure and $K_{n,i}$ is the initial stiffness (functions of E_0) (Bisdom et al. 2016a, Barton and Bandis 1980, Barton et al. 1985).

This methodology requires several parameters to work which are based from the mechanics of the reservoir rock. Magnitude and orientation of the main horizontal stress in the region is estimated from recent geomechanics work undertaken on the Sabria field (confidential souce). JCS is estimated from Uniaxial Compressive Strength tests on samples from the Sarbia field under reservoir conditions (confidential source). JRC is estimated from literature based on irregular fracture surfaces and high fracture wall strength (expected from deep reservoirs) (Bisdom et al. 2016a).

6.4.2. Fracture Aperture Results

The analytical modelling was undertaken using ArcGIS where hybrid fracture model was imported and normal stress calculations (fig.6.12 A) were applied to the fractures to determine aperture (fig.6.12 B).

The normal stress results show that the apertures that are perpendicular (302°) to the main horizontal stress (036°) experience the highest stress of up to 98.2 MPa, whilst the fractures parallel to this main stress (240°) experience low stress. The E-W trending background joints show variation in normal stress applied depending on size of fracture. Shear displacement results are heavily influenced by fracture length, and therefore the longer fractures show the most displacement.

The mechanical aperture varied from 0.170mm to 0.258mm at an average of 0.196mm. The wider apertures are mainly situated along the fractures orientated parallel to the main horizontal stress, whilst fractures perpendicular formed the lowest aperture. The long fractures, in particular the fractures orientated E-W contain a wide aperture where fracture length is a strong control on the aperture size. The conjugate fracture orientated 240°shows a higher aperture than the conjugate set orientated 302°(fig.6.11). Therefore, in general the sets of fractures conjugate contain unequal aperture size, one set wider than the other. The background joint system is heavily influenced by length, where the widest fractures in the system (fig.6.11) are up to 0.258mm).

Analytical hydraulic aperture modelling was also attempted, however showed a significant decrease in aperture. This is likely due to the assumption that JRC is equal to JRCmob (Bisdom et al. (2016a)) which is not true for all fractures and therefore results in a much lower aperture.

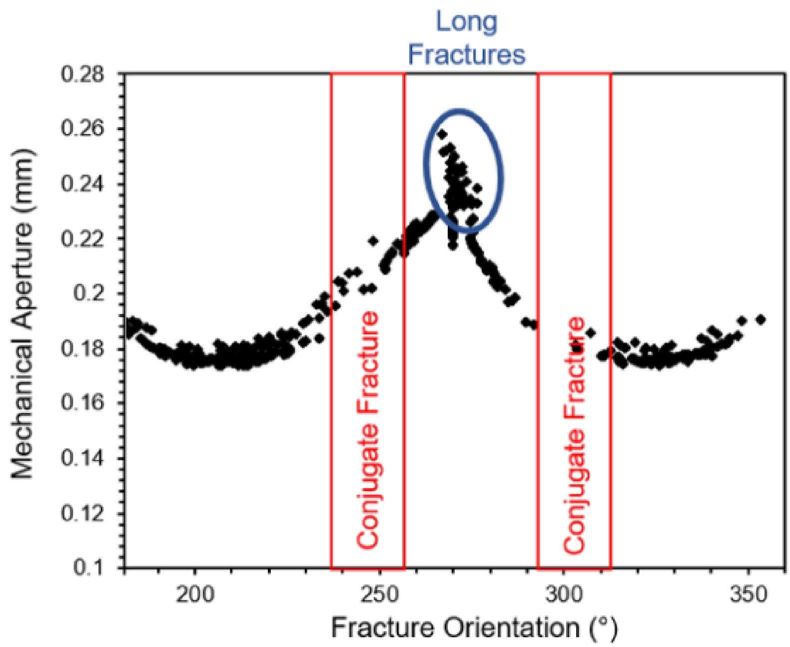

Figure 6.11: Mechanical aperture results as a function of fracture orientation.

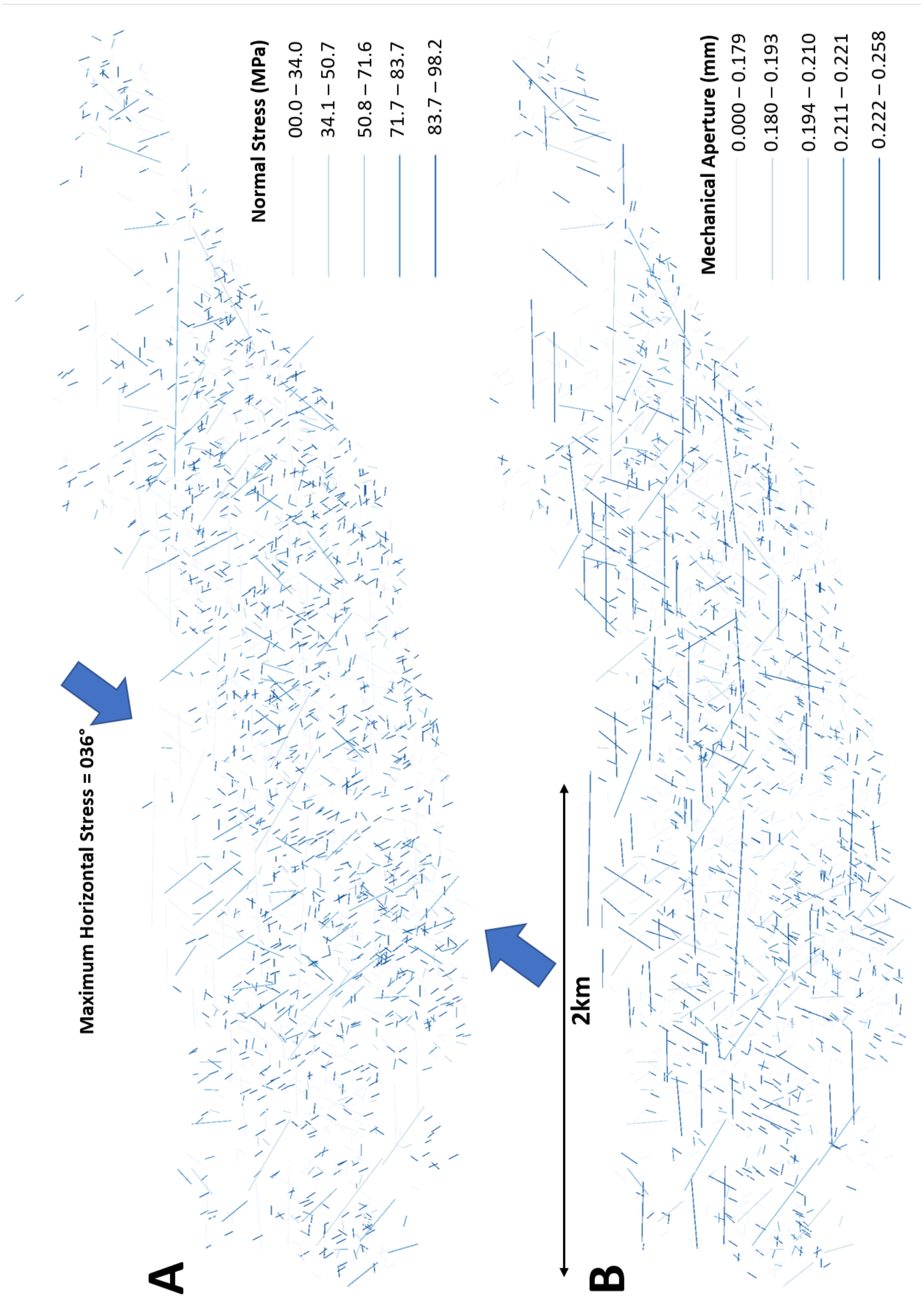

Figure 6.12: A. Normal Stress applied to each fracture based on a maximum horizontal stress of 104MPa at 036°. B. Mechanical Aperture Results

6.5. Discussion

The results of the DFN modelling show the fractures are well connected and distributed throughout the system and thus making them an important aspect to the reservoir flow in the SCB. The distributed nature of these fractures throughout the system of folds make them an excellent target for the modelling. The modelling indicates the estimate of P32 values in the conjugates are around $0.043m^2/m^3$ whilst the background joint lineations are lower around $0.033m^2/m^3$. This shows that, similar to what was observed in the outcrop, the large conjugate system is dominant in the subsurface.
The DFN modelling technique is an established method, but not the most effective method of distributing fractures in models. The method is fully stochastic and driven by the outcrop and well data. To relate the MOVE output to the subsurface better, a number of deterministic fractures were applied to form a hybrid fracture model to gauge a sense of the larger discontinuities at depth. This better links the DFN to real fractures at depth and adds additional detail to the overall fracture network model.

An issue that arised in the DFN modelling is computation limitations. The final model incorporates the only central region in the field, which contains the best fracture zones. The northern and southern regions are larger in volume and therefore would take considerably longer to process the fracture networks. Future work could apply DFN modelling on these regions to better constrain the distribution of the network there, however for the scope of this thesis, the central region provides a good insight in the network at depth and the links between the surface interpretations and subsurface analysis.

Fracture aperture modelling is applied to complement and reduce the uncertainty in the DFN model in regards to flow implications. The fracture aperture modelling provides an additional insight to understanding which fractures are more likely to contribute to flow in the subsurface under the current stress conditions. The results of this indicate that the conjugate fracture set orientated 302°are more open than the fracture set orientated 240°due to the current stress orientation of 036°. The joint fractures varied in aperture size dependent on the fracture length. Therefore, the longer fractures observed in figure 6.8 could be good flow paths combined with the long fractures orientated 302°for the Paleozoic units.

This modelling focused on the fractures in the Paleozoic units, however since the conjugate fracture system is distributed in the Triassic, Permian and Paleozoic (due to the late Hercynian shortening event), these fractures could enable flow in other reservoirs. The Permian contains tight reservoirs in the SCB and where fractures could play a key role in improving reservoir transmissibility (Bruna et al. 2019a). The implications on the timing for the shortening event indicate that the early Triassic reservoirs are likely to be fractured in with the same conjugate network of fractures. Therefore these fractures could influence production rates from the TAGI reservoirs in the SCB. It is important to understand the effect of the fractures through flow testing in these reservoirs as the fracture networks could either improve flow or promote compartmentalisation, increasing the water cut and decreasing the recoverable oil.

This is an analytical approach to the modelling and does not take fully into account slip of the fractures between one another. The methodology, as specified by Bisdom et al. (2016a) shows that the geometric analytical approach and the FE numerical approach yield similar results. However, results of the FE approach can then be used in further modelling phases, including fluid flow modelling which is a vital stage in testing the fractures capability with either production data from the field itself of numerical flow modelling using simulators in house. Therefore consideration should be taken in future research to apply this technique to the fracture network model.

7

Discussion

This thesis presents two main scopes of research, the interpretation of a shortening event in the Jeffara and Southern Chotts Basins and the impact of this event on the fracture networks at depth in the SCB. This chapter will discuss the techniques used and improvements in future work that could be applied.

7.1. Data Collection and Integration

7.1.1. Surface Data

The fieldwork in the Jeffara Basin focused primarily on the Permian and Triassic rocks of the TdM and Kirchaou. This enabled the vast collection of bedding and fracture measurements along with samples for future work. Fractured pavements were imaged and used in the fracture characterisation. The volume of measurements reduced the uncertainties in sampling, improving the analysed data. Further investigations could have been undertaken north and south of the TdM. This would have allowed a better view of the variations in bedding in the lower Triassic units and the Jurassic units away from the main Tebaga high. Additional work could also have been undertaken at Sidi Toui which contains good exposures of mid-late Triassic units for further fracture analysis. It would be useful for any future missions to the region to account for these possible exposures.

Utilising the selfie stick for capturing the fracture pavements provides a low cost and permit free method for imaging the pavements. Whilst this method produced a wealth of good data (orientation [high fisher values] and fracture intensity), this process is time-consuming. In the case for pavements 3 and 4 this process took several hours to image. Issues also arise in processing the imagery of the larger pavements, such as pavement 3 which contains over 800 merged images requiring considerable computing power and time. Taking this into account and whilst this process worked, drone imagery is a far preferred option for imaging pavements. Unfortunately, due to the current laws in Tunisia, acquiring permits for the drone is difficult and it is hoped for future work that this can be undertaken. Not only does the drone capture a larger area of the pavements (such as the Triassic ”moonscape”, or the flanks of the TdM), the images are automatically georeferenced. Drone imagery should be done in conjunction with the measurement stations as this provides a multiscale approach to pavement analysis (hand measurements, selfie stick pavements, drone imagery). This is an important part of fracture characterisation as it considers the concept of Representative Elementary Volume (REV). At different scales, the heterogeneity of objects (fractures/discontinuities) varies. Whilst REV is not discussed in this work, analysing fractures at different scales is important to understanding the various fractures that are detected at each scale. Therefore, imaging the surface fractures at various scales provides an solid base for linking with the data at depth (e.g. borehole - fine scale; seismic - large scale).

Satellite imagery was also a useful tool for gathering information in gaps that were left from the fieldwork mission, in particular along the Jeffara Escarpment. This data was invaluable for measuring the large open folds in the Triassic and Jurassic south of the TdM and integrating this into the cross-sections. This methodology required to the use of topographic satellite data which has an uncertainty value (approx. 5m). This can create variation in the measurements collected. Therefore, to limit this uncertainty, measurements were taken at each chosen location multiple times and averaged, resulting in more accurate results for the bedding in the Triassic and Jurassic. This was coupled with comparing the satellite data with outcrop data collected from the field limiting variability.

7.1.2. Subsurface Data

Subsurface data in the SCB allowed for analysis and interpretation directly to the target reservoirs and thus applying the knowledge gained from the work in the Jeffara Basin to these units.

The well data from Well-1 and Well-2 is excellent for analysing fractures in the Paleozoic reservoirs. This work characterised the different fracture sets that were present then relating this to the seismic data and the overall structural framework. Well data can be influenced by FMI imaging resolution and picking bias whereby certain fracture sets could be missed and extrapolating P10 values from wells becomes difficult. Additional wells were also present to north where interpretations were gathered from Roskam (2016) which estimated aperture sizes for the fractures at depth, however further work could utilise these wells for fracture intensity, orientation and height measurements. It should be noted that whilst estimating aperture values from the wells is good, these measurements are usually overestimated and therefore aperture modelling such as the method used in this thesis is beneficial in reevaluating aperture size (Bisdom et al. 2016a, Davatzes and Hickman 2010).

Seismic data analysis and seismic attributes work provided a modern day approach to fracture evaluation. This gave an insight into the larger fractures and discontinuities at depth in the SCB. The seismic attribute analysis used OpendTect which allowed for easier workflows in applying the data and improving the imaging of fractures at depth. REV is an important concept to consider, and identifying fractures from seismic comes with limitations. Seismic resolution can be an issue, and whilst this is high quality land seismic, the resolution of this data could impact the results. However, since analysis focused on high angle discontinuities on a horizontal plane, resolution issues and uncertainty is reduced. Seismic analysis was limited to the 3D cube in the NW of the SCB. New reprocessed seismic is becoming available which could be useful for exploring the fracture networks elsewhere in the SCB. Additional seismic is also being acquired further into the SCB. Given the understanding from this work, similar fracture distribution of conjugate sets would be expected. The new seismic is closer to the Jeffara Escarpment and TdM, and would provide better links in the subsurface between the Jeffara Basin to the SCB.

7.2. Fracture Prediction in the Subsurface

The fracture network and aperture modelling integrated all the data together into a predictive model for the fractures at depth in the Paleozoic reservoirs and how they contribute to flow. Computational limitations to this type of modelling limited the scope of the final fracture model and future modelling should account for the North and South regions in volume to better understand the impact of the network in these zones.

Furthermore, more advanced methods are available for modelling fracture networks such as MPS (Bruna et al. 2019c). This method would apply the pavement and (acquired) drone imagery of the surface fractures as ”training images” for the simulation to then model fracture networks of the system. This then, in the case of the SCB, to subsurface data as well utilising the fractures observed in the seismic attribute analysis (fig.7.1) as additional ”training images. This method would better constrain the variation in fracture orientation and intensity at depth (especially in the fracture/fault zones) and overall reduce uncertainty in the fracture model.

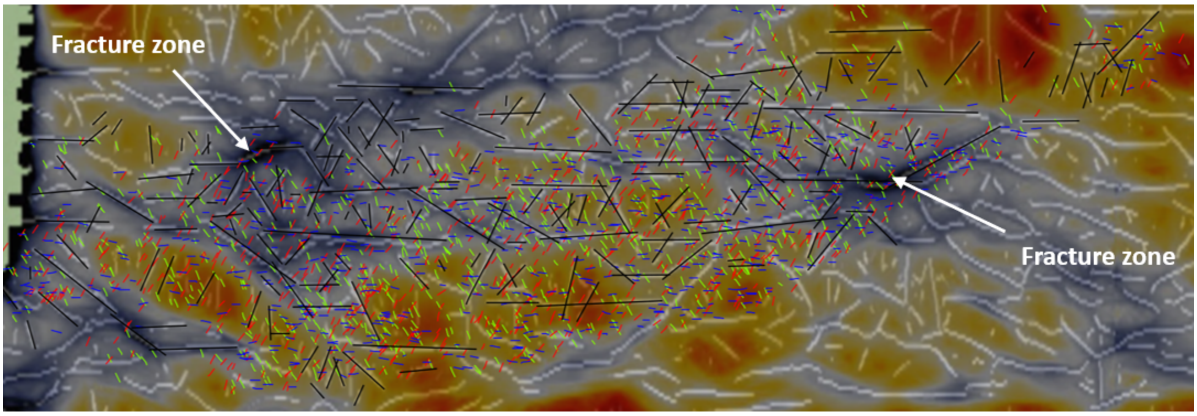

Figure 7.1: FL and TFL seismic attributes and final fracture model showing areas where fracture zones occur which could be further modelling using the MPS technique with training images

The aperture modelling uses an analytical method which does not take into account slip along the fracture intersections. This has an impact a the small scale, influencing the fracture aperture size. Utilising the FE methods of aperture modelling will provide better results in regards to the interaction between fractures in the network an take into account changes to local stress between sets. Furthermore, FE modelling also creates an output from which flow testing can be undertaken. It is useful to test fracture models with pressure data from the field (wells) or with dynamic reservoir modelling to check the suitability of the fracture model. Dynamic flow modelling will also quantify how much the fractures are contributing the reservoir flow and how they affect production. This will provide important insights for future work and development of the reservoirs in the SCB.

7.3. Structural Framework

The updated structural framework presented in this thesis has implications to the interpretation of the late Palaeozoic and early Mesozoic tectonics in Central Tunisia. A late Hercynian shortening phase is proposed between the Permian and early Jurassic orientated N-S causing folding in the Permian and Triassic units and creating a distributed fracture network throughout the system. This has been constrained from the surface and subsurface data which focuses on the Tebaga High in the Jeffara Basin. Structures observed in the SCB links westwards the Tebaga High and the subsurface. Timing the deformation is observed through the thinning and wedging of the mid-late Triassic and Jurassic units towards the high. This shortening phase can be linked to the large scale regional events in Tunisia and Northern Africa during the Mesozoic. This phase predates the major extension of the Tethys Ocean which does not affect Central Tunisia until the mid-Mesozoic and therefore a late Hercynian shortening event can fit between the Permian and the major Jurassic extension (Gharbi et al. 2020, Raulin et al. 2011, Mejri et al. 2006).

The fractures observed indicate a distributed network of conjugate fractures throughout open folds. To allow for a distributed network, fracturing during shortening occurs early on during the LPS phase. This is contrary to most fracture models that imply that fracturing occurs during folding creating extensional orthogonal fractures on fold axis (Watkins et al. 2018, 2015, and references therein). These fractures are not significantly observed in outcrop and therefore it is poorly understood whether they are distributed at depth. The model presented in this thesis (fig.7.2) shows a distributed network of conjugate fractures formed during a regional stress of 001°. These sets form in both the Paleozoic and late Permian to early Triassic units. Two other distributed sets are observed in the Paleozoic units that form background joints observed in seismic and wells. The current regional stress situation of 036°affects the openness of the fracture sets at depth.

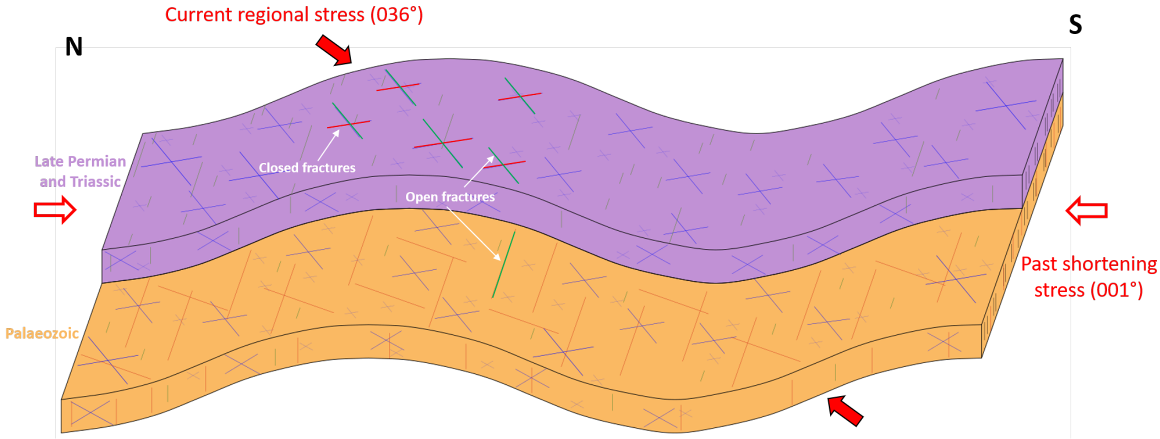

Figure 7.2: Open fold fracture model showing the past and present regional stress orientations and likely open fractures

7.4. Future Research

There is scope for future research building on this work in the Jeffara and Southern Chotts Basins. Work should be undertaken further along the Jeffara Escapement to detail the nature of the Triassic and Jurassic units north and south of the Tebaga High. This would better constrain the folding and thickness changes experienced by these units, especially to the north where the Permian-Jurassic disappears. Apatite Fission Track (AFT) dating work will quantify better the timing of exposure of the Permian and lower Triassic rocks during the mid-late Triassic and Jurassic periods. These details will better constrain the updated structure framework presented in this thesis. It may also be beneficial to explore the affects of this late Hercynian shortening to other basin in the region in Algeria and Libya (e.g. Ghadames Basin) and whether fracture networks are similarly affected.

Drone work should be undertaken along the TdM and around Kirchaou and Sidi Toui to capture the fracture pavements at a larger scale to better constrain how the REV affects the surface networks. This should be done in conjunction with further subsurface analysis of the additional seismic blocks to the southwest, further building on the fracture analysis already undertaken.

Building with this, innovative fracture modelling techniques such as MPS modelling should be applied on the large scale pavement images and seismic attribute slices to create improved fracture network models of the SCB. These should also focus on other reservoir units such as the Permian carbonates and the TAGI units which are within the same structural framework as the Ordovician reservoirs. The Triassic sands are a well known reservoir unit and open fracture networks could play a key role in production of hydrocarbons from them (Kraouia et al. 2018). Furthermore, applying FE modelling to the fracture apertures will allow for flow testing using either production data from the Sabria field or in house flow simulation techniques (e.g. DARTS) to better quantify the contribution of fractures to reservoir flow.

8

Conclusions

This thesis project answered the following research questions:

1. **What is the structural nature of the Tebaga de Medenine?**
   The TdM forms a structural high in the Jeffara Basin formed of folded Permian and early Triassic units onto which mid-late Triassic and early Jurassic units are thin towards and wedge onto. This structure can be extrapolated west into the SCB.

2. **What is the regional structural history during the Permian to Cretaceous in the Jeffara Basin?**
   The period between the Permian and early Jurassic in the Jeffara Basin is characterised by a shortening event (observed in the TdM). This event formed a large topographic high (TdM) and open folding. This corresponds with a late Hercynian compression phase in the region. These highs are then eroded during the late Jurassic and Cretaceous when major rifting affected the basins.

3. **How does this history affect the fractures observed units at the surface?**
   Two main joint sets were observed as a result of the shortening event on the surface: 1) a conjugate fracture system (striking at 240°, 302°), 2) a stylolite orientated in E-W. The orientation of these confirm a shortening in the N-S direction.

4. **How does the geological history of the region drive fracture generation in the Southern Chotts Basin?**
   The fold axis of the TdM can be extrapolated westwards through to the plays in the SCB. Fractures found on the surface are also represented at depth through analysis of both seismic and well data. The distributed network of fractures is observed in a hybrid fracture model (DFN and deterministic from seismic) representing the fracture network at depth.

5. **What are the implications of these fractures to the reservoir flow in the Southern Chotts Basin plays?**
   The fracture network is well connected in the reservoir by fractures with varying aperture. The aperture of the fractures varies under the current stress regime by orientation and length. Long fractures and fractures orientated 240°present the widest aperture. Since the history of these fractures is linked with the shortening phase during the late Hercynian, these fractures are predicted to be found in the Ordovician, Permian and TAGI reservoirs in the SCB. These fractures have implications on the transmissibility of the reservoirs, especially the Permian units which have a low bulk rock permeability and the TAGI units which are susceptible to compartmentalisation.

Bibliography

Aissaoui, N., Acheche, M., Ben Yacoub, J., M'rabet, A., Nehdi, T., Pezzino, F., and Smaoui, J. (1996). Silurian acacus new play in southern tunisia. In *Proceedings of the 5th Exploration and Production Conference, Entreprise Tunisienne d'Activites Petrolières Memoir*, volume 10, pages 1–14.

Amadei, B., Savage, W., and Swolfs, H. (1987). Gravitational stresses in anisotropic rock masses. In *International Journal of Rock Mechanics and Mining Sciences & Geomechanics Abstracts*, volume 24, pages 5–14. Elsevier.

Balti, T., Nasr, I. H., and Inoubli, M. H. (2018). Petrophysical characterization of upper permian reservoir in southern tunisia. In *Conference of the Arabian Journal of Geosciences*, pages 169–171. Springer.

Barton, N. (2014). Non-linear behaviour for naturally fractured carbonates and frac-stimulated gas-shales. *First Break*, 32(9).

Barton, N. and Bandis, S. (1980). Technical note: Some effects of scale on the shear strength of joints. *International Journal of Rock Mechanics and Mining Sciences*, 17:69–73.

Barton, N., Bandis, S., and Bakhtar, K. (1985). Strength, deformation and conductivity coupling of rock joints. In *International journal of rock mechanics and mining sciences & geomechanics abstracts*, volume 22, pages 121–140. Elsevier.

Bisdom, K. (2016). Burial-related fracturing in sub-horizontal and folded reservoirs: Geometry, geomechanics and impact on permeability. *TU Delft*. PhD Thesis.

Bisdom, K., Bertotti, G., and Nick, H. M. (2016a). A geometrically based method for predicting stress-induced fracture aperture and flow in discrete fracture networks. *AAPG Bulletin*, 100(7):1075–1097.

Bisdom, K., Bertotti, G., and Nick, H. M. (2016b). The impact of different aperture distribution models and critical stress criteria on equivalent permeability in fractured rocks. *Journal of Geophysical Research: Solid Earth*, 121(5):4045–4063.

Bishop, W. F. (1975). Geology of Tunisia and adjacent parts of Algeria and Libya. *AAPG bulletin*, 59(3):413–450.

Blenkinsop, T. G. (2008). Relationships between faults, extension fractures and veins, and stress. *Journal of Structural Geology*, 30(5):622–632.

Bodin, S., Petitpierre, L., Wood, J., Elkanouni, I., and Redfern, J. (2010). Timing of early to mid-cretaceous tectonic phases along north africa: New insights from the jeffara escarpment (libya–tunisia). *Journal of African Earth Sciences*, 58(3):489–506.

Boote, D. R., Clark-Lowes, D. D., and Traut, M. W. (1998). Palaeozoic petroleum systems of north africa. *Geological Society, London, Special Publications*, 132(1):7–68.

Bouaziz, I., Saidi, M., Belhaj Mohamed, A., et al. (2014). Oil-oil correlation and potential source rocks in the chotts basin tunisia. In *International Petroleum Technology Conference*. International Petroleum Technology Conference.

Bouaziz, S. (1995). Etude de la tectonique cassante dans la plate-forme et l'atlas sahariens (tunisie méridionale): Evolution des paléochamps de contraintes et implications géodynamiques. *Thése d'Etat de l'Université de Tunis II*, page 485.

Bouaziz, S., Barrier, E., Soussi, M., Turki, M. M., and Zouari, H. (2002). Tectonic evolution of the northern african margin in tunisia from paleostress data and sedimentary record. *Tectonophysics*, 357(1-4):227–253.

Brouwer, F. and Huck, A. (2011). An integrated workflow to optimize discontinuity attributes for the imaging of faults. In *Attributes: New Views on Seismic Imaging—Their Use in Exploration and Production. GCSSEPM, 31st Annual Conference Publication*, volume 496, page 533.

Bruna, P.-O., Bertotti, G., Ben Amor, S., Nasri, A., and Ouahchi, S. (2019a). Analysis of the pre- and post variscan unconformity deformations: new insights for the characterisation of the ordovician and triassic reservoirs in the southern chotts basin, tunisia. In *PESGB Africa EP conference*.

Bruna, P.-O., Lavenu, A. P., Matonti, C., and Bertotti, G. (2019b). Are stylolites fluid-flow efficient features? *Journal of Structural Geology*, 125:270–277.

Bruna, P.-O., Straubhaar, J., Prabhakaran, R., Bertotti, G., Bisdom, K., Mariethoz, G., and Meda, M. (2019c). A new methodology to train fracture network simulation using multiple-point statistics. *Solid Earth*, 10(2):537–59.

Busson, G. (1965). Esquisses géologiques de la région de medenine, foum tatahouine, sidi toui, bir fatnassia (sud-tunisien). *Centre National de la recherche scientifique*.

Busson, G. (1972). Principes, méthodes et résultats d'une étude stratigraphique du mésozoïque saharien. *Mémoires du Museum National d'Histoire Naturelle, Série C*.

Condie, K. C. (2003). Supercontinents, superplumes and continental growth: the neoproterozoic record. *Geological Society, London, Special Publications*, 206(1):1–21.

Cosgrove, J. (2015). The association of folds and fractures and the link between folding, fracturing and fluid flow during the evolution of a fold–thrust belt: a brief review. *Geological Society, London, Special Publications*, 421(1):41–68.

Craig, J., Rizzi, C., Said, F., Thusu, B., Lüning, S., Asbali, A., Keeley, M., Bell, J., Durham, M., Eales, M., et al. (2008). Structural styles and prospectivity in the precambrian and palaeozoic hydrocarbon systems of north africa. *The Geology of East Libya*, 4:51–122.

Daniels, R. and Emme, J. (1995). Petroleum system model, eastern algeria, from source rock to accumulation: when, where and how. In *Proceedings of the seminar on source rocks and hydrocarbon habitat in Tunisia*, volume 9, pages 101–124.

Davatzes, N. C. and Hickman, S. H. (2010). Stress, fracture, and fluid-flow analysis using acoustic and electrical image logs in hot fractured granites of the coso geothermal field, california, usa.

Derguini, K. (2005). Hydrocarbon potential of Maatoug permit. Technical report, ETAP.

Dershowitz, W. S., Herda, H. H., et al. (1992). Interpretation of fracture spacing and intensity. In *The 33th us symposium on rock mechanics (USRMS)*. American Rock Mechanics Association.

Dhaoui, M., Gabtni, H., Jallouli, C., Jleilia, A., Mickus, K. L., and Turki, M. M. (2014). Gravity analysis of the precambrian basement topography associated with the northern boundary of ghadames basin (southern tunisia). *Journal of Applied Geophysics*, 111:299–311.

Doglioni, C., Fernandez, M., Gueguen, E., and Sabat, F. (1999). On the interference between the early apennines-maghrebides backarc extension and the alps-betics orogen in the neogene geodynamics of the western med iterranean. *Bollettino della Società geologica italiana*, 118(1):75–89.

El Rabia, A., Inoubli, M. H., Ouaja, M., Abidi, O., Sebei, K., and Jlailia, A. (2018). Salt tectonics and its effect on the structural and sedimentary evolution of the jeffara basin, southern tunisia. *Tectonophysics*, 744:350–372.

ETAP (2001). Tunisian Stratigraphic Chart. Available at `http://www.etap.com.tn/`.

ETAP (2020). List of concessions. Available at `http://www.etap.com.tn/`.

Fabre, J. (1988). African paleozoic series-an approach. *Journal of African Earth Sciences*, 7(1):1–40.

Fekirine, B. and Abdallah, H. (1998). Palaeozoic lithofacies correlatives and sequence stratigraphy of the saharan platform, algeria. *Geological Society, London, Special Publications*, 132(1):97–108.

Ferjani, A. B., Burollet, P. F., and Mejri, F. (1990). *Petroleum geology of Tunisia*. Enterprise Tunisienne dÁctivités Pétrolières.

Fisher, R. A. (1953). Dispersion on a sphere. *Proceedings of the Royal Society of London. Series A. Mathematical and Physical Sciences*, 217(1130):295–305.

Fossen, H. (2016). *Structural geology*. Cambridge University Press.

Frizon de Lamotte, D., Raulin, C., Mouchot, N., Wrobel-Daveau, J.-C., Blanpied, C., and Ringenbach, J.-C. (2011). The southernmost margin of the tethys realm during the mesozoic and cenozoic: Initial geometry and timing of the inversion processes. *Tectonics*, 30(3).

Frizon de Lamotte, D., Tavakoli-Shirazi, S., Leturmy, P., Averbuch, O., Mouchot, N., Raulin, C., Leparmentier, F., Blanpied, C., and Ringenbach, J.-C. (2013). Evidence for late devonian vertical movements and extensional deformation in northern africa and arabia: integration in the geodynamics of the devonian world. *Tectonics*, 32(2):107–122.

Gabtni, H., Jallouli, C., Mickus, K. L., Zouari, H., and Turki, M. (2009). Deep structure and crustal configuration of the jeffara basin (southern tunisia) based on regional gravity, seismic reflection and borehole data: How to explain a gravity maximum within a large sedimentary basin? *Journal of Geodynamics*, 47(2-3):142–152.

Gale, J. F., Laubach, S. E., Olson, J. E., Eichhubl, P., and Fall, A. (2014). Natural fractures in shale: A review and new observationsnatural fractures in shale: A review and new observations. *AAPG bulletin*, 98(11):2165–2216.

Galeazzi, S., Point, O., Haddadi, N., Mather, J., and Druesne, D. (2010). Regional geology and petroleum systems of the illizi–berkine area of the algerian saharan platform: An overview. *Marine and Petroleum Geology*, 27(1):143–178.

Garfunkel, Z. and Derin, B. (1984). Permian-early mesozoic tectonism and continental margin formation in israel and its implications for the history of the eastern mediterranean. *Geological Society, London, Special Publications*, 17(1):187–201.

Gharbi, M., Masrouhi, A., Bellier, O., and Youssef, M. B. (2020). The southern atlas front in tunisia: Regional-scale geometry and structural evolution. In *Arabian Plate and Surroundings: Geology, Sedimentary Basins and Georesources*, pages 137–160. Springer.

Guiraud, R., Bosworth, W., Thierry, J., and Delplanque, A. (2005). Phanerozoic geological evolution of northern and central africa: an overview. *Journal of African Earth Sciences*, 43(1-3):83–143.

Gutierrez, M. and Youn, D.-J. (2015). Effects of fracture distribution and length scale on the equivalent continuum elastic compliance of fractured rock masses. *Journal of Rock Mechanics and Geotechnical Engineering*, 7(6):626–637.

Harris, P. M. (1985). Depositional environments of carbonate platforms. *Colo. Sch. Mines Q*, 80(4):3.

Healy, D., Rizzo, R. E., Cornwell, D. G., Farrell, N. J., Watkins, H., Timms, N. E., Gomez-Rivas, E., and Smith, M. (2017). Fracpaq: A matlab™ toolbox for the quantification of fracture patterns. *Journal of Structural Geology*, 95:1–16.

Hilley, G. E., Arrowsmith, J. R., and Amoroso, L. (2001). Interaction between normal faults and fractures and fault scarp morphology. *Geophysical Research Letters*, 28(19):3777–3780.

IAG (1967). Geodetic reference system 1967, Special Publication 3. *Bulletin Géodésique*, page 116.

Ishii, E. (2016). Far-field stress dependency of the failure mode of damage-zone fractures in fault zones: Results from laboratory tests and field observations of siliceous mudstone. *Journal of Geophysical Research: Solid Earth*, 121(1):70–91.

Jabir, A., Cerepi, A., Loisy, C., and Rubino, J.-L. (2020). Stratigraphy, sedimentology and paleogeography of a paleozoic succession, ghadames and jefarah basin, libya and tunisia. *Journal of African Earth Sciences*, 163:103642.

Jaglan, H., Qayyum, F., and Hélène, H. (2015). Unconventional seismic attributes for fracture characterization. *First Break*, 33(3).

Jamieson, J. and Herman, G. (2014). Dynamic 3-Point Geological-Plane Solver. *NJ Geological Water Survey*. Available at `http://www.impacttectonics.org/GeoTools/3ppops.html`.

Jing, L. and Stephansson, O. (2007). Chapter 10 - Discrete Fracture Network (DFN) Method. In Jing, L. and Stephansson, O., editors, *Fundamentals of Discrete Element Methods for Rock Engineering*, volume 85 of *Developments in Geotechnical Engineering*, pages 365 – 398. Elsevier.

Keeley, M. (1994). Phanerozoic evolution of the basins of northern egypt and adjacent areas. *Geologische Rundschau*, 83(4):728–742.

Kilani-Mazraoui, F., Razgallah-Gargouri, S., and Mannai-Tayech, B. (1990). The permo-triassic of southern tunisia—biostratigraphy and palaeoenvironment. *Review of Palaeobotany and Palynology*, 66(3-4):273–291.

Kraouia, S., El Asmi, A. M., Ben Salem, A., and Saidi, M. (2018). Geopetroleum assessment of the ordovician and triassic reservoirs in the chotts region and maturity modeling of their supplying source rock (fegaguira formation). In *14th Tunisian Petroleum Exploration and Production Conference*. ETAP.

Lavier, L. L. and Buck, W. R. (2002). Half graben versus large-offset low-angle normal fault: Importance of keeping cool during normal faulting. *Journal of Geophysical Research: Solid Earth*, 107(B6):ETG–8.

Lazzez, M., Zouaghi, T., and Youssef, M. B. (2008). Austrian phase on the northern african margin inferred from sequence stratigraphy and sedimentary records in southern tunisia (chotts and djeffara areas). *Comptes Rendus Geoscience*, 340(8):543–552.

Li, J. Z., Laubach, S., Gale, J., and Marrett, R. (2018). Quantifying opening-mode fracture spatial organization in horizontal wellbore image logs, core and outcrop: application to upper cretaceous frontier formation tight gas sandstones, usa. *Journal of Structural Geology*, 108:137–156.

Lüning, S. (2005). *AFRICA | North African Phanerozoic*, pages 12–25.

Lüning, S., Craig, J., Loydell, D., Storch, P., and Fitches, B. (2000). Lower silurian 'hot shales' in north africa and arabia: regional distribution and depositional model. *Earth-Science Reviews*, 49(1):121 – 200.

Lüning, S., Kolonic, S., Geiger, M., Thusu, B., Bell, J., and Craig, J. (2009). Infracambrian hydrocarbon source rock potential and petroleum prospectivity of nw africa. *Geological Society, London, Special Publications*, 326:157–180.

Marrett, R., Ortega, O. J., and Kelsey, C. M. (1999). Extent of power-law scaling for natural fractures in rock. *Geology*, 27(9):799–802.

Mathieu, G. (1949). *Contribution à l'étude des monts troglodytes dans l'extrême Sud-Tunisien: géologie régionale des environs de Matmata medenine et Foum-Tatahouine*, volume 4.

Mazarine Energy B.V. (2019). Mazarine Energy and ETAP Discover Oil in Sidi Marzoug-1 Well. *Mazarine Energy*. Available at `https://mazarine-energy.com`.

Mejri, F., Burollet, P. F., and Ferjani, A. B. (2006). *Petroleum geology of Tunisia: A renewed synthesis*. Enterprise tunisienne d'activités pétrolières.

Narr, W., Schechter, D. S., and Thompson, L. B. (2006). *Naturally fractured reservoir characterization*, volume 112. Society of Petroleum Engineers Richardson, TX.

NASA and CNES (2019). Global Topography and Gravity Data from TOPEX/Poseidon Satellite Mission. *Scripps Institution of Oceanography, University of California*. Available at `https://topex.ucsd.edu/cgi-bin/get_data.cgi`.

Nederveen, R. (2018). Factors controlling fracture characteristics in chalk formations in the dutch offshore: Results from a study based on seismic attributes. *TU Delft*. Master Thesis.

Nelson, R. (2001). *Geologic analysis of naturally fractured reservoirs*. Elsevier.

Niven, E. B. and Deutsch, C. V. (2010). Relating different measures of fracture intensity. *CCG Annual Report-Paper 103, Centre for Computational Geostatistics*.

Olsson, R. and Barton, N. (2001). An improved model for hydromechanical coupling during shearing of rock joints. *International Journal of Rock Mechanics and Mining Sciences*, 38(3):317–329.

Perthuisot, V. (1981). Diapirism in northern tunisia. *Journal of Structural Geology*, 3(3):231–235.

Raulin, C., de Lamotte, D. F., Bouaziz, S., Khomsi, S., Mouchot, N., Ruiz, G., and Guillocheau, F. (2011). Late triassic–early jurassic block tilting along e–w faults, in southern tunisia: New interpretation of the tebaga of medenine. *Journal of African Earth Sciences*, 61(1):94–104.

Redfern, J., Owusu, K., Bradley, G.-M., and Charton, R. (2019). NARG Database. *North African Research Group*. Available at `http://www.narg.org.uk/`.

Reeh, G., Boote, D., and Reston, T. (2019). Structural history of the jefarrah fault system, nw libya. In *18th PESGB/HGS Conference (Africa EP)*. PESGB.

Rohde, J. R. (1986). Determination of far-field stress from localized stress concentrations. *Iowa State University*. PhD Thesis.

Roskam, P. (2016). Sub-seismic deformation in the sabria oilfield, central tunisia. *TU Delft*. Master Thesis.

Ross, C. A. and Ross, J. R. (1988). Late paleozoic transgressive-regressive deposition.

Roure, F., Brun, J.-P., Colletta, B., and Van Den Driessche, J. (1992). Geometry and kinematics of extensional structures in the alpine foreland basin of southeastern france. *Journal of Structural Geology*, 14(5):503–519.

Rouvier, H. (1977). Géologie de l'extrême nord-tunisien. *Thesis, These es Sci., Univ. Paris VI, France*.

Sandwell, D. T. and Smith, W. H. (2009). Global marine gravity from retracked geosat and ers-1 altimetry: Ridge segmentation versus spreading rate. *Journal of Geophysical Research: Solid Earth*, 114(B1).

Scotese, R. C. and Barrett, S. F. (1990). Gondwana's movement over the south pole during the palaeozoic: evidence from lithological indicators of climate. *Geological Society, London, Memoirs*, 12(1):75–85.

Soua, M. (2013). First evidence of tunnel valley-like formation during the late ordovician "subgalacial" period in southern tunisia influence on the jeffara sandstone reservoir quality. *SPE Journal*.

Soua, M. (2014). Paleozoic oil/gas shale reservoirs in southern tunisia: An overview. *Journal of African Earth Sciences*, 100:450–492.

Stampfli, G., Borel, G., Cavazza, W., Mosar, J., and Ziegler, P. (2001). Palaeotectonic and palaeogeographic evolution of the western tethys and peritethyan domain (igcp project 369). In *Episodes*, page 222.

Stampfli, G. M. and Borel, G. (2002). A plate tectonic model for the paleozoic and mesozoic constrained by dynamic plate boundaries and restored synthetic oceanic isochrons. *Earth and Planetary Science Letters*, 196(1-2):17–33.

Tissot, B., Espitalié, J., Deroo, G., Tempere, C., and Jonathan, D. (1984). Origin and migration of hydrocarbons in the eastern sahara (algeria).

Toomey, D. F. (1991). Late permian reefs of southern tunisia: Facies patterns and comparison with the capital reef, southwestern united states. *Facies*, 25(1):119–145.

Villeneuve, M., Bassot, J., Robineau, B., Dallmeyer, R., and Ponsard, J. (1991). The bassaride orogen. In *The West African orogens and circum-atlantic correlatives*, pages 151–185. Springer.

Watkins, H., Butler, R. W., Bond, C. E., and Healy, D. (2015). Influence of structural position on fracture networks in the torridon group, achnashellach fold and thrust belt, nw scotland. *Journal of Structural Geology*, 74:64–80.

Watkins, H., Healy, D., Bond, C. E., and Butler, R. W. (2018). Implications of heterogeneous fracture distribution on reservoir quality; an analogue from the torridon group sandstone, moine thrust belt, nw scotland. *Journal of Structural Geology*, 108:180–197.

Zaafouri, A., Haddad, S., and Mannaî-Tayech, B. (2017). Subsurface permian reef complexes of southern tunisia: Shelf carbonate setting and paleogeographic implications. *Journal of African Earth Sciences*, 129:944–959.

Zargouni, F. (1985). Tectonique de l'atlas meridionale de la tunisie. evolution geometrique et cinematique des structures en zone de cisaillement. *Doctoral thesis, Louis Strasbourg University*.

Zeeb, C., Gomez-Rivas, E., Bons, P. D., and Blum, P. (2013). Evaluation of sampling methods for fracture network characterization using outcrops. *AAPG bulletin*, 97(9):1545–1566.

Zouari, H., Turki, M. M., Delteil, J., and Stephan, J.-F. (1999). Tectonique transtensive de la paléomarge tunisienne au cours de l'aptien-campanien. *Bulletin de la Société géologique de France*, 170(3):295–301.

A

Tunisian Stratigraphic Chart

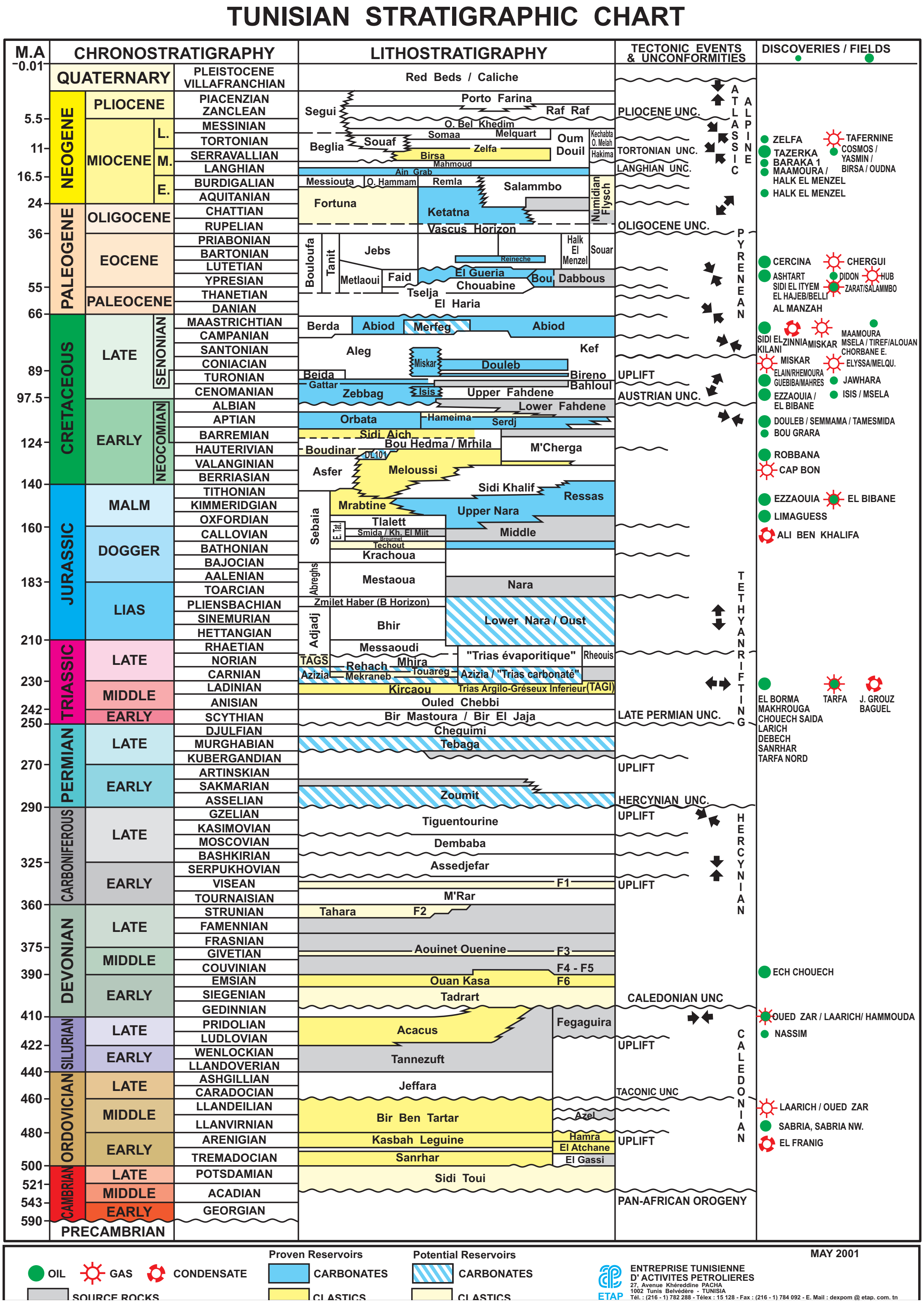

Figure A.1: Tunisian Stratigraphical Chart (ETAP 2001)

B

Field Measurements

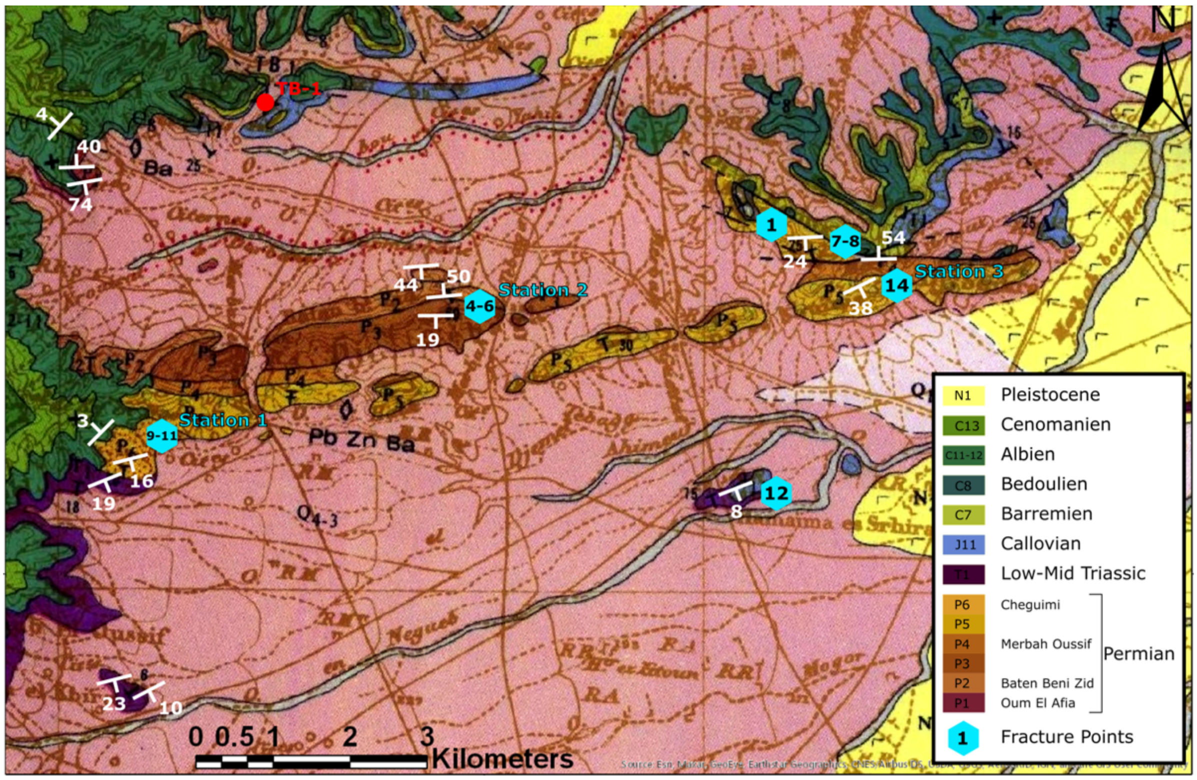

Figure B.1: Field measurements and fracture station locations in the TdM

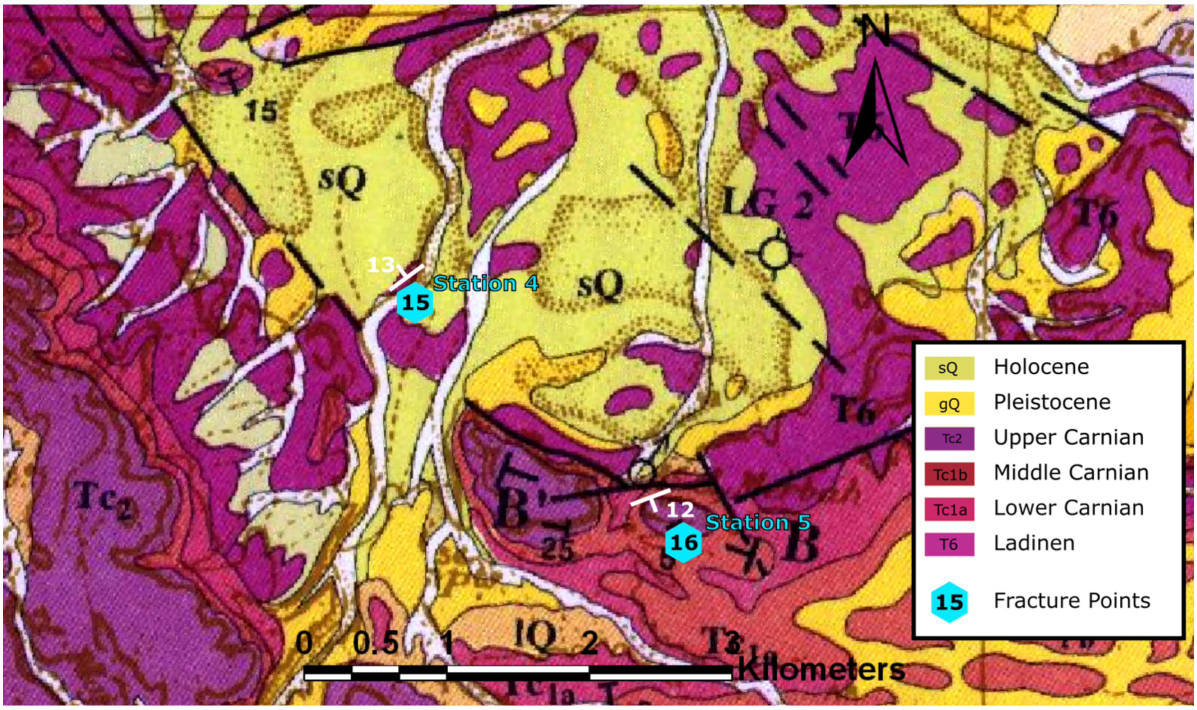

Figure B.2: Field measurements and fracture station locations in Kirchaou

C

Seismic Data

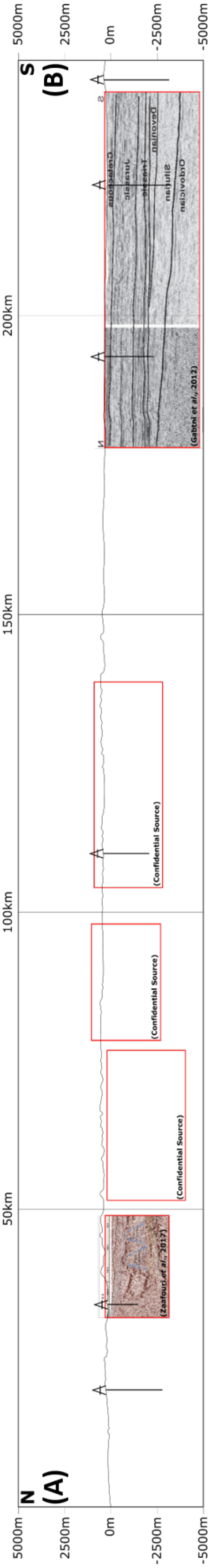

Figure C.1: Seismic lines and wells interpreted in the N-S regional cross-section (see fig.3.2 for line of section)

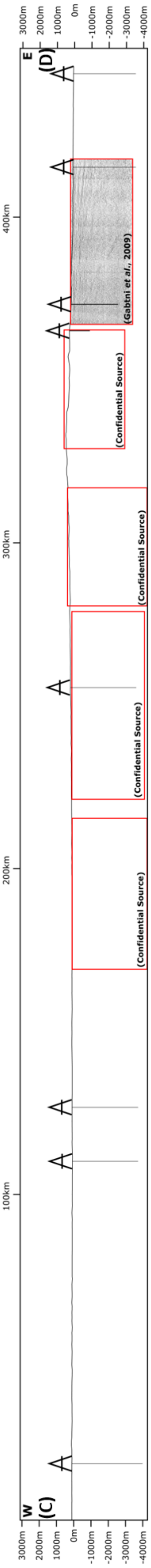

Figure C.2: Seismic lines and wells interpreted in the E-W regional cross-section (see fig.3.2 for line of section)

D

Dynamic 3-Point Geological-Plane Solver

D.1. Theory and Tutorial

The Dynamic 3-Point Geological-Plane Solver is a tool that utilises satellite topographic data to determine the bedding nature of geologic units using the 3-point rule (Jamieson and Herman 2014). The software can be downloaded from the ImpactTectonics website.

The nature of planes can be determined from using 3 points on the plane. When the coordinates of these three points is known, the plane can be calculated. In the real world, knowing the 3D coordinates of three locations along a bedding plane, the dip azimuth and angle is the calculated result. The tool extracts the 3D spatial coordinates from NASA World Wind Globe that are picked along a visible edge of a geological plane. The distances and spatial bearings between each of the three coordinates are calculated from the longitude and latitude using the Haversine Formula:

$$\Theta = \frac{d}{r}$$

where:
Θ is the angle and d is the distance between two points on a sphere with radius r.

and:

$$d = 2r\left(\sqrt{\sin^2\left(\frac{\gamma_2 - \gamma_1}{2}\right) + \cos\gamma_1 \cos\gamma_2 \sin^2\left(\frac{\lambda_2 - \lambda_1}{2}\right)}\right)$$

where:
γ_1 and γ_2 are the latitude of point 1 and point 2. λ_1 and λ_2 are the longitude of point 1 and point 2.

Since the three points on the plane also form vectors, using cross-product and algebraic multiplication of the directional components, a plunge angle and azimuth of a vector normal to the geologic plane can be calculated. This plunge angle and azimuth represent the bedding angle and azimuth of the geological plane.

The tool automatically applies the formula and calculations to the three chosen points by the user and outputs a bedding angle and azimuth.

The tool interface (fig.D.1) allows for points to be picked on a 3D NASA world globe (yellow pins). These form the 3 points on the bedding plane. The output of the calculation from these points is shown in the red box (strike, dip, quadrant, azimuth). Multiple bedding measurements can be made (in multiples of 3 points), and can be exported as a KML file into Google Earth, from which the results can be extracted. It is recommended that multiple bedding calculations be made for each bedding to reduce uncertainty in picking.

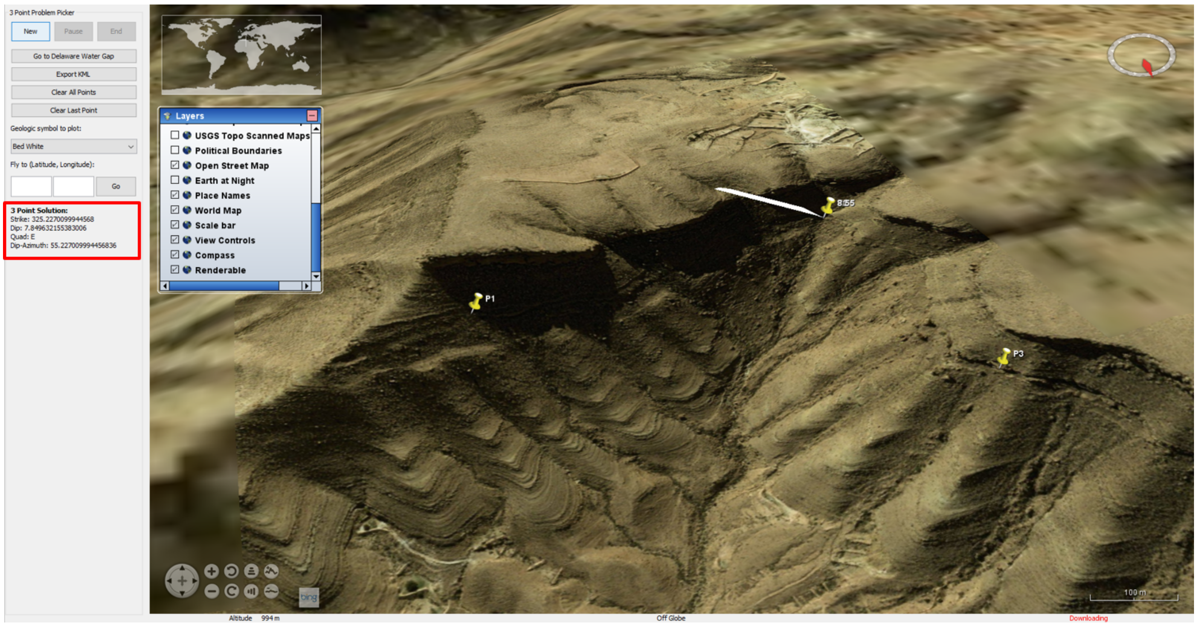

Figure D.1: Solver interface

E

OpendTect Seismic Attributes Results

Seismic attribute analysis followed the workflow specified in Chapter 5. The seismic attributes were calculated using OpendTect, a free to use software specialising in innovated methods of manipulating seismic data. The workflow created by Jaglan et al. (2015) aims at highlighting the fault and fracture data. The results of each stage of the workflow are as follows:

The first step is the input of the 3D seismic cube via the Petrel Link.

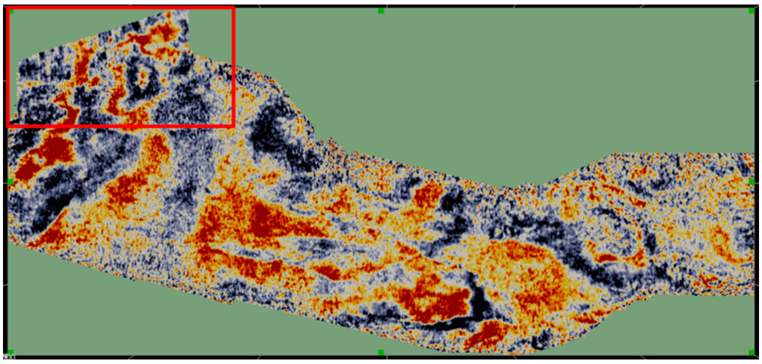

Figure E.1: Full seismic cube input (bounding box area marked in red)

A bounding box is defined to focus the attribute analysis. Attributes can take time in computing and therefore reducing the seismic cube size is important for an efficient workflow.

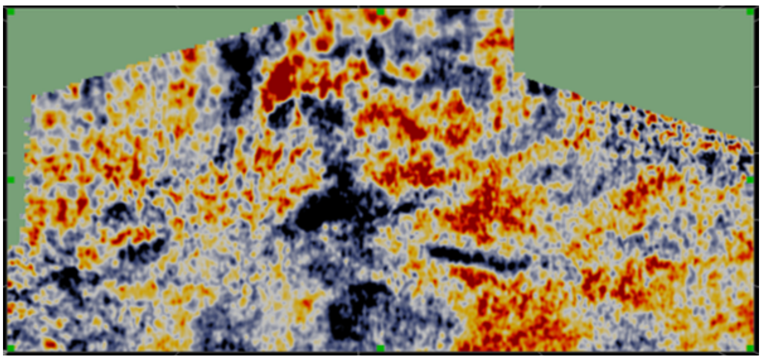

Figure E.2: Bounding box focussing on the north western region of the 3D cube

A steering cube is set up using the Phase Gradient Steering (median) which highlights structural data. This is the cube from which all analysis is undertaken from. The first of which is calculating the Dip Filters (DSMF, DSDF).

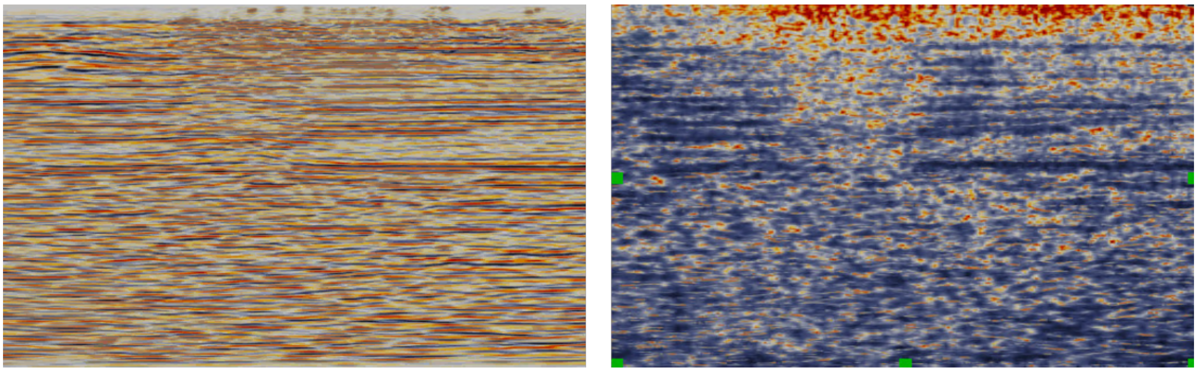

Figure E.3: Dip Filters. Left: DSMF. Right: DSDF

The FEF is then applied to the seismic cube using a combination of DSMF and DSDF. Similarity is used to gauge the quality of the seismic, if the seismic is good (similarity is high), DSMF is applied to the steering cube. Likewise, if the seismic is poor (similarity is low), DSDF is applied. This causes the effect of smoothed seismic, and sharp fault breaks.

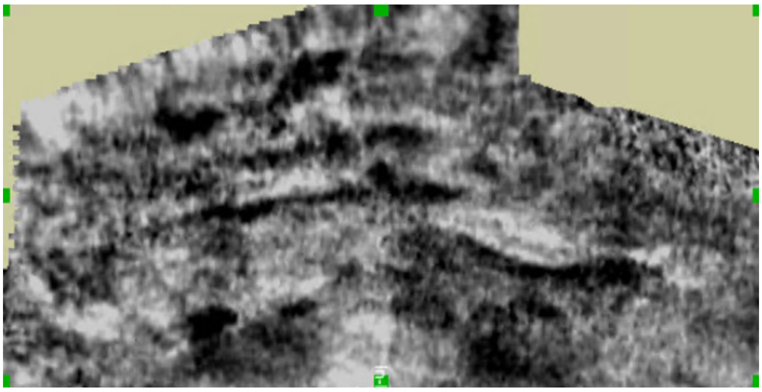

Figure E.4: Fault Enhancement Filter output

Similarity is updated from the FEF attribute cube to be used for analysis. The similarity attribute is sharper than before, as the data is filtered and steered towards faults and fractures.

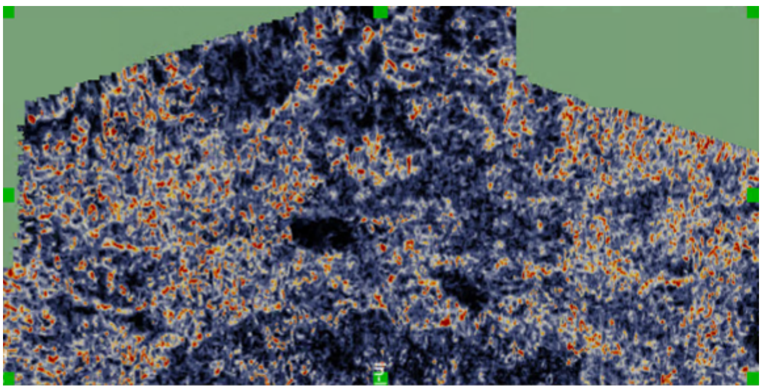

Figure E.5: Updated similarity attribute derived from the FEF attribute. Cutoff value = 0.7

Fault likelihood (FL) and thinned fault likelihood (TFL) is calculated using the FEF attribute. TFL is an attribute which provides accurate and sharp faults and fractures using the power of semblance. The algorithm scans the range of fault dips to identify the maximum likelihood of this lineation occurring. The output is sharp fault and fracture edges on both horizontal and vertical slices. From the FL attribute, detected lineations can be extracted using the Extract Fault tool. The output from this tool is the lineation strike, dip and length.

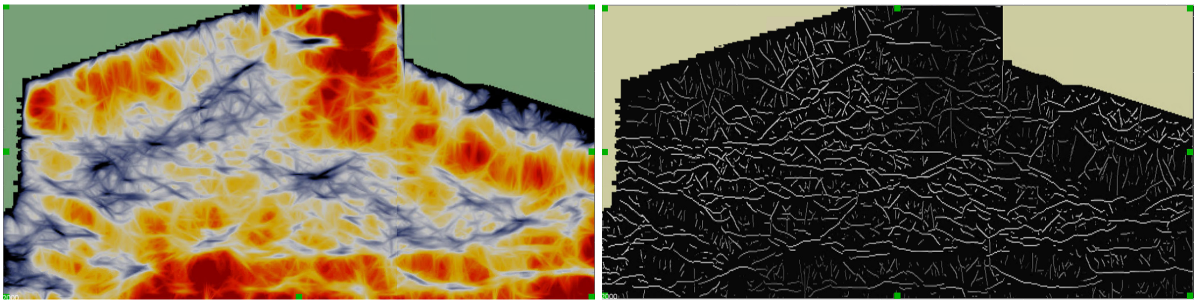

Figure E.6: Left: Fault Likelihood attribute. Right: Thinned Fault Likelihood attribute

Fracture proximity and density are two additional attributes that can be used to estimate the regions in the seismic where fractures are appearing and highlight fracture zones. Fracture proximity is useful for pin-pointing locations with maximum fracture activity within a given radius by tracking the distance along a z-slice from a trace location to a fracture. Fracture density highlights areas of high dense fractures. This attribute improves the visualisation of potential fracture anomalies through computing the ratio of ”number of classified fracture traces” to the ”number of total traces” in a given radius. The anomaly threshold is determined from other curvature/coherence attributes such as Max Curvature.

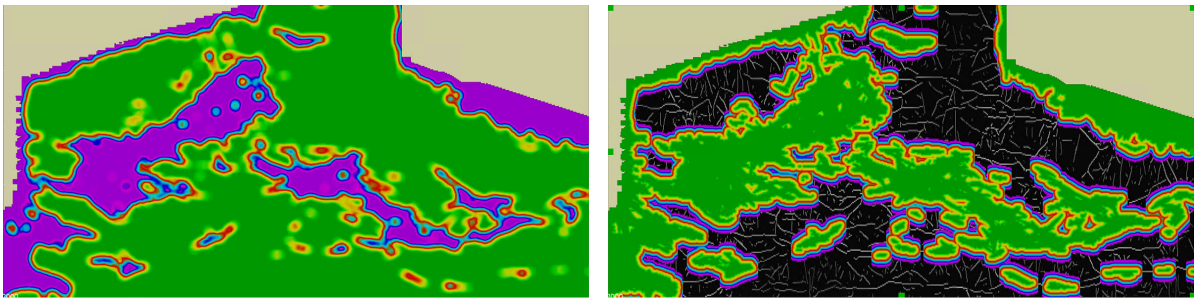

Figure E.7: Left: Fracture density output. Trace threshold - 0.4, Radius - 150m. Right: Fracture proximity output. Trace threshold - 0.4, Radius - 250m.